WORLD METEOROLOGICAL ORGANIZATION

GLOBAL ATMOSPHERE WATCH

WORLD DATA CENTRE FOR GREENHOUSE GASES

WMO WDCGG DATA SUMMARY

WDCGG No. 30

GAW DATA

Volume IV-Greenhouse Gases and Other Atmospheric Gases

PUBLISHED BY
JAPAN METEOROLOGICAL AGENCY
IN CO-OPERATION WITH
WORLD METEOROLOGICAL ORGANIZATION

MARCH 2006

Acknowledgements

The present issue of *Data Summary* summarizes the latest status of greenhouse gases and related gases in the globe. The Data Summary was prepared by the WMO World Data Centre for Greenhouse Gases (WDCGG) in cooperation with the World Meteorological Organization (WMO) using the data from the global observation network that consists of many contributors (Appendix: LIST OF CONTRIBUTORS). These organizations and individuals are involved in observations and research at stations and laboratories which measure greenhouse gases and other atmospheric gases within the framework of the WMO Global Atmosphere Watch (GAW), and other cooperative monitoring and research programmes. The WDCGG thanks all of the organizations and individuals for their efforts in maintaining the observation programme and for their continuous provision of data, particularly the NOAA global air sampling network. Some contributors may not be explicitly acknowledged in this publication owing to lack of space, but it should be noted that all of the organizations and individuals that have submitted data to the WDCGG equally contributed to this new issue of *Data Summary*.

CONTENTS

Summary

This issue of *Data Summary* covers the results of basic analyses of greenhouse gas mixing ratios submitted to the WMO World Data Centre for Greenhouse Gases (WDCGG). The observations range from 1968 to 2004, and only data that reached the WDCGG by September 2005 were analyzed. This *Data Summary* includes analyses of the monthly mean mixing ratios of global, hemispheric and zonal greenhouse and related gases, and provides useful information on the state of mixing ratios of these gases.

Only monthly mean mixing ratios were used in the analyses in the Data Summary. Of course, it is also appreciated that some stations submit daily and hourly mean mixing ratios, which may be more appropriate for analyzing the variations on various time-scales. All the submitted data are available on the WDCGG web site (http://gaw.kishou.go.jp/wdcgg.html).

In this Summary, the symbols ppm, ppb, ppt are used as the units of mixing ratio for traditional convenience. They correspond to the SI units μmol/mol, nmol/mol, pmol/mol in respectively.

The CO_2 mixing ratio can be seen on both a seasonal scale and a long-term scale. Annual growth rates (yearly differences in mixing ratio) are derived from the deseasonalised long-term trend.

The analytical results are summarized below for each greenhouse and related gas:

1. Carbon Dioxide (CO_2)

The level of Carbon Dioxide (CO_2), which of all the greenhouse gases contributes most to global warming, has been increasing since the pre-industrial period. Global mean mixing ratio has reached a new high in 2004 at 377.1 ppm, which increased by 1.8 ppm during the last year. This mixing ratio corresponds to 135% of the pre-industrial level. Mixing ratios peak in northern high and mid-latitudes, suggesting strong net sources in these areas.

The global growth rate varies significantly interannually and was 1.9 ppm/year on average for the latest 10 years (1994-2004). The high growth rates in 1987/1988, 1997/1998 and 2002/2003, which exceeded 2 ppm/year, resulted from the warm events related to El Niño-Southern Oscillation (ENSO). The anomalously strong El Niño event in 1997/1998 brought about worldwide high increases in 1998. The exceptionally low growth rates in 1992, including negative values for northern high and mid-latitudes, were caused by low global temperatures following the eruption of Mt. Pinatubo in 1991.

Amplitudes of the seasonal cycle are clearly large in northern high and mid-latitudes and small in the Southern Hemisphere. The northern seasonal cycle mainly reflects seasonal variation in the absorption/emission in the biosphere there, while the southern cycle reflects oceanic variations and biomass burning in addition to the influence of the biosphere. In southern low latitudes, an annual cycle cannot be seen clearly but a semiannual cycle can. This is probably due to two opposing factors — the direct influence of sources and sinks there and the propagation of the out-of-phase seasonal variation from the Northern Hemisphere.

2. Methane (CH_4)

CH_4 is the second most significant greenhouse gas, and its level has been increasing since the beginning of the 19th Century. Global mean mixing ratios reflect an annual increase, and the annual averaged mixing ratio was 1783 ppb in 2004, which was the same as that in 2003. This level was the highest mixing ratio since the beginning of the worldwide observation. The mixing ratio corresponds to 255% of that in the pre-industrial level.

The annual mixing ratios peak in the northernmost latitudes and fall toward the southernmost latitudes, suggesting significant net sources in northern latitudes.

The global growth rate was 11 ppb/year on average for the period 1984-1990, but the rates decreased markedly from the 1980s to the 1990s. The global growth rate for the latest 10 years (1994-2004) was 3.7 ppb/year. Growth rates decreased significantly in some years, including 1992, when negative values were recorded in northern high latitudes, and 1996, when growth almost stopped in many regions. However, both hemispheres experienced high growth rates in 1998, caused by an exceptionally high global mean temperature. The global growth rates decreased to almost zero in 2000-2001, but the growth rates increased again with the occurrence of the 2002 /2003 El-Niño event.

Monthly mean mixing ratios have a seasonal variation with high mixing ratios in winter and low mixing ratios in summer. Unlike CO_2, amplitudes of the seasonal cycle are large for CH_4, not only in the Northern Hemisphere but also in southern high and mid-latitudes. In southern low latitudes, a distinct semi-annual component with a secondary maximum in boreal winter overlays the annual component. This is attributed to the large-scale transportation of CH_4 from the Northern Hemisphere.

3. Nitrous Oxide (N_2O)

Nitrous oxide (N_2O) is an important greenhouse gas, and its level is increasing on a global scale. Data for N_2O submitted to the WDCGG show that mixing ratios are increasing in both hemispheres. Global mean mixing ratio has reached a new high in 2004 at

318.6 ppb, which increased by 0.7 ppb during the last year. The mean growth rate of the global mean mixing ratio during the latest 10 years (1994 - 2004) was 0.8 ppb/year. This mixing ratio corresponds to 118% of the pre-industrial level.

4. Halocarbons

Halocarbons, most of which are anthropogenic, are effective greenhouse gases and some also act as ozone-depleting compounds. Levels of some halocarbons (CFCs, etc.) increased in the 1970s and 1980s, but have now almost ceased increasing as a result of regulation of production and emission under the Montreal Protocol on Substances that Deplete the Ozone Layer and its Adjustments and Amendments.

Mixing ratios of CFC-11 peaked around 1992 and then started decreasing. CFC-12 increased slowly, but growth has almost stopped in recent times. CFC-113 growth stopped in the early 1990s, and over the last decade has shown a trend of decreasing slightly. Mixing ratios of HCFC-141b and HCFC-142b are increasing linearly. Mixing ratios of CCl_4 are decreasing slowly. Mixing ratios of CH_3CCl_3 peaked around 1992 and thereafter clearly started to decrease.

The mixing ratios of HCFCs, which are the industrial replacements of CFCs, are increasing at rapid rates, although their mixing ratios are small.

5. Surface Ozone (O_3)

Ozone (O_3) plays important roles in the atmospheric environment through radiative and chemical processes. It absorbs UV radiation in the stratosphere, making a temperature profile, and circulates the atmosphere with its absorbed energy. It also absorbs IR radiation, and is thus one of the greenhouse gases.

Variation in the mixing ratio of O_3 near the surface, so-called surface ozone, reflects various processes there. While some of the O_3 in the troposphere comes from the stratosphere, the rest is chemically produced in the troposphere through oxidation of CO or hydrocarbons in the presence of rich NO_x.

Many stations at various locations measure the mixing ratio of surface ozone. As the seasonal and interannual variations are relatively large, it is difficult to identify a global long-term trend.

6. Carbon Monoxide (CO)

Carbon monoxide (CO) is not a greenhouse gas, but brings influences the mixing ratios of greenhouse gases by affecting hydroxyl radicals (OH). Its mixing ratio in northern high latitudes has been increasing since the mid-19th Century. The mean global mixing ratio was 94 ppb in 2004. The mixing ratio is high in the Northern Hemisphere and low in the Southern Hemisphere, suggesting substantial anthropogenic emissions in the Northern Hemisphere.

Although the global mixing ratio of CO was increasing before the mid-1980s, the growth stopped or the mixing ratio subsequently decreased after then (WMO, 1999a). There was large fluctuation in the growth rate, however, with high positive rates followed by high negative rates in northern latitudes and southern low latitudes from 1997 to 1999. The growth rates in the Northern Hemisphere increased again in 2002.

Monthly mean mixing ratios show a seasonal variation with large fluctuations in the Northern Hemisphere and small fluctuations in the Southern Hemisphere. This seasonal cycle is driven by industrial emissions, biomass burning, large-scale transportation, and variations in OH mixing ratio which acts as a sink.

7. Nitrogen Monoxide (NO) and Nitrogen Dioxide (NO_2)

Nitrogen oxides (NO_x, i.e., NO and NO_2) are not greenhouse gases, but influence mixing ratios of important greenhouse gases by affecting OH. In the presence of NO_x, CO and hydrocarbons are oxidized to produce ozone (O_3), which affects the Earth's radiative balance as a greenhouse gas and the oxidization capacity of the atmosphere by reproducing OH.

Most of the stations reporting NO_x data to the WDCGG are located in Europe. NO_x has large temporal and geographic variability, and it is difficult to identify a long-term trend. In Europe, NO_2 mixing ratios are generally higher in southern regions than in northern regions.

8. Sulphur Dioxide (SO_2)

Sulphur dioxide (SO_2) is not a greenhouse gas but a precursor of atmospheric sulphate (H_2SO_4) aerosol. Sulphate aerosol is produced by SO_2 oxidation through photochemical gas-to-particle conversion. SO_2 has also been a major source of acid rain and deposition throughout industrial times.

Most of the stations reporting SO_2 data to the WDCGG are located in Europe. Generally, in Europe, SO_2 mixing ratios are higher in southern regions than in northern regions.

1. Introduction

Human activities have been shown to have major impacts on the global environment. Since the beginning of the industrial revolution, mankind has increasingly made use of land, water, minerals and other natural resources, and future population and economy growths will result in further increases in our impact on the environment. As the global climate, biogeochemical processes and natural ecosystems are closely interlinked, changes in any one of these systems may affect the others and be detrimental to humans and other organisms. Emissions of man-made gaseous and particulate matter alter the energy balance of the atmosphere, and consequently affect interactions between the atmosphere, hydrosphere, and biosphere. Nevertheless, we do not yet have a sufficient understanding of either the chemical processes that occur within the atmosphere or the interrelationships between the atmosphere, the hydrosphere, and the biosphere. This lack of understanding regarding the chemical processes of the atmosphere and the oceans is due mainly to a paucity of observation data.

The World Meteorological Organization (WMO) launched the Global Atmosphere Watch (GAW) Programme in 1989 to promote systematic and reliable observation of the global environment, including greenhouse gases (CO_2, CH_4, CFCs, N_2O, *etc.*) and other related gases (*e.g.*, CO, NO_x, and SO_2) in the atmosphere. In October 1990, the WMO established the World Data Centre for Greenhouse Gases (WDCGG) at the Japan Meteorological Agency (JMA) in Tokyo as one of the GAW World Central Facilities to collect, archive, and distribute data regarding greenhouse and related gases in the atmosphere and oceans. In August 2002, the WDCGG took over the role of the Data Centre for Surface Ozone from the Norwegian Institute for Air Research (NILU) and began to collect surface ozone data from a number of observation sites throughout the world participating in GAW and other scientific monitoring programmes (Appendix: LIST OF OBSERVING STATIONS).

With regard to issues involving global warming, the Kyoto Protocol, in which quantified emission limitations and reductions were agreed upon based on the United Nations Framework Convention on Climate Change, came into force in February 2005. The WMO begins annual publication of the WMO Greenhouse Gas Bulletin in March 2006 that briefly summarizes the state of greenhouse gases in the atmosphere. The WDCGG is needed for swifter and smoother exchange of such data.

Since its establishment, the WDCGG has provided its users with data and other information through its regular publications: *Data Report*, *Data Catalogue*, *Data Summary,* and *CD-ROM* (Appendix: LIST OF WMO WDCGG PUBLICATIONS). All data and information are now available on the WDCGG web site, which aims to improve accessibility to data, information, and products in line with the Strategy of the Implementation of the Global Atmosphere Watch Programme (2001-2007) published in June 2001 and its Addendum for the Period 2005-2007 (WMO, 2001; WMO, 2004).

This strategy also requests that GAW facilities, including World Data Centres, build a data bank that can provide good analyses in cooperation with the scientific research community. To meet this request, the WDCGG has increased its analytical activities, and made the contents of the annual *Data Summary* more comprehensive. Global and integrated analyses used to monitor global changes in mixing ratios of greenhouse gases have become important tasks of the WDCGG. Other important tasks include the revision and improvement of the contents of the *Data Summary* based on comments from data contributors and scientists, and to provide scientists and policy makers with more advanced analytical information. The WDCGG welcomes comments and suggestions regarding the *Data Summary* and its other publications. It is expected that the analytical information presented here will not only stimulate the use of data regarding greenhouse and other gases, but will also increase appreciation of the value of the GAW program.

The WDCGG thanks all the data contributors, including those involved in measurement at the numerous sites worldwide, for their efforts in maintaining the observation programme and for their continuous provision of data.

Mailing address:

WMO World Data Centre for Greenhouse Gases (WDCGG)
c/o Japan Meteorological Agency
1-3-4, Otemachi, Chiyoda-ku, Tokyo 100-8122, Japan

E-mail: wdcgg@hq.kishou.go.jp
Telephone: +81-3-3287-3439
Facsimile: +81-3-3211-4640
Web Site: http://gaw.kishou.go.jp/wdcgg.html

Note:

The WDCGG requests acknowledgement from data users by the appropriate citation of the contributors and data sources when they use any data or information provided by the WDCGG. Data users should refer to the GAW Station Information System (GAWSIS) at the GAW web site (http://www.wmo.ch/web/arep/gaw/gaw_home.html) or the WDCGG web site for details on the GAW Country Contacts, what measurements are being made, and the investigators responsible. The information at the GAWSIS and the World Data Centres is updated in cooperation with the WMO Secretariat.

2. Analysis

The WDCGG collects, archives and distributes observation data regarding mixing ratios of greenhouse gases, and also provides analytical results on the collected data.

This publication presents long-term trends and seasonal variations in mixing ratios of CO_2, CH_4 and CO derived for the global, hemispheric and zonal means. For N_2O, global and hemispheric long-term trends are presented. For halocarbons, surface O_3, NO_x and SO_2, only time series of monthly mean mixing ratios are presented because only a small number of sites have submitted observation data.

In this Summary, the symbols of ppm, ppb, and ppt are used as units of mixing ratio for traditional convenience. They correspond to the SI units μmol/mol, nmol/mol, and pmol/mol, respectively.

The following sections explain the methods used for analysis for CO_2, CH_4, CO and N_2O. Refer to the respective chapters for the other parameters.

2-1. Site selection for global, hemispheric and zonal mean mixing ratios

For CO_2, global, hemispheric and zonal mean statistics are derived from the selected sites whose standard gases have traceability to the WMO standard gas that is hosted by the Central Calibration Laboratory (CCL). The WMO standard for CH_4 was established in 2005, so that the standard has not prevailed yet. Thus, for CH_4, the statistics are derived from the selected sites that employ the WMO standard gas or employ standard gases whose difference from the WMO standard gas has been scientifically determined. For N_2O, the statistics are also derived from the selected sites that employ the WMO standard or employ standard gases whose difference from the WMO standard has been scientifically determined.

As ground-based sites observe air at a lower boundary layer, the measured mixing ratios of gases, such as CO_2, CH_4 and CO, which have sources and/or sinks on the Earth's surface, may show localised characteristics in a lower boundary layer depending on weather conditions, *etc.*

These data incorporate very useful information for investigating the power of local sources and sinks. However, for global scale analysis, it is necessary to use data that can be considered as representative mixing ratios averaged over a reasonable geographical area and in a whole boundary layer, *i.e.*, background data. Background data can usually be extracted from the total data through appropriate selection criteria, which are chosen for each site.

In this study, observation sites that were considered to offer data appropriate for the purpose were selected. In some cases, *e.g.*, where the observatory was in a marine area, even data without any selection criteria may be regarded as background data. In contrast, it could be difficult to select background data in other cases where the observatory was located in woodland or near a densely populated city.

Finally, site selection was performed objectively as described below, based on data in a reasonable scattered range of the total data in the same latitudinal zone. The latitudinal distribution of the annual mean mixing ratios normalised with respect to the South Pole, which were calculated from the monthly mean mixing ratios, was fitted with the LOESS model curve (Cleveland *et al.*, 1988). Sites with mixing ratios lying more than $\pm 3\sigma$ from this curve were rejected and this process was iterated until all of the remaining sites lay within $\pm 3\sigma$ from the fitted curve. The selected sites are listed in Plate 3.1 for CO_2, Plate 4.1 for CH_4, Plate 5.1 for N_2O and Plate 8.1 for CO with asterisks. List of the selected sites for CO_2, CH_4 and N_2O is available on the WDCGG web site (http://gaw.kishou.go.jp/wdcgg.html).

2-2. Trend analysis

The time series of greenhouse gas mixing ratios, which is often produced by removing local effects with very short-term variations, represents integration of variations on different time scales. The two major components of variation in CO_2 mixing ratio are seasonal variations and long-term trends. Many researchers have attempted to decompose observation data into these two components by objective curve fitting (Keeling *et al.*, 1989), digital filtering (Thoning *et al.*, 1989; Nakazawa *et al.*, 1991), or both (Conway *et al.*, 1994; Dlugokencky *et al.*, 1994).

Trend analysis approximating variations in the sum of seasonal variations by Fourier harmonics and long-term trends by low-pass filtering with a cut-off frequency of 0.48 cycles/year was performed for each selected site. Refer to the previous Summary (WDCGG No. 22) for details.

2-3. Estimation of value for periods without data for zonal mean calculation

The number of sites used for trend analysis outlined above varied during the analysis period. Moreover, data were frequently excluded due to pauses in the observation. When the calculations are performed without considering changes in the number of the sites used in the analysis, the values, such as the zonal growth rate, fluctuate with the change in the number of available sites. These fluctuations were particularly evident in the early period when few sites were available.

However, if we select only those sites for which data

are available throughout the whole analysis period, the data from many newly established sites will not be reflected in the analysis. To use as many sites as possible and to avoid gaps accompanying changes in the number of sites, the estimated values for the periods for which no data were included in the zonal mean calculations. The values were estimated by interpolation and extrapolation as follows.

First, sites requiring interpolation were selected. A provisional seasonal variation was calculated from the longest consecutive data set for each site with all the same Lanczos filters (Duchon, 1979) as described in the previous Summary. Then, linear interpolation was performed for the data from which the provisional seasonal variation was subtracted. The complete variation was then retrieved by adding the provisional seasonal variation.

Next, the sites requiring extrapolation were selected. The provisional long-term trend and the seasonal variation were calculated from the interpolated data set with the same filter. Extrapolation was then performed for the long-term trend as its growth rate traces the zonal mean growth rate calculated from those of the other sites in the same latitudinal zone. Subsequently, the complete variation was retrieved by adding the site's own provisional seasonal variation. Here, each zone was created every 30° of latitude.

The zonal mean mixing ratios were calculated from the continuous data set, derived in the above procedure, by determining the arithmetic mean for the sites included in each latitudinal zone for every 20° or 30°. The zonal mean in the early stage of the analysis period may have lower accuracy than that in the latest stage. Although the data sets were partly estimated, the completeness of data was assumed to be advantageous for trend analysis of the zonal mean.

2-4. Calculation of global and hemispheric means

Global and hemispheric means were calculated by averaging the zonal means, taking into consideration the area ratio of each latitudinal zone.

The deseasonalised long-term trend and growth rate for the globe, both hemispheres and each latitudinal zone were calculated again with the filter from the global, hemispheric and zonal means. To derive the trend for the whole period, we assumed provisional data extending from both ends followed the linear trend for the whole period. Therefore, analyzed trends at both ends may depart from the actual values.

Here, we summarise the characteristics of global, hemispheric and zonal mean mixing ratios by presenting the time series of monthly mean mixing ratios, deseasonalised long-term trends, annual growth rates and the averaged seasonal cycle.

3.
CARBON DIOXIDE
(CO_2)

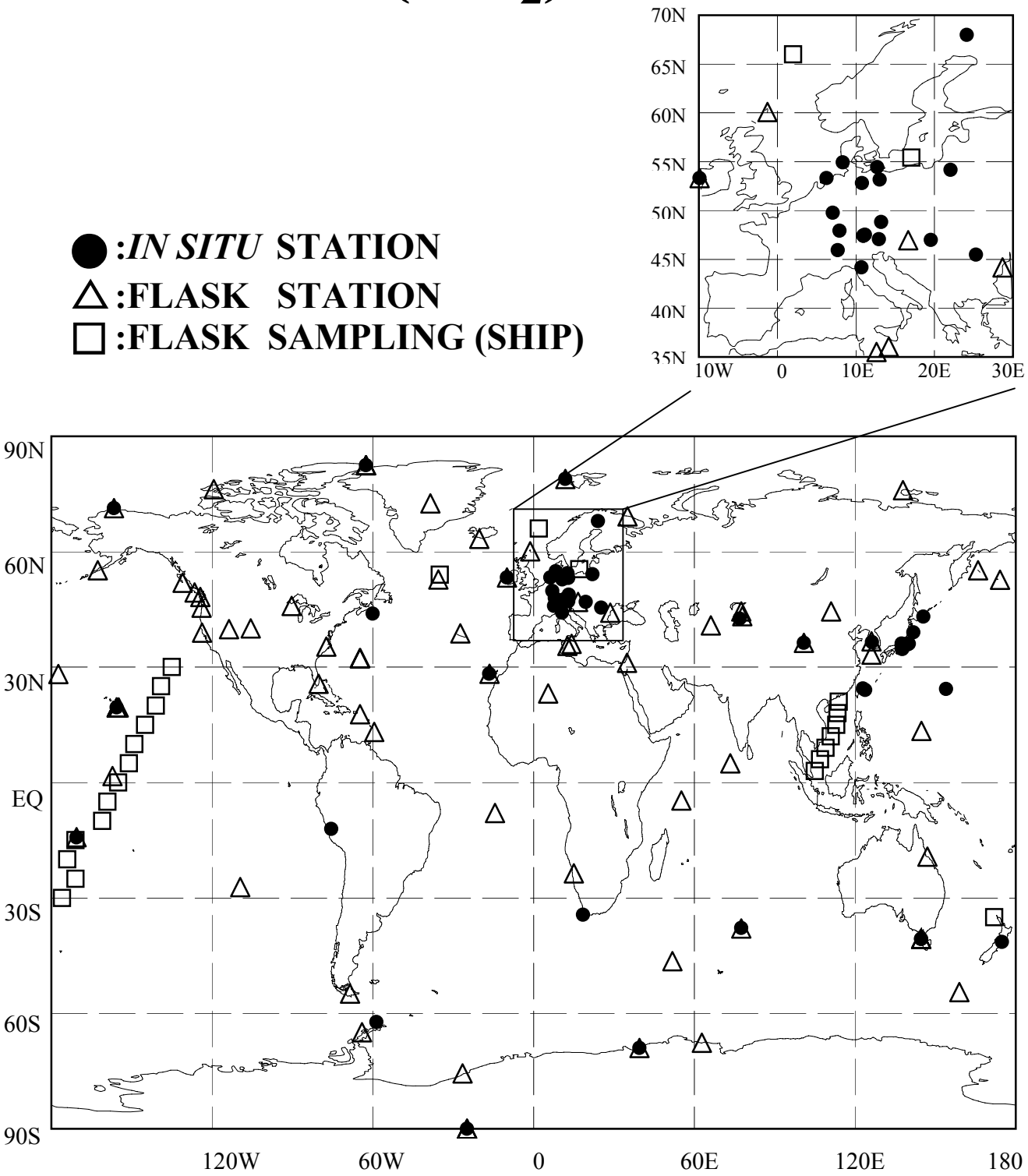

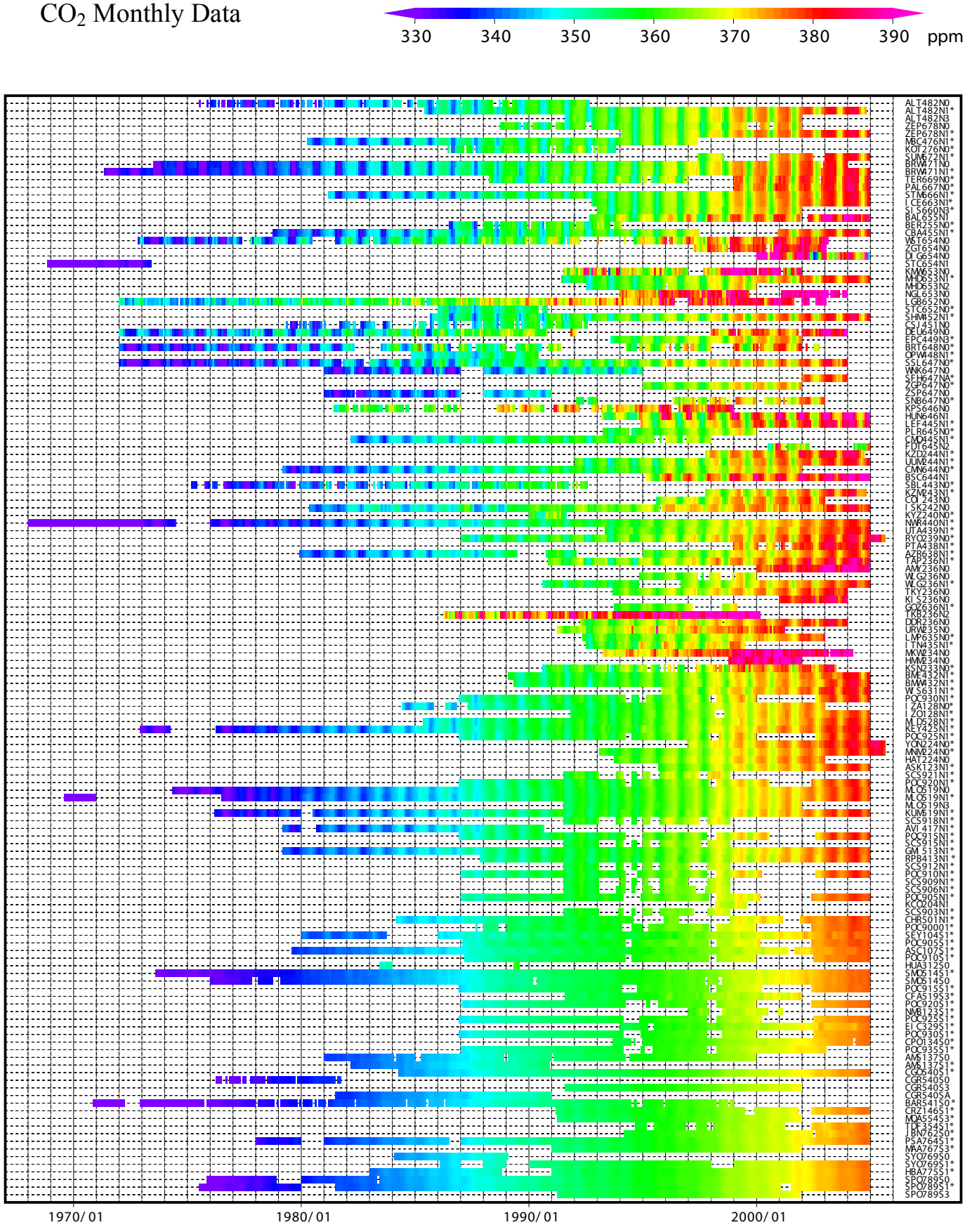

Plate 3.1 Monthly mean CO_2 mixing ratios for all sites reported to the WDCGG illustrated in colors that change with the mixing ratio. The sites are set from north to south. Though some stations reported data at two or three different altitudes, only data at the lowest altitudes are illustrated. The monthly value at the site which has submitted only original (hourly) data before selection is calculated by the WDCGG as an arithmetic mean, and may become high for reflecting the mixing ratio influenced in plant breathing at nighttime in the lower boundary layer. Site index with an asterisk shows the site used in the analysis shown in Plate 3.2. (see Chapter 2)

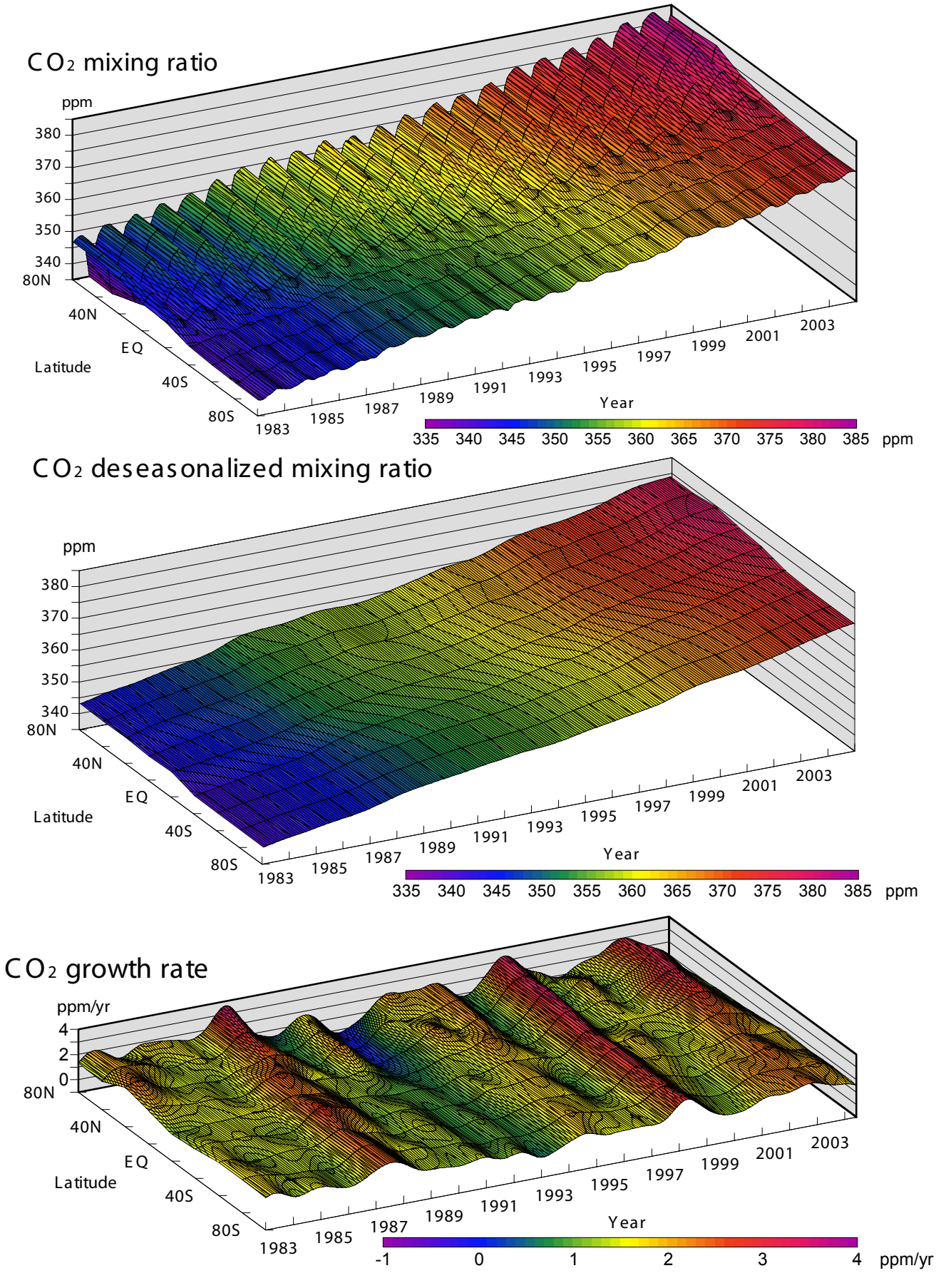

Plate 3.2 Variation of zonally averaged monthly mean CO_2 mixing ratios (top), deseasonalized mixing ratios (middle), and growth rates (buttom). Zonally averaged mixing ratios are calculated for each 20° zone. Deseasonalized mixing ratios and growth rates are derived as described in Chapter 2.

3. Carbon Dioxide (CO_2)

Basic information on CO_2 with regard to environmental issues

Carbon dioxide (CO_2) is a significant greenhouse gas that has strong absorption bands in the infrared region and is the largest contributor to the greenhouse effect. CO_2 contributed to 60% of the radiative forcing due to the increase in well-mixed greenhouse gases after the industrial revolution (IPCC, 2001).

The balance between emission and absorption at the surface of the earth or ocean determines the mixing ratio of CO_2 in the atmosphere. About 750 Gigatonnes of carbon is stored in the atmosphere as CO_2. This carbon in atmospheric CO_2 is exchanged with two other large reservoirs, the terrestrial biosphere and the ocean. The CO_2 is exchanged between the atmosphere and terrestrial biosphere mainly through absorption by photosynthesis and emission from plant respiration and decomposition of organic soils. These biogenic activities vary with season, resulting in large seasonal variations in CO_2 levels. Transport of CO_2 from the atmosphere to the ocean or in the opposite direction occurs according to the differences in CO_2 mixing ratio, which varies with season and sea region.

The atmospheric CO_2 mixing ratio has never exceeded the current level during the past 420,000 years (IPCC, 2001). Based on the results of ice core studies, the mixing ratio of atmospheric carbon dioxide in the pre-industrial level was about 280 ppm (IPCC, 2001). The levels of anthropogenic emission of CO_2 have been increasing from the beginning of the industrial era, and the emitted CO_2 has been distributed into the atmosphere, oceans and terrestrial biosphere, which serve as reservoirs of CO_2 in the global carbon cycle. However, the whole global carbon cycle, which is comprised mainly of CO_2, has not yet been revealed. About half of this anthropogenic CO_2 emission has increased CO_2 in the atmosphere and the rest has been removed by sinks, including the terrestrial biosphere and ocean uptake. However, the amount of removal depends strongly on the year (Figure 3.1).

Carbon isotopic studies have demonstrated the importance of the terrestrial biosphere and oceans as sources and sinks (Francey *et al.*, 1995; Keeling *et al.*, 1995; and Nakazawa *et al.*, 1993, 1997a). On the other hand, the atmospheric O_2 content is dependent mainly on O_2 removal by burning of fossil fuels, and O_2 release from the terrestrial biosphere. Therefore, the uptake of carbon by the terrestrial biosphere and the ocean can be evaluated from O_2 (O_2/N_2) measurements combined with CO_2 measurements (IPCC, 2001). IPCC (2001) showed that the ocean and the terrestrial biosphere respectively absorbed about 27% and 22% of CO_2 emitted from the burning of fossil fuel in the 1990s, while the remaining 51% contributed to the annual increase in CO_2 level in the atmosphere.

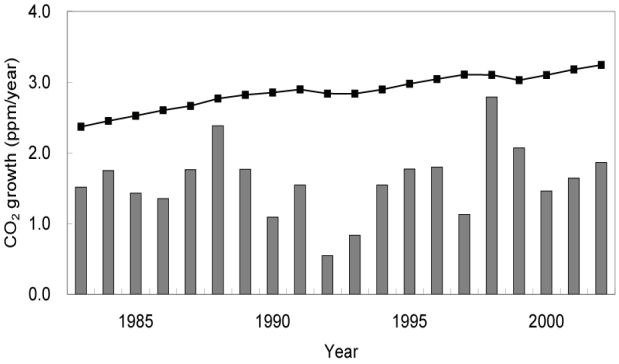

Fig. 3.1 Time series of annual mean CO_2 growth rates in the atmosphere calculated from observation data (column) and from anthropogenic emission data (thin line with dots). CO_2 emissions were calculated by CDIAC based on the United Nations Energy Statistics, and the observed growth rate was calculated by the WDCGG. Note that observational CO_2 abundance in the atmosphere is expressed by mixing ratio with respect to dry air, but CO_2 mixing ratio from anthropogenic emission is calculated based on the atmosphere including water vapor that is usually less than 1% in mixing ratio.

Large amounts of CO_2 are exchanged among these reservoirs, and the global carbon cycle is coupled with the climate system on seasonal, interannual and decadal time scales. Accurate understanding of the global carbon cycle is essential for the estimation of future CO_2 mixing ratios in the atmosphere.

The map at the beginning of this chapter shows observation sites that submitted CO_2 mixing ratio data to the WDCGG by December 2004. These sites include *in situ* stations performing continuous measurement as well as flask-sampling stations, such as those in the NOAA/GMD network. In addition to such fixed stations, mobile stations on ships and aircraft, and other stations that measure event data also report their data to the WDCGG (Appendix: LIST OF OBSERVATION STATIONS).

Annual variations in CO_2 in the atmosphere

The monthly mean CO_2 data from all the stations that submitted to the WDCGG are shown in Plate 3.1. In this plate, mixing ratio levels are illustrated in different colours. Global, hemispheric and zonal mean background mixing rations were analysed based on selected stations (see the caption to Plate 3.1). The three-dimensional representations of latitudinal distribution of atmospheric CO_2 mixing ratio, deseasonalized mixing ratios and the growth rate

(yearly difference of mixing ratio) are shown in Plate 3.2. These three-dimensional representations (CO_2 carpets) indicate that the amplitudes of seasonal mixing ratio variations are large in the northern mid-latitudes, but the seasonal variation is indistinct in the Southern Hemisphere; the increases in mixing ratio occur in the Northern Hemisphere prior to the Southern Hemisphere, and propagate to the Southern Hemisphere, and the inter-annual variation of growth rates occurs largely in the Northern Hemisphere.

Figure 3.2 shows the global monthly mean mixing ratios with the long-term trends and growth rate from 1983 to 2004. The global average mixing ratio has reached a new high in 2004 at 377.1 ppm, which increased by 1.8 ppm during the last year. This mixing ratio corresponds to 135% of the pre-industrial level.

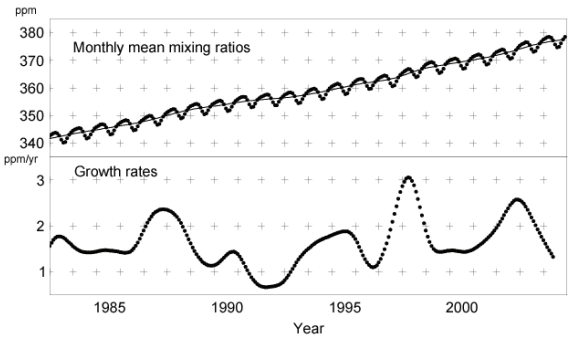

Fig. 3.2 Monthly mean mixing ratios (thick line and dots) and deseasonalized long-term trends (thin line) (top), and growth rate (bottom) from 1983 to 2004 for the globe.

The mean global growth rate during the latest 10 years (1994–2004) was 1.9 ppm/year. The global growth rate of CO_2 shows a large inter-annual variation. During the above period, the maximum and minimum global growth rates were 3.1 ppm/year in April 1998 and 0.7 ppm/year in March 1992, respectively. High growth rates exceeding 2 ppm/year were seen in 1987/1988, 1997/1998 and 2002/2003.

Figure 3.3 shows the monthly mean mixing ratios and their long-term trends from 1983 to 2004 for each 30° latitudinal zone. Long-term increases in both hemispheres and seasonal variations in the Northern Hemisphere are clearly observed.

As shown in Figure 3.4, the growth rates fluctuated between –0.3 and 3.5 ppm/year, and variability in the growth rate was relatively large in northern high latitudes. All growth rates were high in 1987/1988, 1997/1998 and. 2002/2003. On the other hand, negative values were recorded in northern high latitudes in 1992.

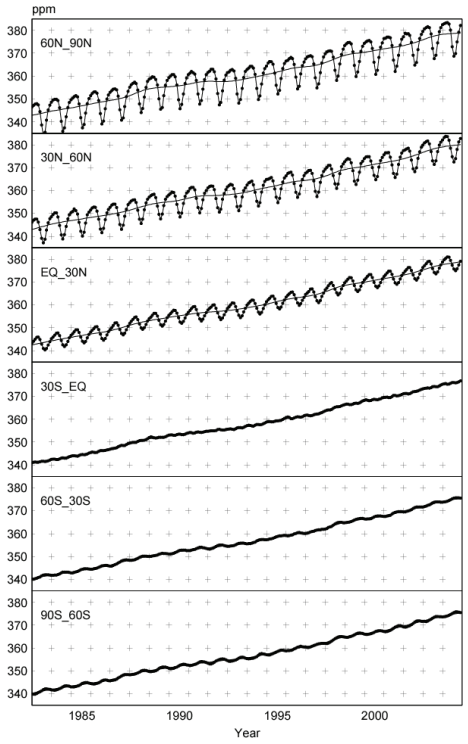

Fig. 3.3 Monthly mean mixing ratios (thick lines and dots) and deseasonalized long-term trends (thin lines) from 1983 to 2004 for each 30° latitudinal zone.

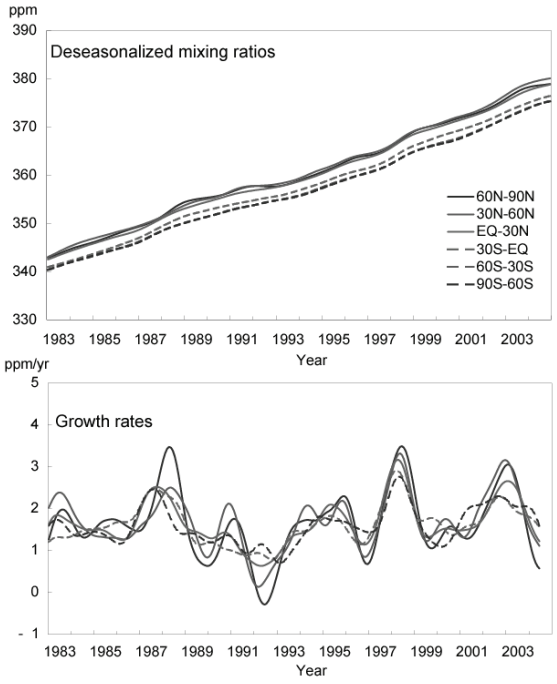

Fig. 3.4 Long-term trends (top) and growth rates (bottom) for each 30° latitudinal zone.

Changes in growth rate are also known to be associated with El Niño-Southern Oscillation (ENSO). El Niño events occurred in 1982/1983, 1986-1988,

1991/1992, 1997/1998 and 2002/2003, and with the exception of 1992, growth rates were high in these years. In addition to those at the surface, the CO_2 growth rates at high altitudes (8-13 km) over the Pacific Ocean are also known to have a similar relationship with ENSO (Matsueda *et al.*, 2002). Ordinarily, there is an up-welling area with CO_2-rich ocean water in the eastern equatorial Pacific, and CO_2 is emitted from the ocean. However, El Niño events suppress this up-welling, which reduces CO_2 emission from the ocean. On the other hand, El Niño events result in high temperature anomalies in many areas globally, particularly in the Tropics, which increase CO_2 emission from the terrestrial biosphere by the enhanced respiration of plants and decomposition of organic matter in the soil (Keeling *et al.*, 1995). Anomalously low precipitation, particularly in the Tropics, also enhances this effect by suppressing plant photosynthesis. These oceanic and terrestrial processes have opposite effects during El Niño events. However, Dettinger and Ghil (1998) suggested that the former effect was limited to the eastern equatorial Pacific, while the latter had a global scale. Thus, the CO_2 response, which is almost synchronous with El Niño events, is due to terrestrial biosphere changes associated with temperature variations on a global scale.

Carbon isotope (^{13}C) studies have also shown that atmospheric CO_2 variations accompanying El Niño events are brought about by the flux between the terrestrial biosphere and the atmosphere, rather than between the ocean and the atmosphere (Keeling *et al.*, 1989; Nakazawa *et al.*, 1993; Morimoto *et al.*, 2000). A strong El Niño event during 1997/1998, which was one of the most severe ENSO events in the 20th Century, brought about high temperatures and low precipitation levels on a global scale during this period (WMO, 1999b), resulting in frequent wildfires and drought in Southeast Asia. Such meteorological conditions perturbed the global carbon cycle, and are considered to intensify CO_2 emission from the terrestrial biosphere. However, an exceptionally low CO_2 growth rate occurred even during the El Niño event in 1991/1992.

The injection of 14-20 Mt of SO_2 aerosols into the stratosphere by the Mt. Pinatubo eruption in June 1991, which affected the radiation budget and atmospheric circulation (Hansen *et al.*, 1992; Stenchikov *et al.*, 2002), resulted in a drop in the global temperature. The reduced CO_2 emission from the terrestrial respiration and from decomposition of organic matter in the soil due to anomalous low temperatures (Conway *et al.*, 1994; Lambert *et al.*, 1995; Rayner *et al.*, 1999), and enhanced CO_2 absorption by intensive photosynthesis due to the increase in diffuse radiation (Gu *et al.*, 2003) contributed to the low CO_2 growth rate despite the El Niño event (Angert *et al.*, 2004).

Figure 3.5 shows a time series of CO_2 growth rates in the tropical area (< ±30° from 1983 to 2004), the SOI (Southern Oscillation Index), the SST anomaly in the eastern equatorial Pacific (4°N-4°S, 150°W-90°W) and the temperature anomaly on land in the Tropics calculated from NCEP (National Centers for Environmental Prediction) reanalysis data. In the figure, the SOI, the SST anomaly and the temperature anomaly are processed as a five-month running mean to display the seasonal variation. The growth rate in the Tropics showed good correspondence with the SOI and SST anomalies with a time lag except in 1992. In addition, the growth rate in the Tropics also showed good correspondence with the temperature anomaly on land in the Tropics, including 1992. These results suggest that the growth rate is related to ENSO events, but that temperature anomalies on tropical land have the closest relationship with CO_2 growth rate in the Tropics. These observations suggest a strong influence of the tropical biosphere on tropical CO_2 mixing ratio.

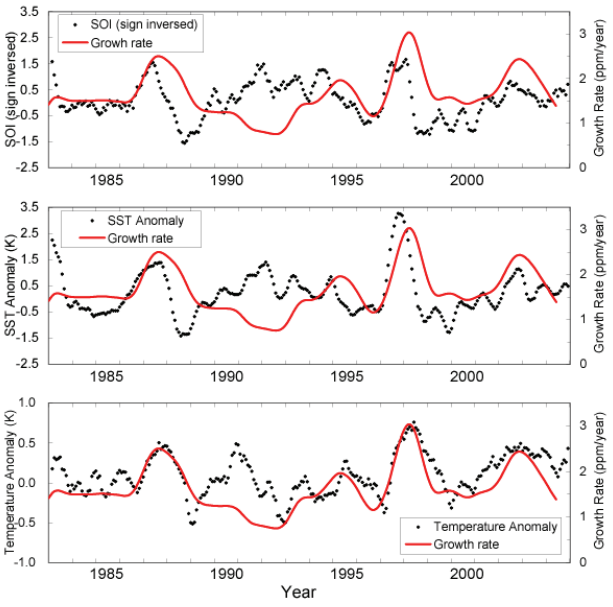

Fig. 3.5 Time series of growth rates in the Tropics (30°N-30°S) and a comparison with the Southern Oscillation Index inversed sign (top), SST anomaly in the eastern equatorial Pacific (4°N-4°S, 150°W-90°W) (middle) and temperature anomaly on land in the Tropics calculated from NCEP reanalysis data (bottom). The solid lines show the growth rates, and the dots show each element (5-month running mean).

Seasonal cycle of CO_2 in the atmosphere

Figure 3.6 shows average seasonal cycles for each 30° latitudinal zone from which the long-term trends were subtracted.

Amplitudes of seasonal cycles are clearly large in northern high and mid-latitudes and small in the

Southern Hemisphere. Ocean uptake (Ramonet *et al.*, 1996) and biomass burning (Wittenberg *et al.*, 1998) are thought to influence the seasonal variation. However, these large seasonal cycles in the Northern Hemisphere are characterized by rapid decreases from June to August and large returns from September to December. They are the result of the activities of the terrestrial biosphere, *i.e.*, CO_2 absorption by photosynthesis, emission by respiration of vegetation, and decomposition of organic matter by microbes in the soil (*e.g.*, Nakazawa *et al.*, 1997b).

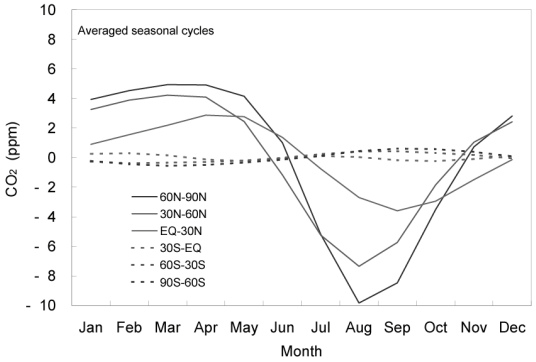

Fig. 3.6 Average seasonal cycles for each 30° latitudinal zone from which the long-term trends were subtracted.

In northern high and low latitudes, the occurrences of their maximum mixing ratios are delayed by one or two months. Minimum mixing ratios appeared in August in northern high and mid-latitudes and in September in northern low latitudes. The peak in low latitudes is delayed because the seasonal variation in high latitudes takes some time to reach the low latitudes (Tanaka *et al.*, 1987), and the seasonal cycle of terrestrial biosphere activity at low latitudes is delayed against that in the mid-latitudes due to the courses of the wet and dry seasons (Nemry *et al.*, 1996).

In the Southern Hemisphere, the seasonal variations showed small amplitudes with a half-year delay due to small amounts of net emission and absorption by the terrestrial biosphere. The seasonal variations of northern mid-latitudes and southern mid-latitudes seemed to be superimposed in the southern low latitudes (0-30°S), while the amplitude was small, suggesting that the large seasonal variation in the Northern Hemisphere influences the Southern Hemisphere. The direct influence of sources and sinks in the Southern Hemisphere might be partially cancelled by propagation of the out-of-phase seasonal variation from the Northern Hemisphere.

Figure 3.7 shows the latitudinal distributions of CO_2 mixing ratios in January, April, July and October in 2004. Latitudinal gradients around 30°N were positive in January and April, and negative in July, corresponding to the large seasonal cycle in northern, mid- and high latitudes.

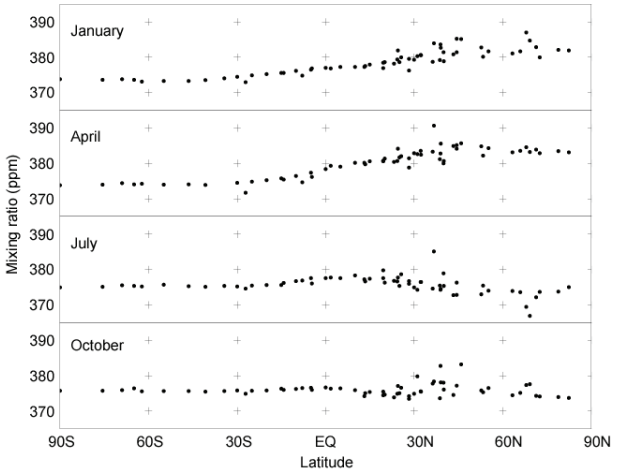

Fig. 3.7 Latitudinal distributions of monthly mean mixing ratios in January, April, July and October 2004.

Annual variation of CO_2 in the upper atmosphere

The Meteorological Research Institute in Japan Meteorological Agency has carried out aircraft-based measurements of trace gases, such as CO_2, at altitudes of 8-13 km over the western Pacific using a commercial flight between Japan and Australia in cooperation with the Japan Airlines Foundation, the Ministry of Land, Infrastructure and Transport, and Japan Airlines since 1993. The observation data are submitted to the WDCGG every year. Fig. 3.8 shows the time series of the atmospheric CO_2 mixing ratios, Deseasonalized mixing ratios and the growth rates in the upper air obtained by these measurements. We used continuous data obtained by linear interpolation. The trend analysis method used was the same as that described in Chapter 2. The CO_2 mixing ratios increased with seasonal variations, similarly to those on the surface. The seasonal variations observed over the Northern Hemisphere also reflected those on the surface, but the amplitudes were smaller.

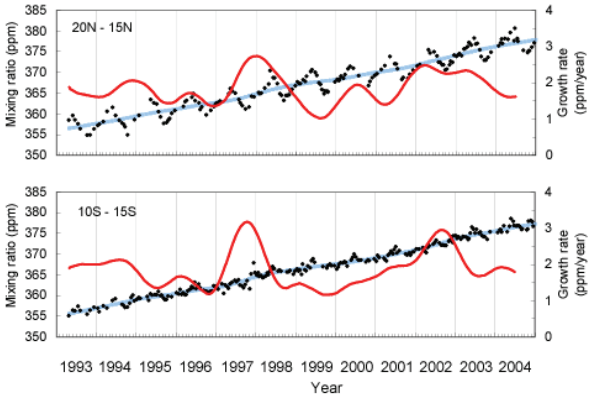

Fig. 3.8 Time series of CO_2 mixing ratios (dots), deseasonalized mixing ratios (dashed lines), and growth rates (solid lines) observed at latitudinal zones of 15-20°N and 10-15°S at altitudes of 8–13 km over the western Pacific.

4.
METHANE
(CH_4)

●:*IN SITU* STATION
△:FLASK STATION
□:FLASK SAMPLING (SHIP)

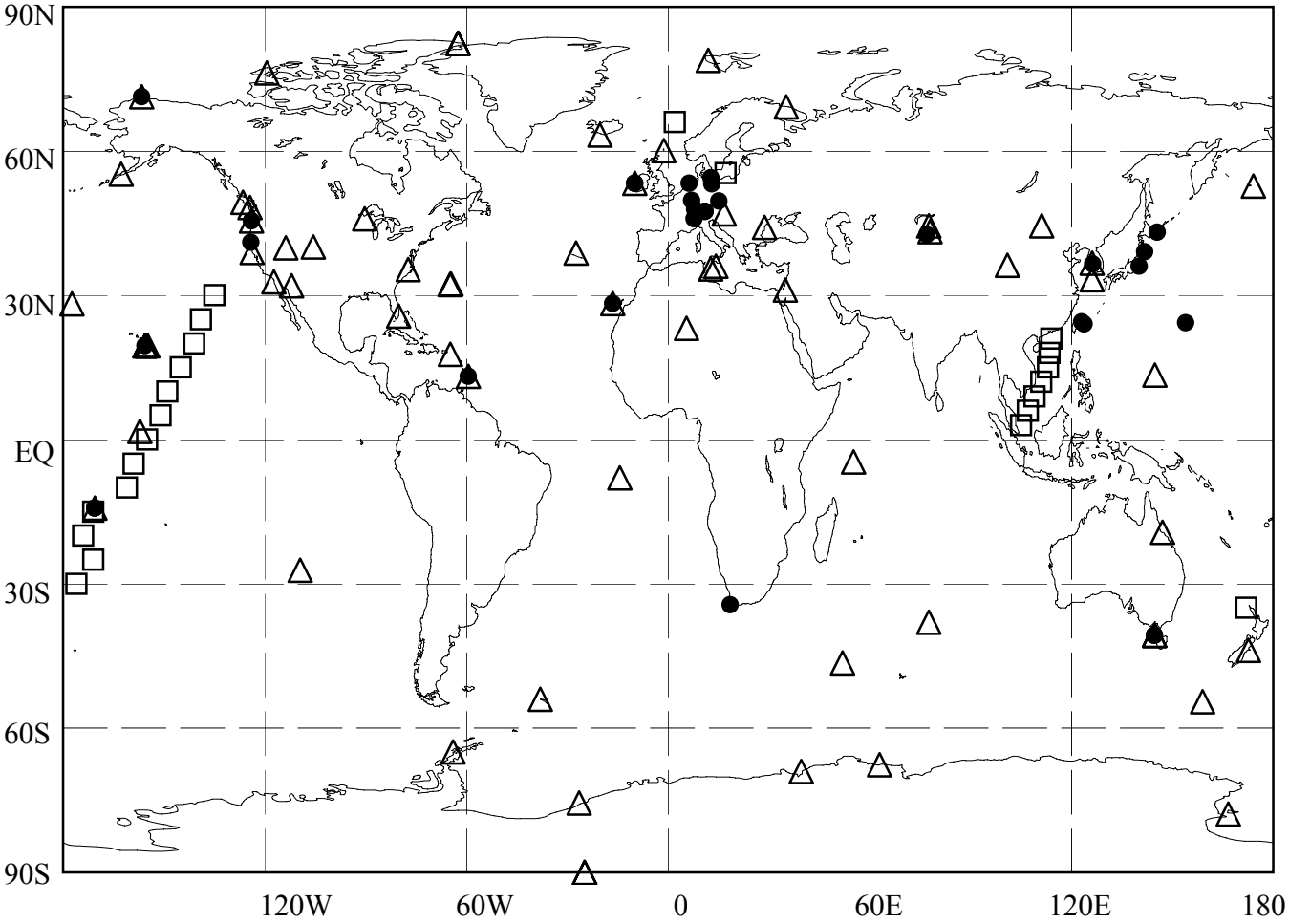

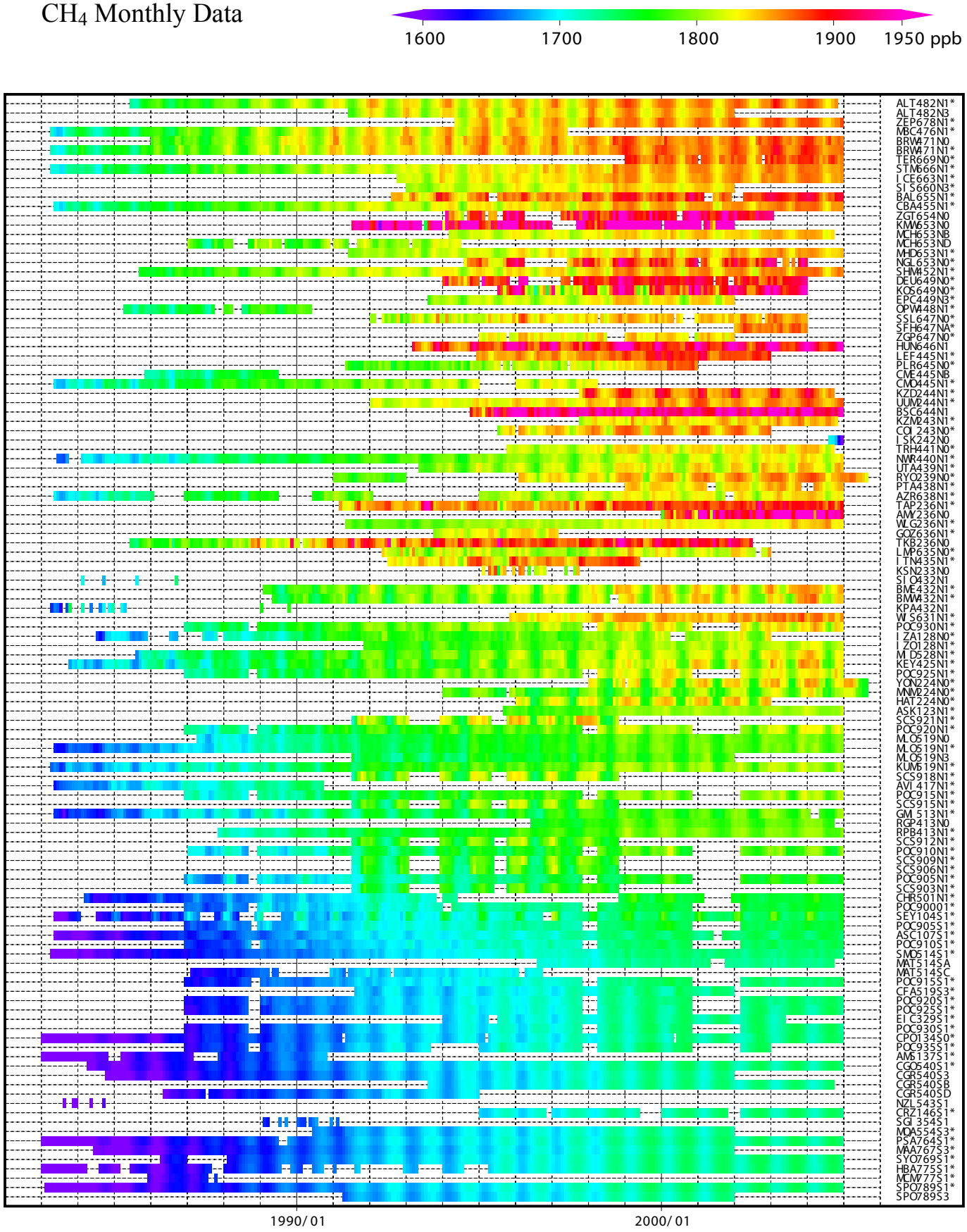

Plate 4.1 Monthly mean CH_4 mixing ratios for all sites reported to the WDCGG illustrated in colors that change with the mixing ratio. The sites are set from north to south. Though some stations reported data at two or three different altitudes, only data at the lowest altitudes are illustrated. The monthly value at the site which has submitted only original (hourly) data before selection is calculated by the WDCGG as an arithmetic mean. Site index with an asterisk shows the site used in the analysis shown in Plate 4.2. (see Chapter 2)

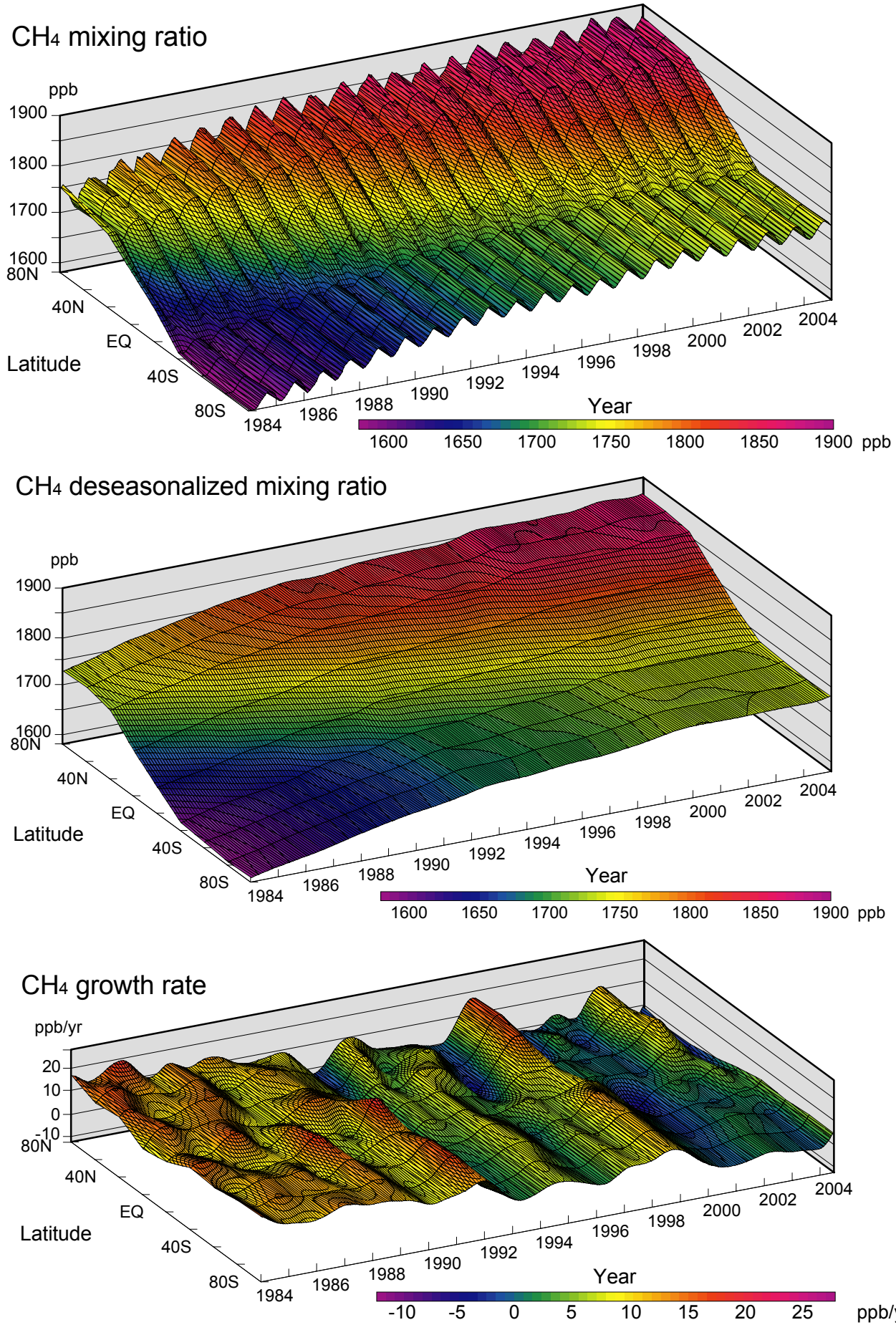

Plate 4.2 Variation of zonally averaged monthly mean CH_4 mixing ratios (top), deseasonalized mixing ratios (middle), and growth rates (buttom). Zonally averaged mixing ratios are calculated for each 20° zone. Deseasonalized mixing ratios and growth rates are derived as described in Chapter 2.

4. Methane (CH_4)

Basic information on CH_4 with regard to environmental issues

Methane (CH_4) is the second most significant greenhouse gas, but is estimated to have 21 times as much radiative forcing as CO_2 per molecule. From 1000 to 1800 A.D., the mixing ratio of CH_4 was about 700 ppb (Etheridge *et al.*, 1998). CH_4 contributed to 20% of the radiative forcing due to increases in levels of greenhouse gases after the industrial evolution (IPCC, 2001).

Atmospheric CH_4 is produced mainly by anaerobic digestion and combustion of fossil fuel, and is removed by reaction with hydroxyl radicals (OH). CH_4 is emitted from both natural and anthropogenic sources, including natural wetlands, oceans, landfills, rice paddies, enteric fermentation, gas drilling and biomass burning. Of the various emissions, about 60% are estimated to have a relationship with anthropogenic activities. Particularly, the increases in energy consumption with landfills, sewage disposal, and fossil fuel use in urban cities have resulted in high mixing ratios of CH_4 in Asia (Bartlett *et al.*, 2004). CH_4 is destroyed by reaction with OH in the troposphere and the stratosphere, reaction with chlorine atoms and oxygen atoms in the excited $O(^1D)$ state in the stratosphere and soil absorption. CH_4 is one of the most important water vapour sources in the stratosphere. The atmospheric lifetime of CH_4 was estimated to be about 9 years. However, the mixing ratio of OH, which decomposes CH_4, is affected by ambient temperature and humidity. In addition, emissions from some sources are dependent on temperature. Therefore, information regarding sources and sinks of CH_4 must be further improved to estimate the atmospheric CH_4 budget.

Analyses of confined air in ice cores in Antarctica and Arctic areas showed that the present CH_4 mixing ratio has not been exceeded during the past 420,000 years (IPCC, 2001). The CH_4 mixing ratio before the industrial revolution was about 700 ppb. The CH_4 mixing ratio had increased after the industrial revolution. However, the increase was very slow in a few years.

The observation sites that submitted CH_4 mixing ratio data to the WDCGG are shown on the map at the beginning of this chapter.

Annual variation in CH_4 levels in the atmosphere

The monthly mean CH_4 data from all the stations that submitted to the WDCGG are shown in Plate 4.1. In this plate, mixing ratio levels are illustrated in different colours. Global, hemispheric and zonal mean background mixing ratios were analysed based on selected stations (see the caption for Plate 4.1). The three-dimensional representations of latitudinal distribution of atmospheric CH_4 mixing ratio, deseasonalized mixing ratios and the growth rate (yearly difference of mixing ratio) are shown in Plate 4.2. These three-dimensional representations (CH_4 carpets) indicate that the amplitudes of seasonal variation of mixing ratio are larger in the Northern hemisphere than in the Southern Hemisphere; the increase in mixing ratio occurs in the Northern Hemisphere prior to the Southern Hemisphere, and propagates to the Southern Hemisphere. The variation in growth rate occurs on a global scale. These features are similar to those of CO_2 (see Section 3). The latitudinal gradient of CH_4 mixing ratio is large from the mid-latitudes in the Northern Hemisphere to the Tropics, suggesting that the major sources located in the high and middle northern latitudes and CH_4 are destroyed with transportation to the Tropics where OH mixing ratios are high.

Measurements of CH_4 mixing ratios in Antarctic and Greenland ice cores indicated that the differences between northern and southern high latitudes ranged from 24 to 58 ppb from 1000 to 1800 A.D. (Etheridge *et al.*, 1998). At present, the difference between the northern and southern high latitudes is about 150 ppb (see Fig. 4.3). This increase is presumably due to increased emissions in the Northern Hemisphere, which are mainly from anthropogenic sources.

Figure 4.1 shows the monthly mean mixing ratios with deseasonalized long-term trends and the growth rate from 1984 to 2004 for the globe. The global mean mixing ratio in 2004 was 1783 ppb, which was the same as that in 2003, and the highest mixing ratio since the beginning of the worldwide observation. The mixing ratio corresponds to 255% of that in the pre-industrial level.

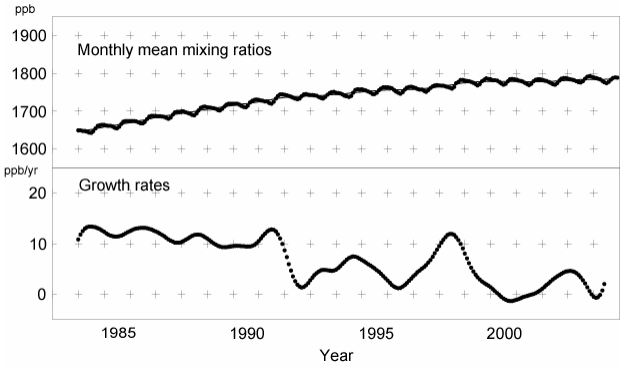

Fig. 4.1 Monthly mean mixing ratios (thick line), deseasonalized long-term trends (thin line) (top) and growth rates (bottom) from 1984 to 2004 for the globe.

The growth rate of CH_4 shows a large interannual variation. During the analysis period, global growth rates reached a maximum in June 1984 at 13 ppb/year and a minimum in October 2000 at -1 ppb/year. The global growth rate of almost zero in 2000-2001 suggested that the global CH_4 budget seemed to have been at a steady-state. Growth rates after the 1990s were generally lower than those during the 1980s. The global mean growth rates were 11 ppb/year for 1984-1990 and 3.7 ppb/year during the latest 10 years (1994-2004). Lelieveld *et al*. (1998) noted that the decrease in global emission of CH_4 brought about a reduction in CH_4 growth rate in the 1990s. However, Dlugokencky *et al.* (1998) and Etheridge *et al.* (1998) reported that the decreased growth rates in the 1990s suggested that global CH_4 mixing ratios are approaching a steady-state where removal of CH_4 is balanced by emission from CH_4 sources.

Figure 4.2 shows the monthly mean mixing ratios and their deseasonalized long-term trends from 1984 to 2004 for each of the 30° latitudinal zones. The seasonal variations were small in the latitudinal zone from the equator to 30°S.

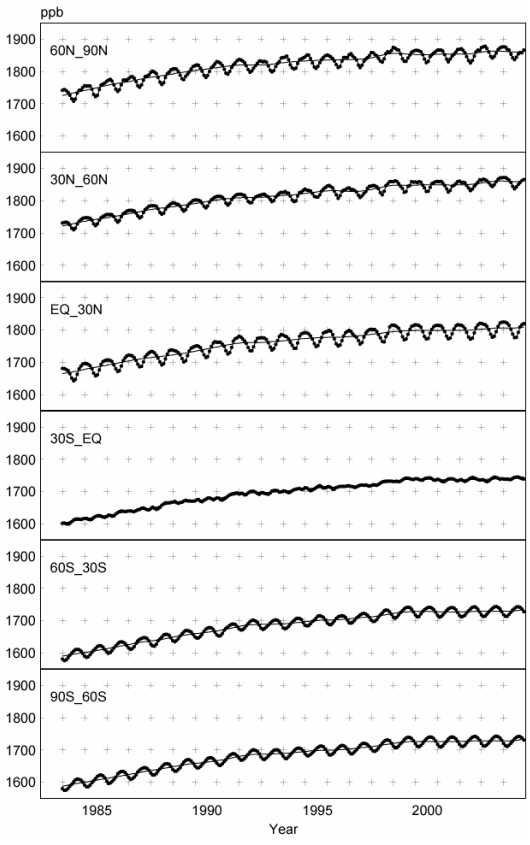

Fig. 4.2 Monthly mean mixing ratios (thick line) and deseasonalized long-term trends (thin line) from 1984 to 2004 for each 30° latitudinal zone.

Figure 4.3 shows the deseasonalized long-term trends and growth rates for each of the 30° latitudinal zones. Deseasonalized long-term trends have the distinct feature of high mixing ratios in northern high and mid-latitudes and low mixing ratios in southern latitudes. Growth rates clearly decreased from the 1980s to the 1990s for all of the latitudinal zones.

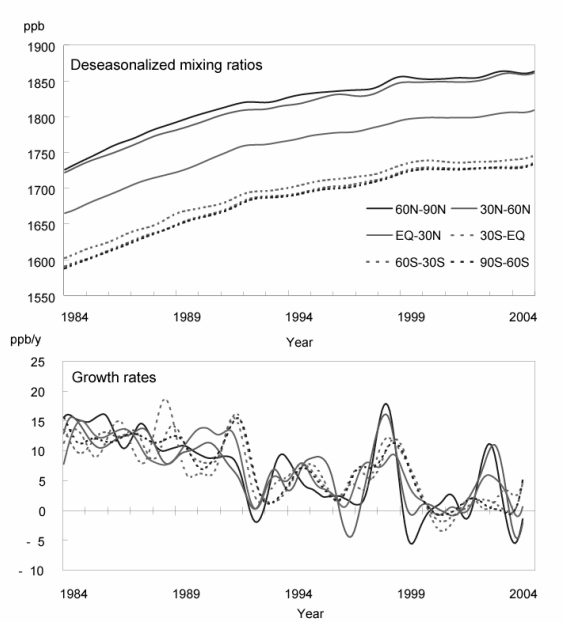

Fig. 4.3 Deseasonalized long-term trends (top) and growth rates (bottom) for each 30° latitudinal zone.

Growth rates in the Southern Hemisphere and Northern Subtropics were large in 1991 and small in 1992 and 1993 for all latitudinal zones, and took negative values in the northern high latitudes in 1992.

The large increase in 1991 may have been caused by decreased OH radical levels due to a reduction in UV radiation as a result of the eruption of Mt. Pinatubo in 1991 (Dlugokencky *et al.*, 1996). Carbon isotope observations suggested that the decrease in 1992 was probably caused by a reduction in biomass burning at low latitudes (Lowe *et al.*, 1997), and analysis of monsoon activity suggested a role of a decrease in emission from wetlands and rice paddy fields due to low temperatures and enhancement of decomposition due to dryness (Lelieveld *et al.*, 1998). The decrease in 1992 may also have been due to an increase in OH radical mixing ratio caused by stratospheric ozone depletion after the eruption of Mt. Pinatubo in 1991 (Bekki *et al.*, 1994).

Growth rates were large in 1998 for all of the latitudinal zones. Dlugokencky *et al.* (2001) suggested that the large growth rates in 1998 were due to increased emissions from the northern high latitudinal zones and the tropical wetlands due to high temperatures and increased precipitation, and partly due to the influence of biomass burning of the boreal forest mainly in Siberia. The growth rates decreased afterward, but the growth rates increased again

corresponding to the occurrence of the 2002 /2003 El-Niño event.

Fig. 4.4 shows the interannual variations in global mean growth rate and global surface temperature anomaly. Global CH_4 growth rates varied along with global mean temperature anomalies in the 1990s, particularly during the period from 1992-1998. High temperature anomalies result in increased CH_4 emission from wetlands and increased removal by increased OH radical levels (Bekki *et al.*, 1997). The relationship between global growth rates and temperature anomalies showed that the former effect exceeds the latter globally. A study of the relationship between CH_4 mixing ratios in ice cores or firn layers and global temperature anomalies also suggested that a large growth rate for the CH_4 mixing ratio follows a high global mean temperature (Etheridge *et al.*, 1998). However, the global mean growth rate in the 1980s did not correspond with the global surface temperature anomaly in the same decade. This suggests that causes other than the global temperature anomaly resulted in the large increase rate in the 1980s.

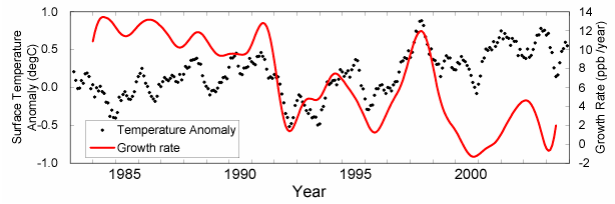

Fig. 4.4 Time series of the global mean CH_4 growth rates and their comparison with temperature anomalies on land from NCEP reanalysis data. The solid lines show the growth rates, and the dots show temperature anomalies (5-month running mean).

Seasonal cycle of CH_4 in the atmosphere

Figure 4.5 shows average seasonal cycles for each of the 30° latitudinal zones. Seasonal cycles are brought about mainly by reaction with OH, a major CH_4 sink in the atmosphere. The strength and timing of the emission from CH_4 sources, such as wetlands and biomass burning, along with transportation of CH_4, also affect the seasonal cycle. The amplitudes of the seasonal cycle were large in the Northern Hemisphere. Unlike CO_2, amplitudes were large in the Southern Hemisphere except at low latitudes. The CH_4 seasonal cycle showed a minimum in summer and a maximum in winter in both hemispheres. The seasonal variation of CH_4 is almost consistent with that of OH, which reacts chemically with CH_4. Southern low latitudes have a distinct semi-annual component, which is superimposed on the annual component of the seasonal cycle at southern mid-latitudes. The secondary maximum occurred in boreal winter due to the trans-hemisphere transportation of CH_4 from the Northern Hemisphere. This phenomenon was seen at stations located in the western Indian Ocean, *e.g.,* Mahe Island and the Seychelles, and in the western and central equatorial Pacific, *e.g.,* Cape Matatula and Samoa.

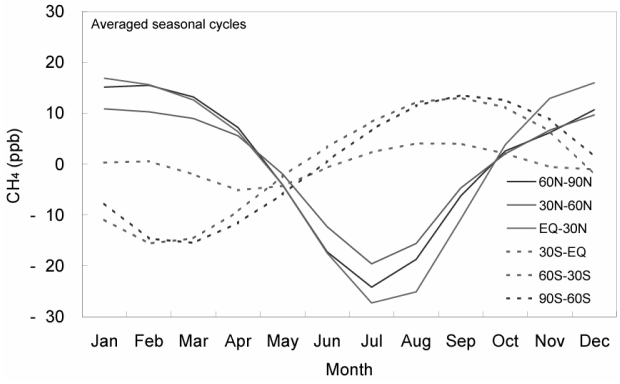

Fig. 4.5 Average seasonal cycles for each 30° latitudinal zone from which the long-term trends were subtracted.

5.
NITROUS OXIDE
(N_2O)

●:*IN SITU* STATION
△:FLASK STATION

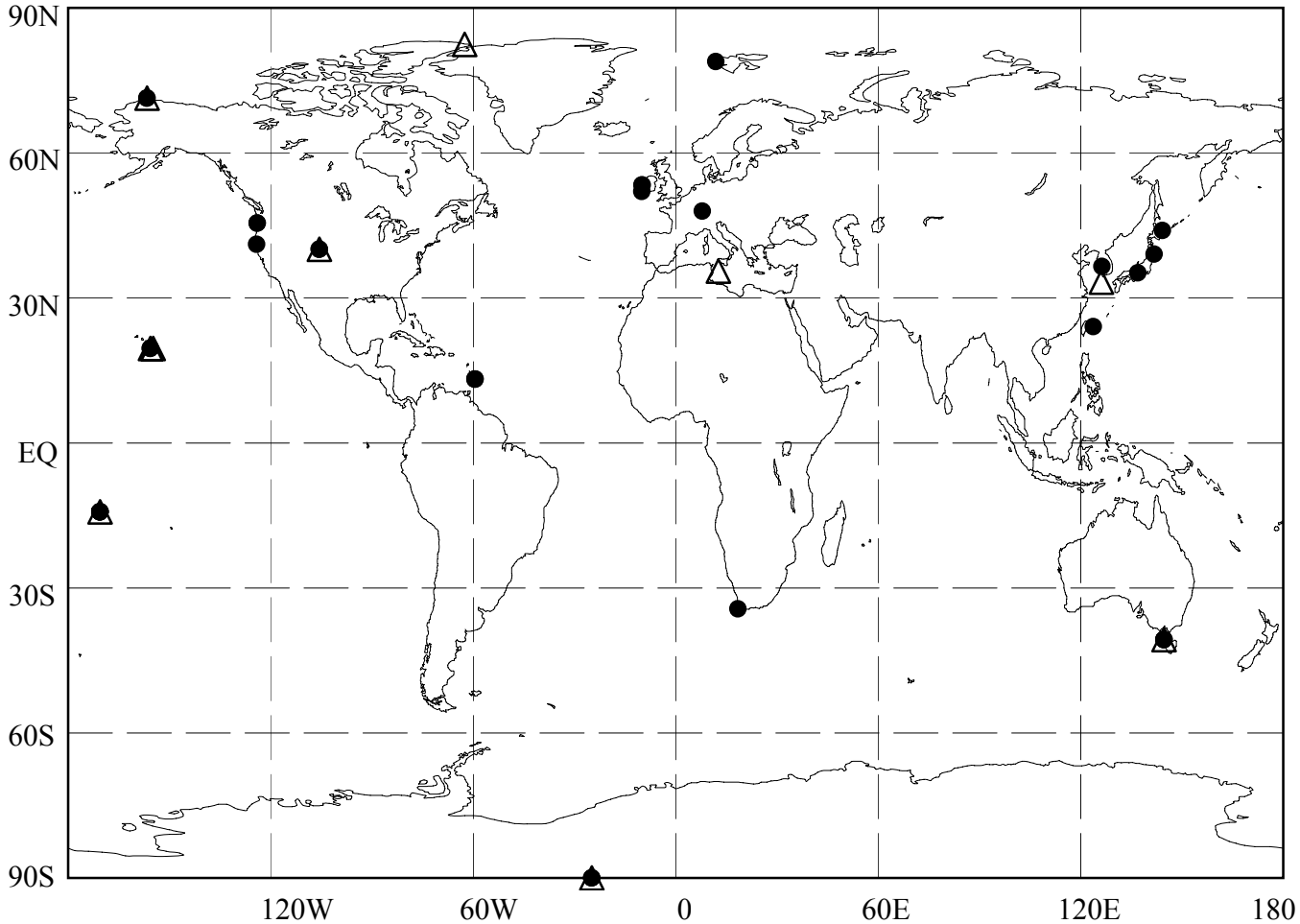

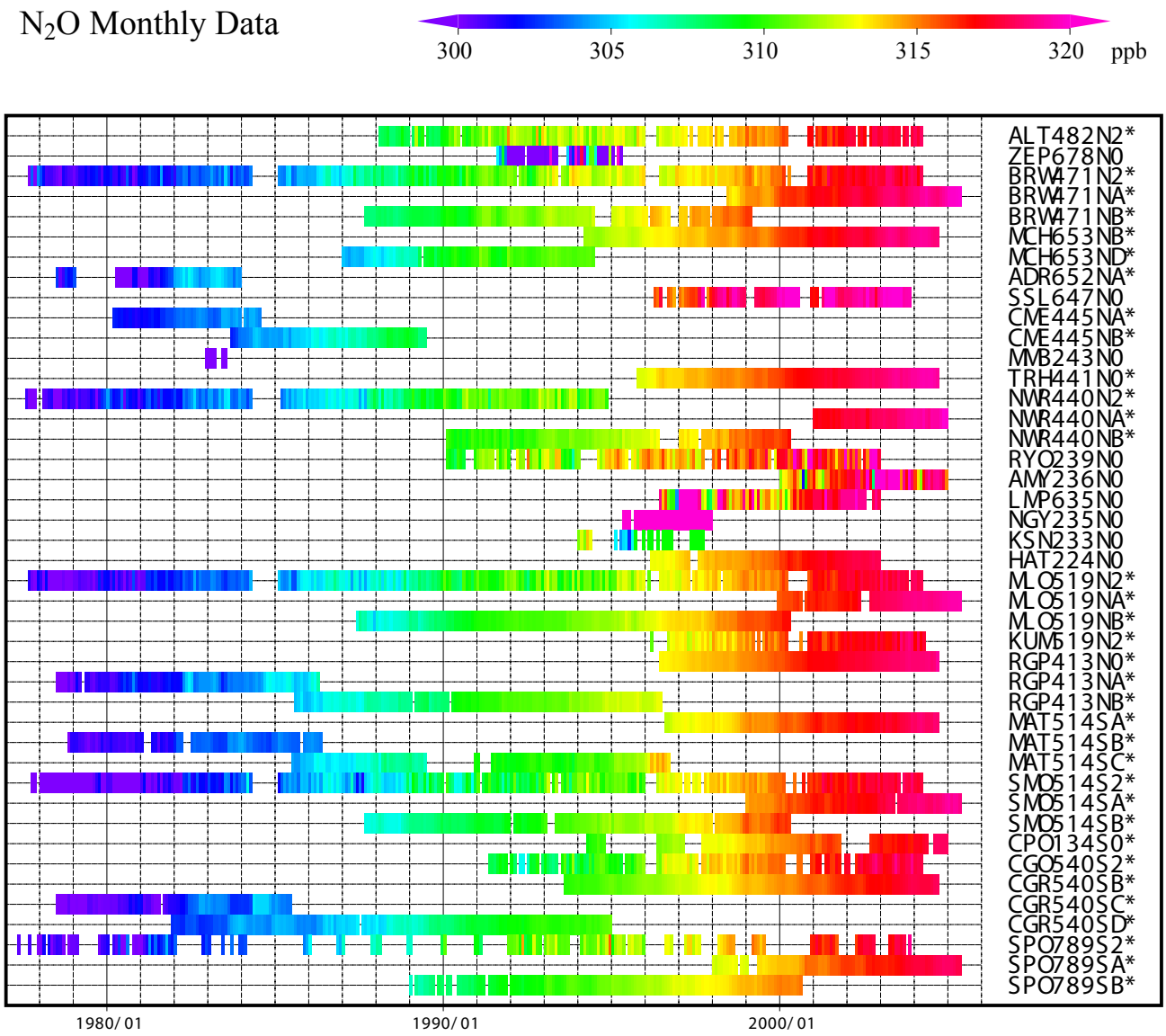

Plate 5.1 Monthly mean N_2O mixing ratios for all sites reported to the WDCGG illustrated in colors that change with the mixing ratio. The sites are set from north to south. Site index with an asterisk shows the site used in the analysis shown in Fig. 5.1. (see Chapter 2)

5. Nitrous Oxide (N_2O)

Basic information on N_2O with regard to environmental issues

Nitrous oxide (N_2O), which is a relatively stable gas in the troposphere, is a greenhouse gas with an "adjustment-time" of 114 years. At present, radiative forcing of N_2O is estimated at 0.15 W/m^2, which is 6% of the total from all of the long-lived and globally mixed greenhouse gases (IPCC, 2001). The atmospheric mixing ratio of N_2O increased steadily from about 270 ppb in pre-industrial times and is now 18% higher than in 1750.

N_2O is emitted into the atmosphere from natural and anthropogenic sources, including the oceans, soil, combustion of fuels, biomass burning, fertiliser use and various industrial processes. One-third of the total amount of emission is considered to be from anthropogenic sources. N_2O is removed from the atmosphere mainly by photo-dissociation in the stratosphere. However, even at this stage, the estimated amounts from sources and sinks have not yet been balanced.

Annual variation of N_2O in the atmosphere

The map at the beginning of this chapter shows observation sites that have submitted N_2O data to the WDCGG. The monthly mean N_2O data from all stations submitted to the WDCGG are shown in Plate 5.1. In this plate, mixing ratio levels are illustrated in different colours. The time series of monthly mean mixing ratios are plotted in Figure 5.1 using a solid line for the stations located in the Northern Hemisphere and a faint line for those in the Southern Hemisphere. The global mean mixing ratio was 318.6 ppb in 2004, which increased by 0.7 ppb during the last year. This mixing ratio corresponds to 118% of the pre-industrial level. The observation data in this figure did not show large fluctuations. The mixing ratios are increasing in both hemispheres, and the difference between both hemispheres is small. The mean increase rate of the global mean mixing ratio during the latest 10 years (1994-2004) was 0.8 ppb/year.

At some stations, the average growth rate (yearly difference of mixing ratio) decreased considerably between 1991 and 1993, but then returned to almost the same rate as that observed during the 1980s. This was suggested to be due to a decrease in the use of nitrogen-based fertilisers, lower biogenic emissions and larger stratospheric losses due to volcanic-induced circulation changes (IPCC, 2001).

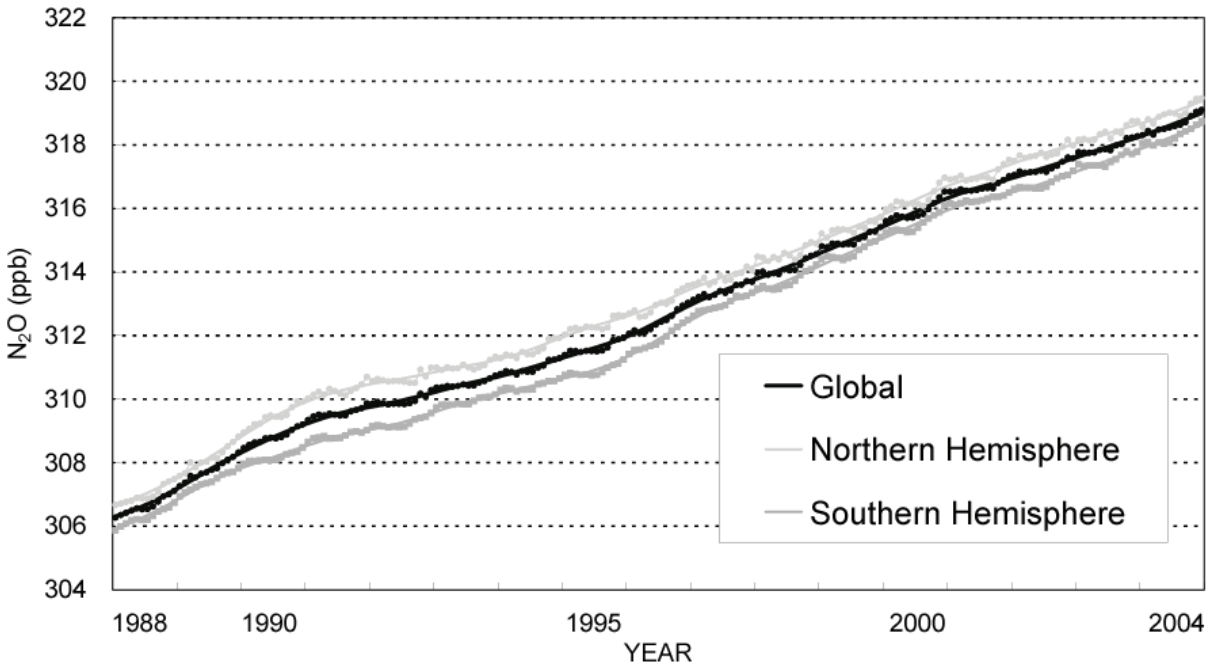

Fig. 5.1 Monthly mean mixing ratios (thin lines) and deseasonalized long-term trends (thick lines) from 1988 to 2004 for the globe (solid line) and both hemispheres (faint lines).

6.
HALOCARBONS

●:*IN SITU* **STATION**
△:**FLASK STATION**

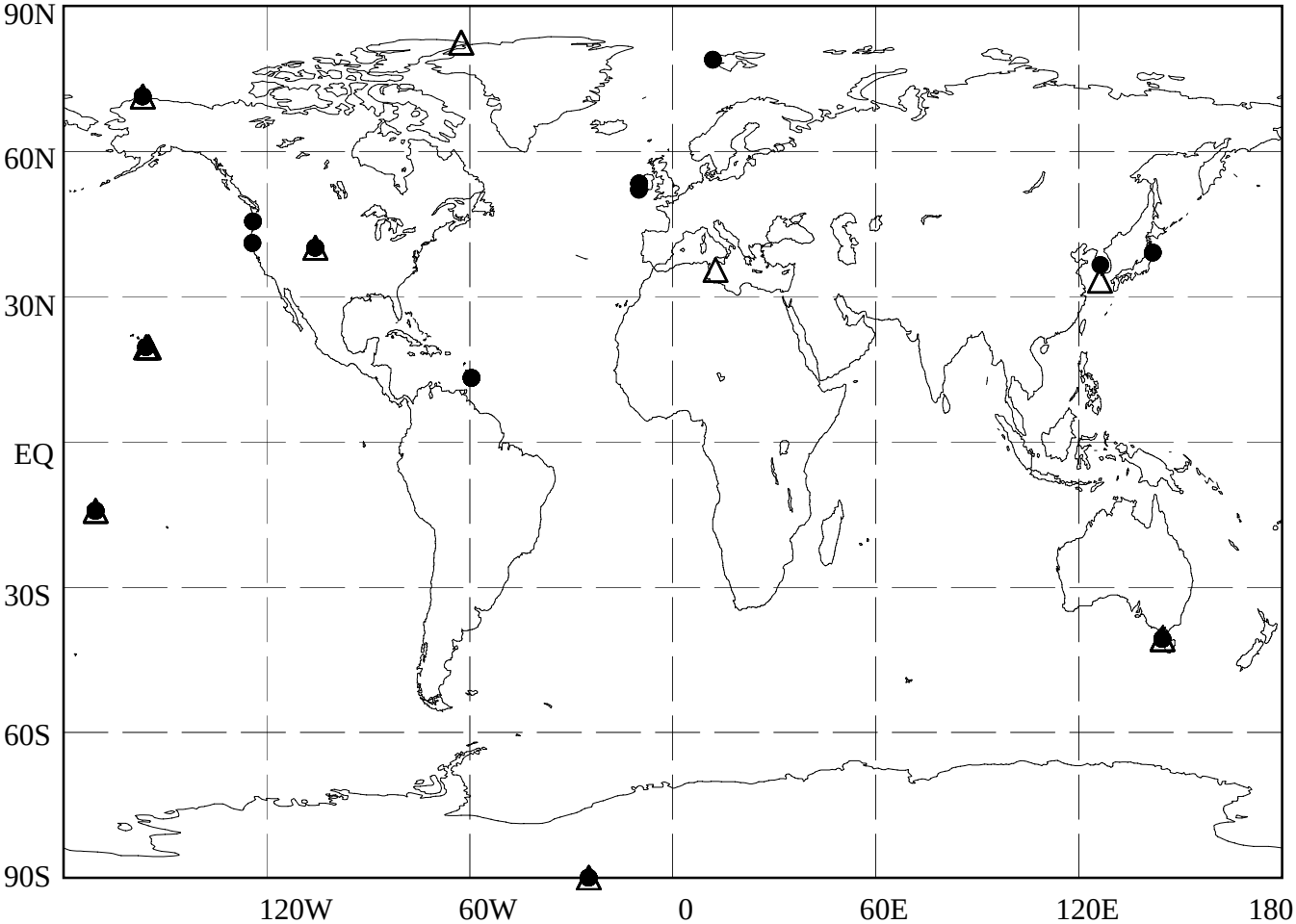

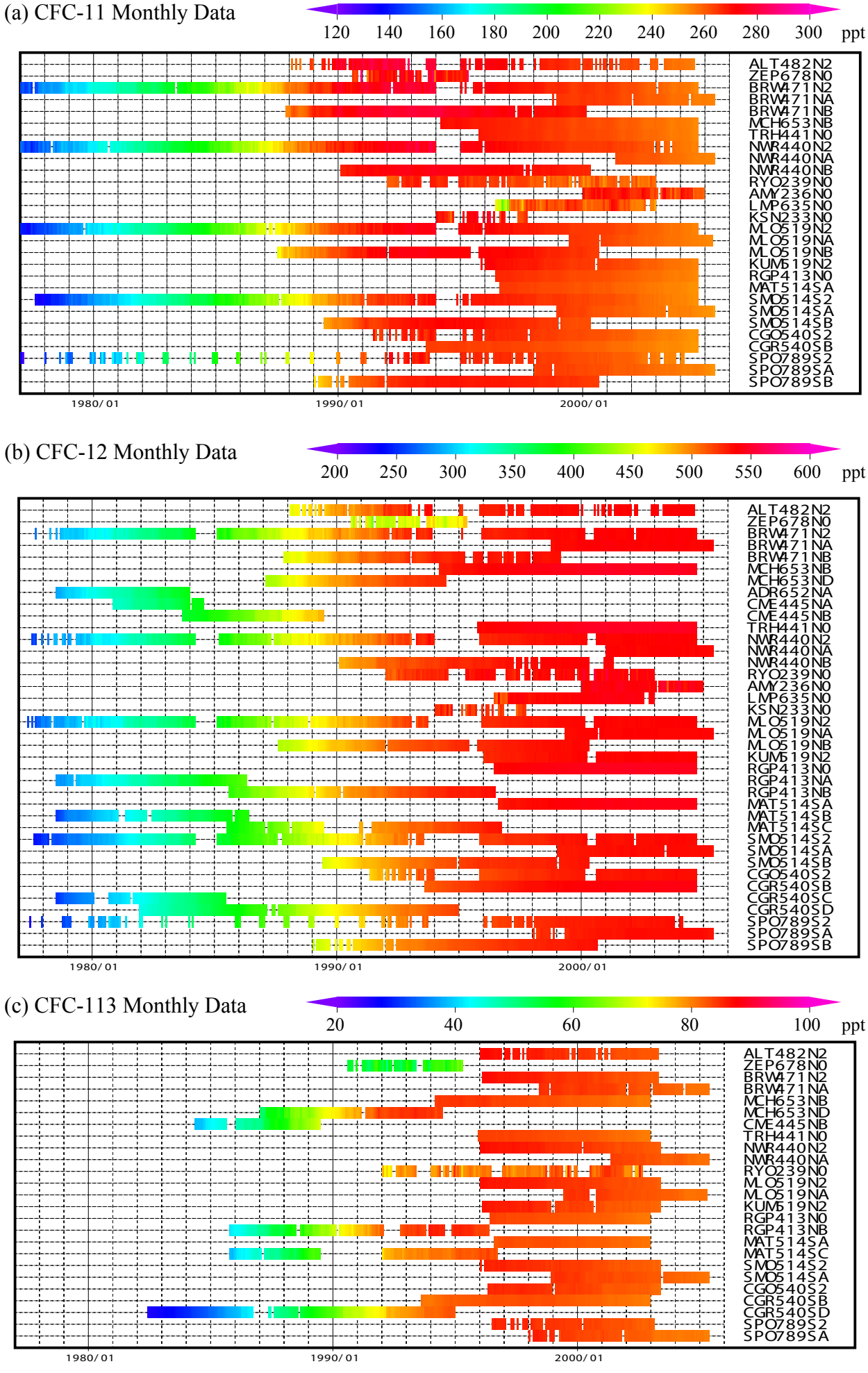

Plate 6.1 Monthly mean (a) CFC-11, (b) CFC-12, (c) CFC-113 mixing ratios for all sites reported to the WDCGG illustrated in colors that change with the mixing ratio. The sites are set from north to south.

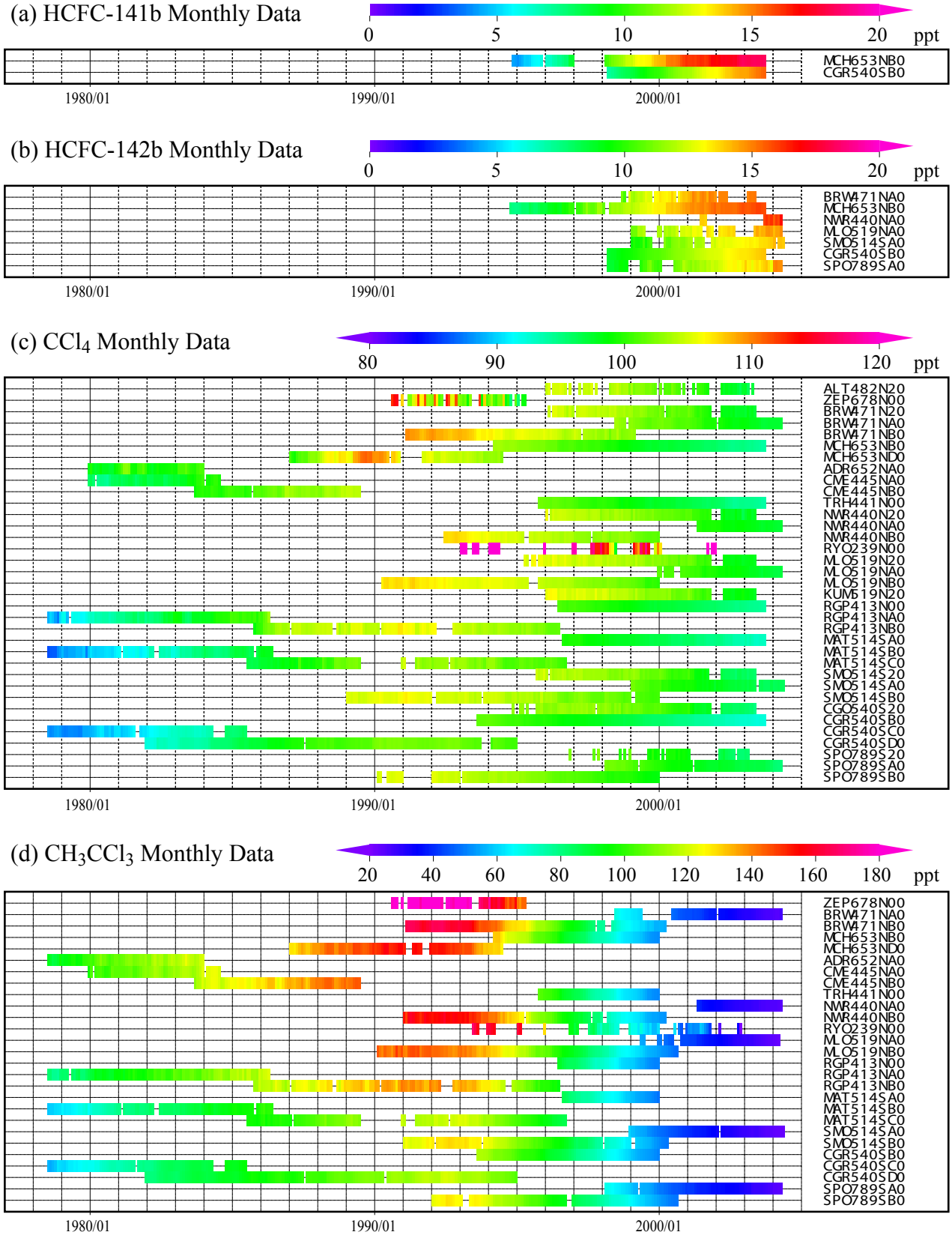

Plate 6.2 Monthly mean (a) HCFC-141b, (b) HCFC-142b, (c) CCl_4, (d) CH_3CCl_3 mixing ratios for all sites reported to the WDCGG illustrated in colors that change with the mixing ratio. The sites are set from north to south.

6. Halocarbons (CFCs, HCFCs, CCl_4 and CH_3CCl_3)

Basic information on halocarbons with regard to environmental issues

"Halocarbon" is a general term for carbon compounds containing one or more halogens, *i.e.*, fluorine, chlorine, bromine or iodine. Most of the halocarbons are industrial products. The chlorofluorocarbons (CFCs) are halocarbons containing fluorine and chlorine but no hydrogen, while hydrochlorofluorocarbons (HCFCs) also contain hydrogen. Carbon tetrachloride (CCl_4) and methyl chloroform (CH_3CCl_3) are produced industrially, while methyl chloride and methyl bromide are halocarbons with natural sources. Halocarbons have very low mixing ratios in the atmosphere, but most have large global warming potential. Thus, halocarbons contributed to 14% of radiative forcing due to increases in levels of long-lived and globally mixed greenhouse gases since the industrial revolution (IPCC, 2001).

Halocarbons are clear, odourless, and innocuous substances, which are readily gasified and liquefied and have low surface tension. Thus, they were commonly used as refrigerants, propellant and detergents for semiconductors, which resulted in a rapid increase in their atmospheric mixing ratios until the mid-1980s. Halocarbons containing chlorine and bromine were found to deplete the ozone layer. The Montreal Protocol on Substances that Deplete the Ozone Layer and its Adjustments and Amendments regulate the production and transportation of ozone-depleting compounds. As a result, global mixing ratios of CFC-11, CCl_4 and CH_3CCl_3 have begun to decrease; the global growth of CFC-113 had stopped by 1996, and that of CFC-12 has decelerated substantially.

A decrease in stratospheric ozone leads to the cooling of the lower stratosphere. However, the increase in halocarbons has a net positive radiative forcing effect on global warming because the positive direct radiative forcing of halocarbons is greater than the negative indirect radiative forcing due to ozone depletion (WMO, 1999a).

CFCs are dissociated mainly by ultraviolet radiation in the stratosphere, and their lifetimes are generally long (*e.g.*, about 50 years for CFC-11). However, HCFCs and CH_3CCl_3, which contain hydrogen, react with hydroxyl radicals (OH) in the troposphere and thus have relatively short lifetimes (*e.g.*, about 5 years for CH_3CCl_3). As the reaction with OH in the troposphere is a major sink for CH_3CCl_3, global measurements of CH_3CCl_3 provide an accurate estimate of the global mixing ratio of OH (Prinn *et al.*, 2001).

Annual variation of halocarbons in the atmosphere

The map at the beginning of this chapter shows observation sites that have submitted halocarbon data to the WDCGG. The monthly mean CFC-11, CFC-12, CFC-113 data from all stations submitted to the WDCGG are shown in Plate 6.1. The monthly mean HCFC-141b, HCFC-142b, CCl_4 and CH_3CCl_3 data from all stations submitted to the WDCGG are shown in Plate 6.2. Figure 6.1 shows the time series of monthly mean mixing ratios of CFC-11, CFC-12 and CFC-113.

Figures 6.2 and 6.3 show the corresponding data for HCFCs, and CCl_4 and CH_3CCl_3, respectively. All monthly data from each station are plotted in these figures. The absolute values of mixing ratios differ from station to station, suggesting that standard gases may not be traceable at each station.

Figures 6.1 and 6.3 showed significant increases in mixing ratios of all compounds during the 1980s in both hemispheres. Long-term trends since around 1990 for each compound are as follows:

CFC-11:	Mixing ratios were at a maximum around 1992 in the Northern Hemisphere and about one year later in the Southern Hemisphere. They have been decreasing slowly since then.
CFC-12:	The growth rates have declined since around 1990 and are now nearly zero in both hemispheres.
CFC-113:	Mixing ratios were at a maximum around 1992 in the Northern Hemisphere and around 1994 in the Southern Hemisphere. Mixing ratios are currently almost constant or decreasing slowly in both hemispheres.
HCFC-141b:	Mixing ratios are increasing linearly.
HCFC-142b:	Mixing ratios are increasing linearly.
CCl_4:	Mixing ratios were at a maximum around 1991 in both hemispheres. Since then, they have been decreasing slowly.
CH_3CCl_3:	Mixing ratios were at a maximum around 1992 in the Northern Hemisphere and around 1993 in the Southern Hemisphere. They have been decreasing almost linearly since then.

Comparison of the stations using identical standard gases revealed that the mixing ratio differences between the two hemispheres were large for all compounds except HCFCs in the 1980s. However, the differences have been decreasing following each compound's mixing ratio peak. The increases in mixing ratios of HCFCs are the result of their continued use as substitutes for CFCs.

The mixing ratios of HCFCs, which are some of the

industrial replacements of CFCs, are increasing. Based on the special report from Intergovernmental Panel on Climate Change (IPCC) and Technology and Economic Assessment Panel (TEAP) (IPCC/TEAP, 2005), They are increasing at rapid rates of +3～+7%, although their mixing ratios are small.

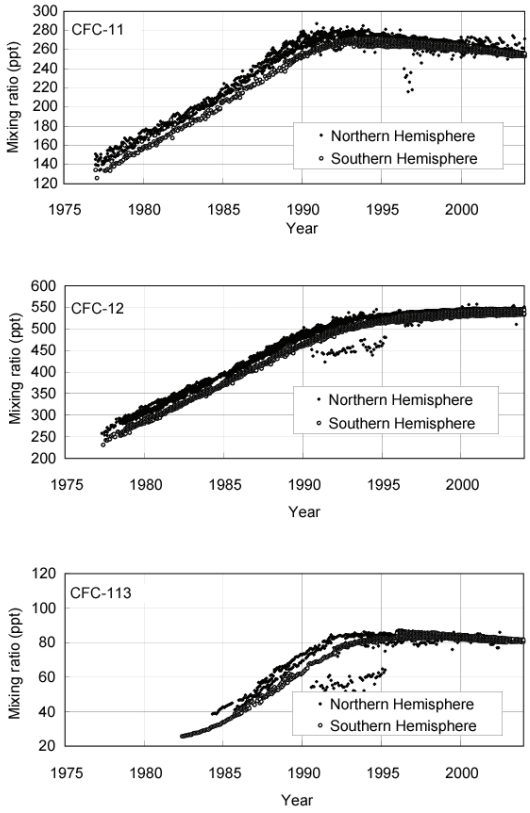

Fig. 6.1 Time series of monthly mean mixing ratios of (a) CFC-11, (b) CFC-12 and (c) CFC-113. Solid circles show the sites located in the Northern Hemisphere and open circles show the sites located in the Southern Hemisphere. Data at all sites reported to the WDCGG are shown.

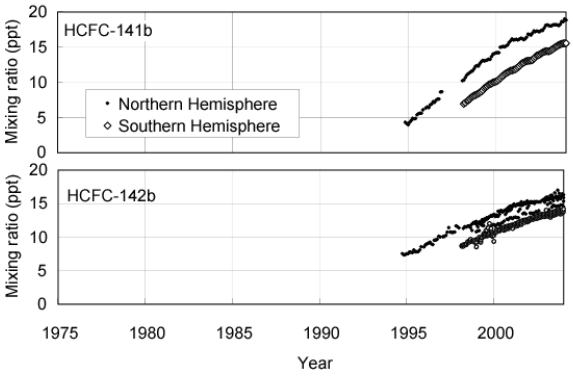

Fig. 6.2 Time series of monthly mean mixing ratios of HCFC-141b (upper panel) and HCFC-142b (lower panel). Solid circles show the sites located in the Northern Hemisphere and open circles show the sites located in the Southern Hemisphere. Data at all sites reported to the WDCGG are shown.

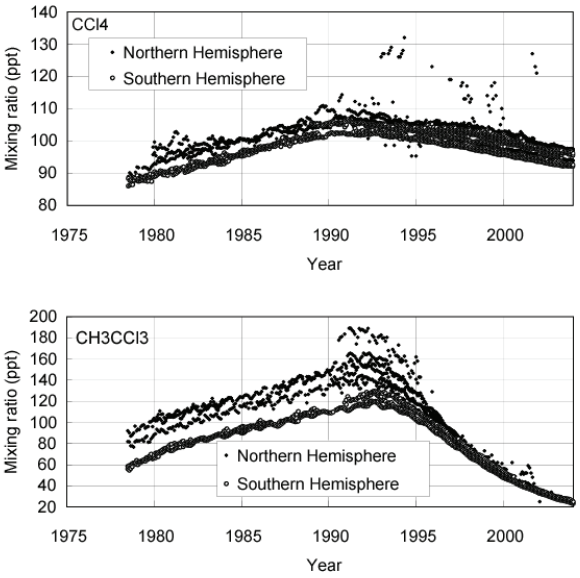

Fig. 6.3 Time series of monthly mean mixing ratios of (a) CCl_4 and (b) CH_3CCl_3. Solid circles show the sites located in the Northern Hemisphere and open circles show the sites located in the Southern Hemisphere. Data at all sites reported to the WDCGG are shown.

7.
Surface OZONE
(O_3)

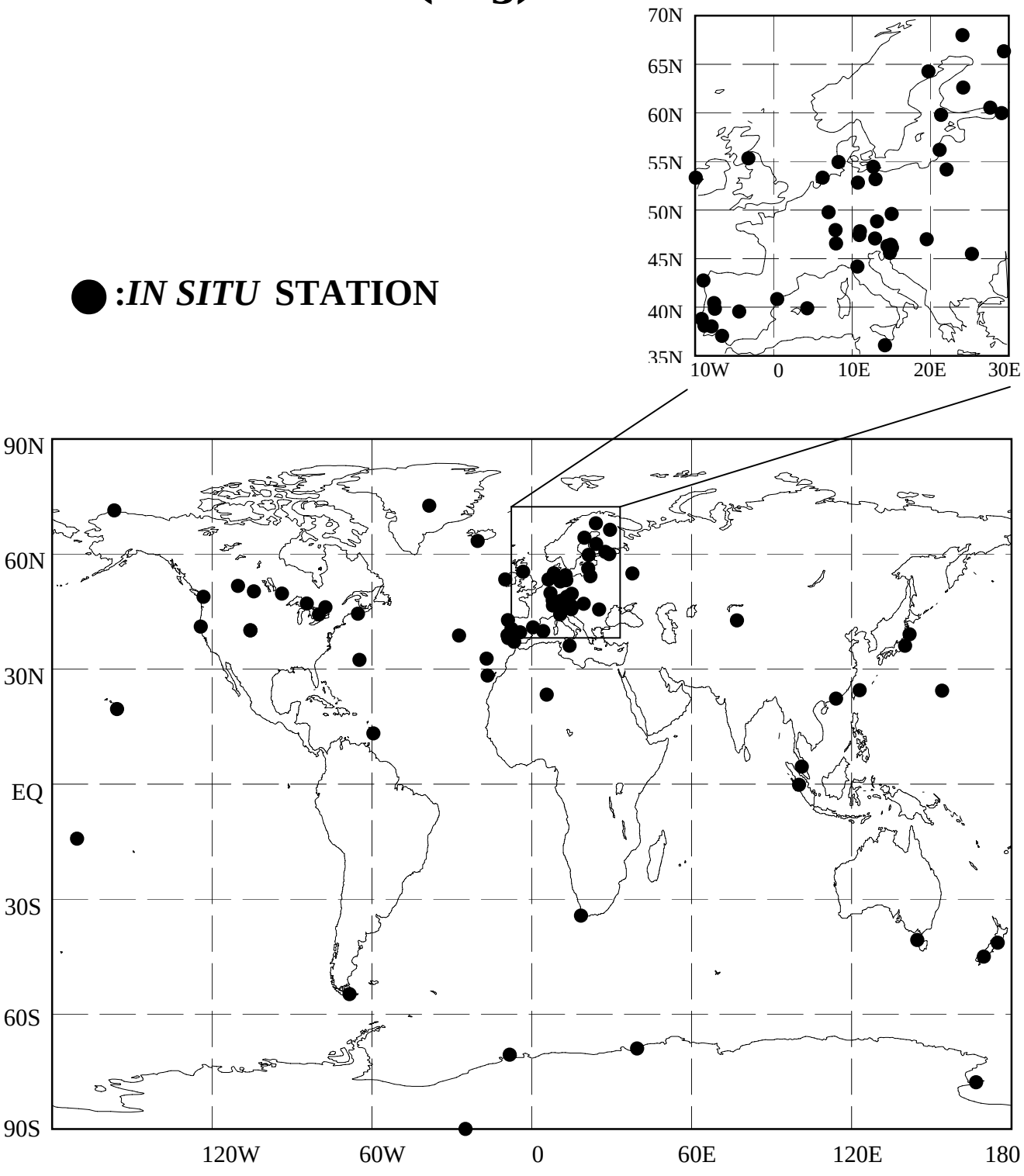

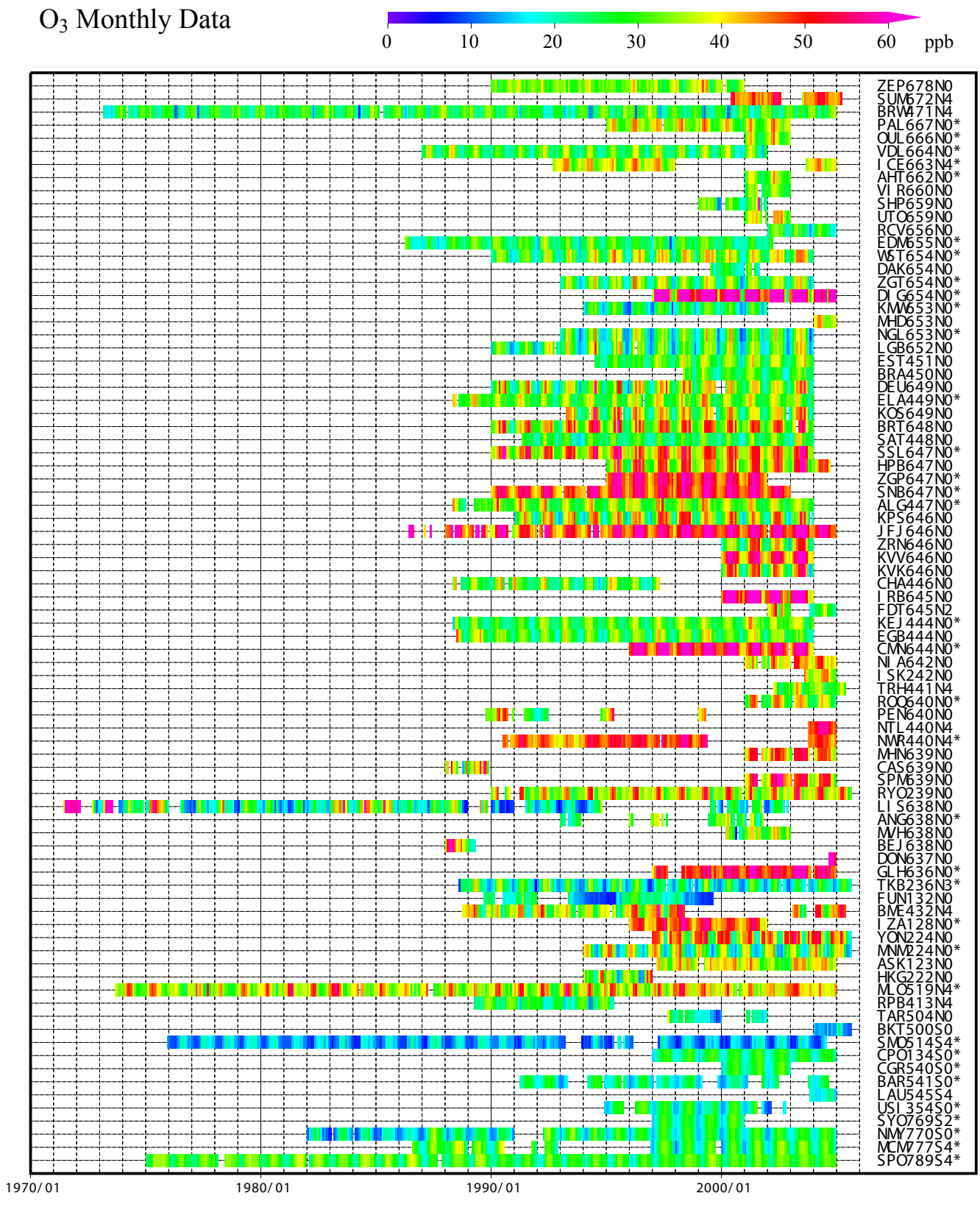

Plate 7.1 Monthly mean O_3 mixing ratios for all sites reported to the WDCGG illustrated in colors that change with the mixing ratio. The sites are set from north to south. It is shown that an asterisk incidental to station index is one peak type in the analysis shown in Fig 7.1.

7. Surface Ozone (O_3)

Basic information on surface ozone (O_3) with regard to environmental issues

Most ozone (O_3) in the atmosphere exists in the stratosphere, with less than 10% being in the troposphere. However, O_3 in the troposphere plays an important role in the atmospheric environment through radiative and chemical processes. O_3 absorbs UV radiation in the stratosphere, and this energy influences the temperature vertical profile and circulation in the stratosphere. O_3 also absorbs IR radiation, and is thus one of the greenhouse gases in the troposphere. This effect is more significant in the upper troposphere, and tropospheric O_3 is the third most important greenhouse gas after CO_2 and CH_4 (IPCC, 2001). O_3 is also a chemically reactive gas producing OH radicals that control atmospheric mixing ratios of many greenhouse gases, such as CH_4 through chemical reactions.

The sources of tropospheric O_3 are intrusions from the stratosphere and photochemical production. Major intrusions from the stratosphere occur by tropopause folding accompanied with low pressure activity in the middle and high latitudes, and unstable mixing in the vicinity of the tropopause around cold vortexes, etc. These intrusions occur around meandering parts of the jet stream. Photochemical production occurs by the reactions of nitrogen oxides with CO and non-methane hydrocarbons under solar radiation (these substances are called "O_3 precursors"). At the same time, O_3 is destroyed mainly through chemical reactions with OH radicals and deposition at the Earth's surface. The latitudinal distributions of O_3 in the middle troposphere have high mixing ratios in the middle and high latitudes in both Hemisphere, and low mixing ratios in the tropics, as shown by Marenco and Said (1989) over the Atlantic Ocean and by Tsutsumi *et al.* (2004) over the Pacific Ocean. As sources are localized and their lifetimes are generally short, the distribution of surface O_3 is also localized and time-variant. Surface O_3 is estimated to have increased since pre-industrial times (IPCC, 2001).

Annual variation of surface O_3

The World Data Centre for surface O_3 was transferred from NILU to JMA in August 2002. The map at the beginning of this chapter shows observation sites that have submitted O_3 data to the WDCGG.

The monthly mean O_3 data from all stations submitted to the WDCGG are shown in Plate 7.1. In the plate, mixing ratio levels are illustrated by different colours. Please note that the data on surface O_3 is reported in two units, *i.e.*, mixing ratio (ppb) and weight per volume ($\mu g/m^3$) at 25°C. Weights per volume ($\mu g/m^3$) are converted to mixing ratios (ppb) as follows:

$$X_p\,[ppb] = (R * T / M / P_0) * 10 * X_g\,[\mu g/m^3]$$

where R is the molar gas constant (8.31451 [J/K/mol]),
T is the absolute temperature reported by an individual station,
M is the molecular weight of O_3 (47.9982), and
P_0 is the standard pressure (1013.25 [hPa]).

The mixing ratio of surface O_3 varies from station to station, many of which are located in Europe. Moreover, the seasonal and interannual variation is relatively large at most stations and so it is difficult to identify a global long-term trend in surface O_3 mixing ratios.

Figures 7.1 and 7.2 show average seasonal cycles from which the long-term trends were subtracted for each 30° latitudinal zone of a single- or multi-peak type. The seasonal cycles for each site can be divided into two types: a single-peak type that has a maximum monthly mean, and a multi-peak type that has more than one annual maximum. One multi-peak type, the Southern Hemisphere site, is not shown in Figure 7.2. The maximum mixing ratio of the single-peak type appears in April in northern high and low latitudes and in May in northern mid-latitudes. The delayed peak in the mid-latitudes may be attributed to air pollution in Europe given that most mid-latitude stations are located on this continent. Relatively high spring maximum mixing ratios were observed at Sonnblick, Niwot Ridge, Assekrem and Mauna Loa, all of which are located at high altitudes (higher than 2700 m).

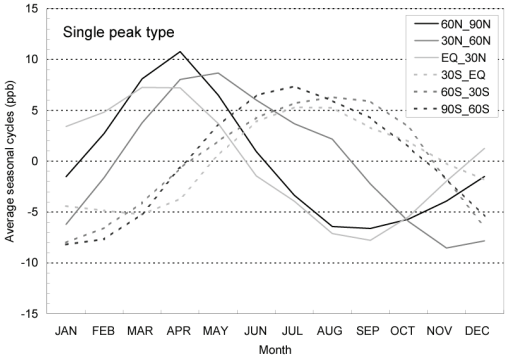

Fig. 7.1 Average seasonal cycles of single-peak type for each 30° latitudinal zone from which the long-term trends were subtracted.

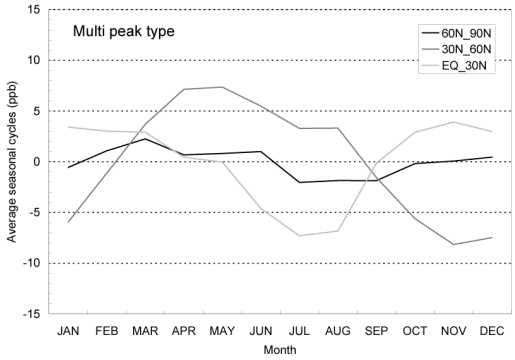

Fig. 7.2 Average seasonal cycles of multi-peak type for each 30° latitudinal zone from which the long-term trends were subtracted.

8.
CARBON MONOXIDE (CO)

●:*IN SITU* STATION
△:FLASK STATION
□:FLASK SAMPLING (SHIP)

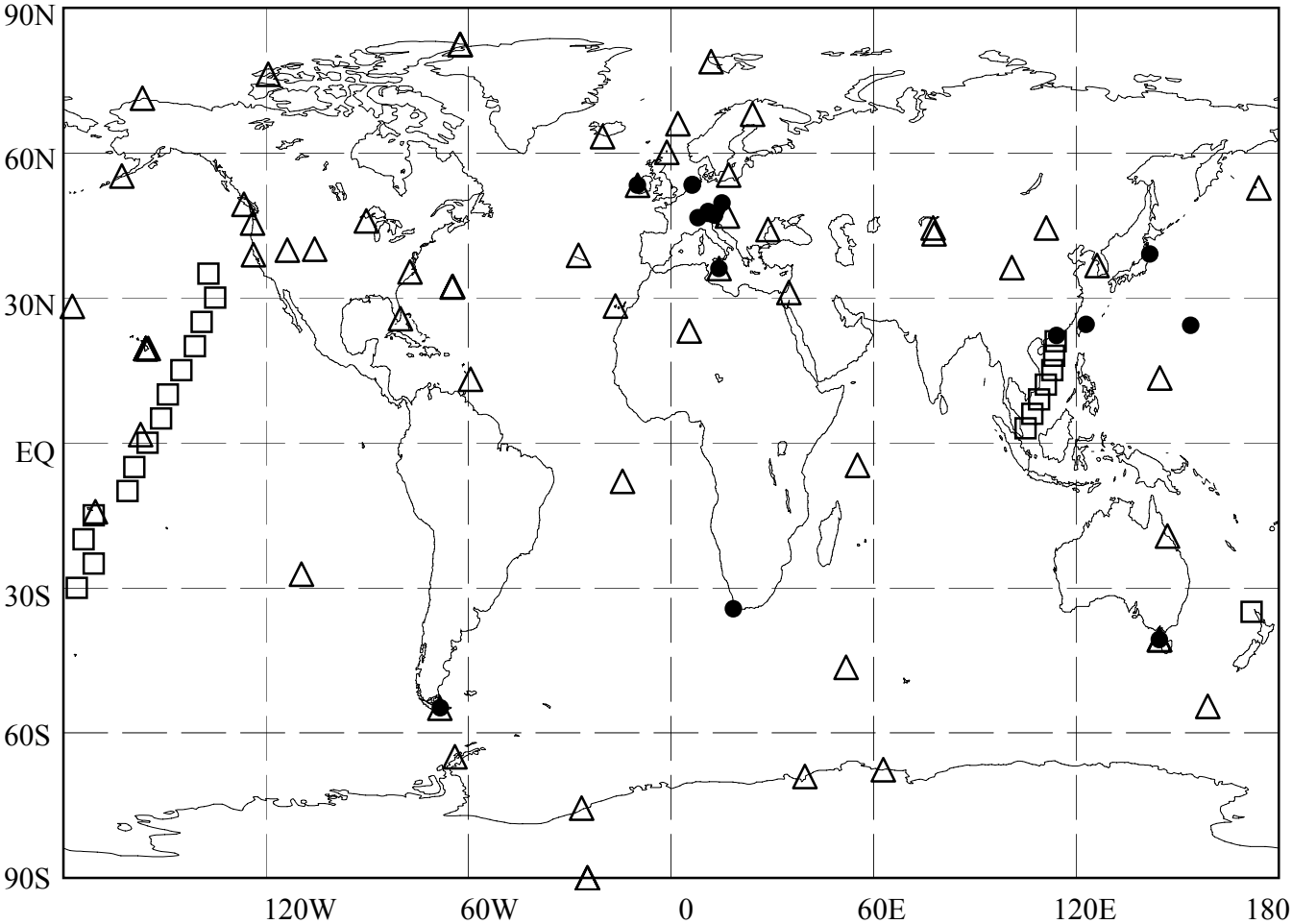

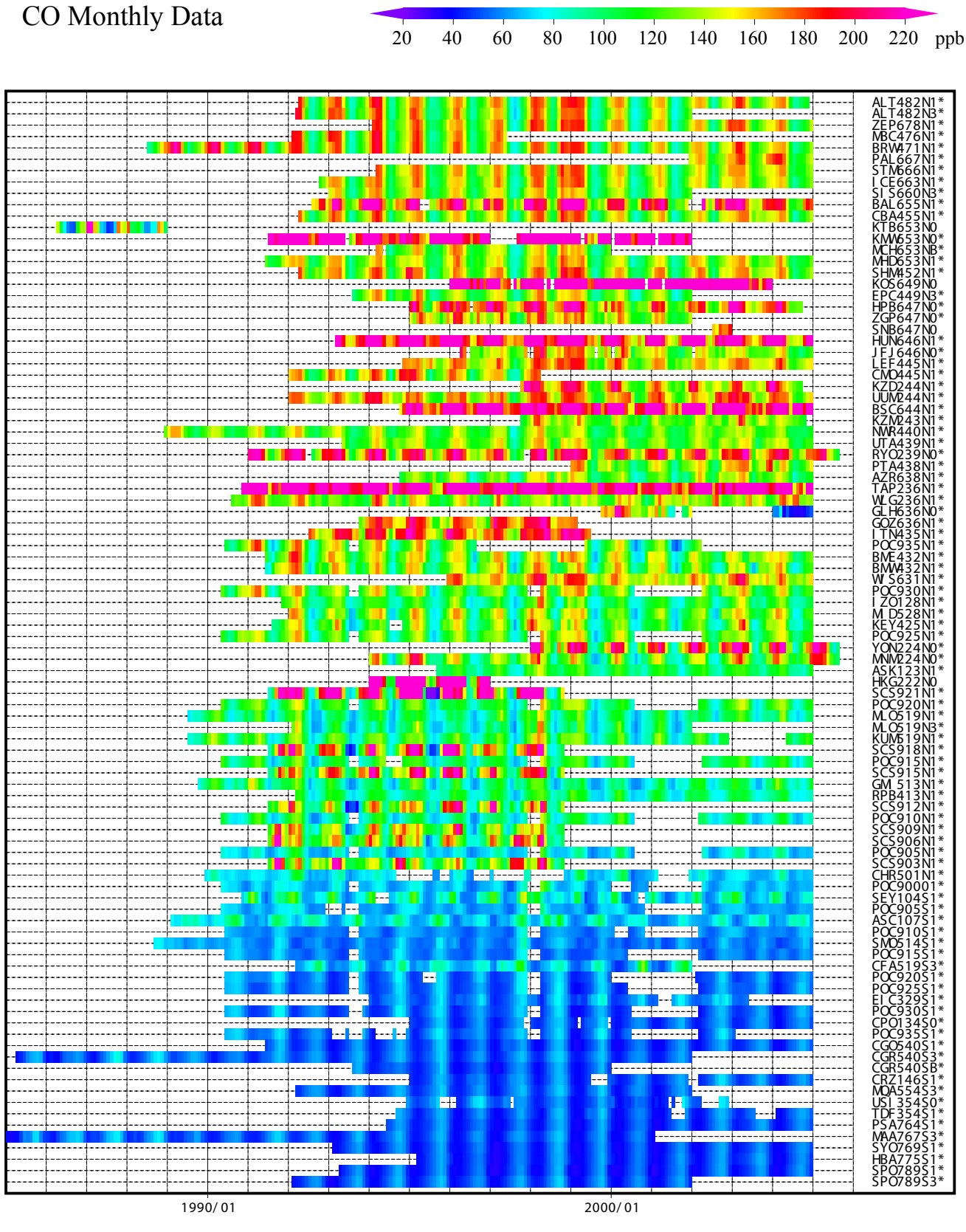

Plate 8.1 Monthly mean mixing ratios of CO for all stations reported to the WDCGG. The stations are set from north to south. Station index with an asterisk shows the station used in the analysis shown in Plate 8.2.
(see Chapter 2)

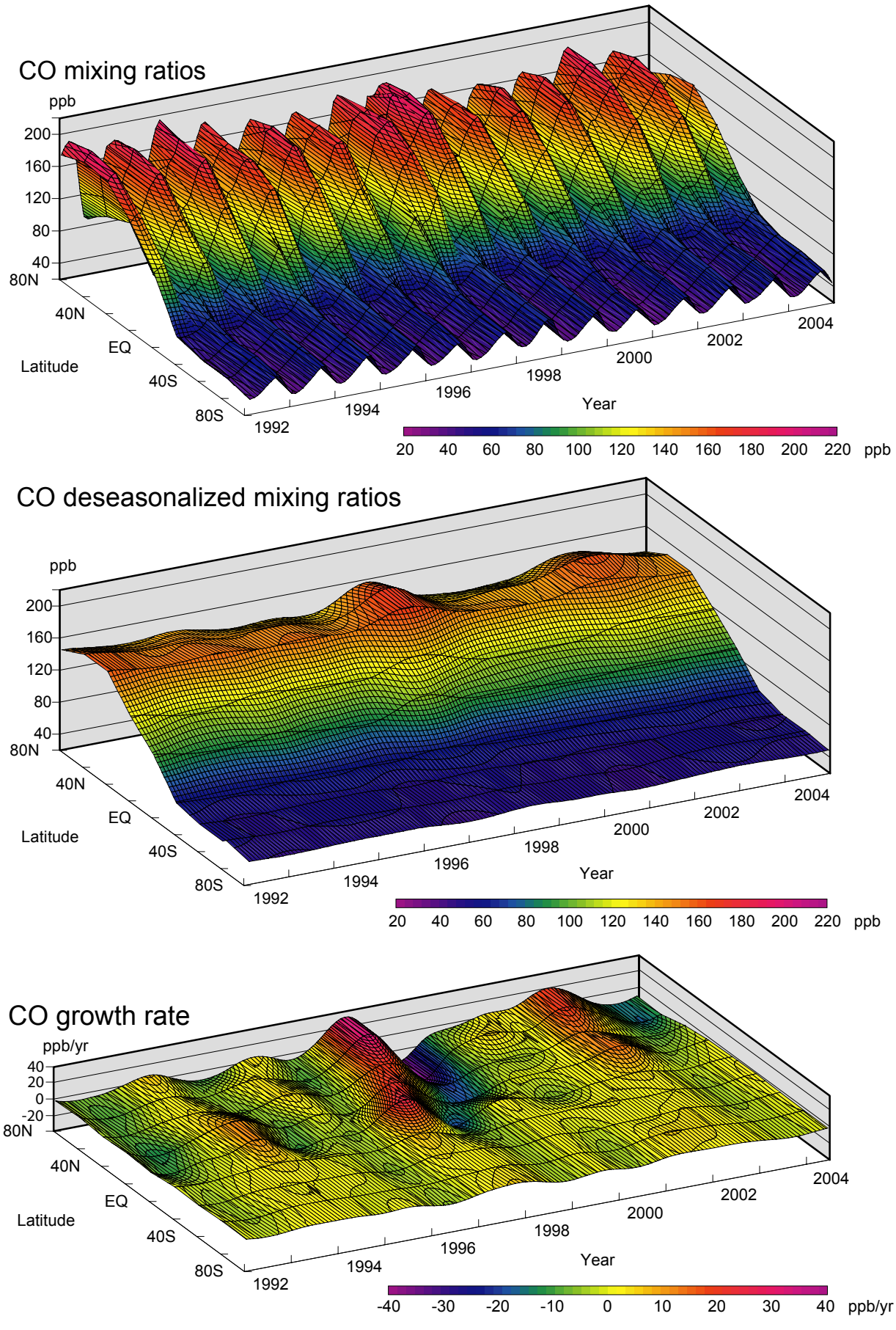

Plate 8.2 Variation of zonally averaged monthly mean CO mixing ratios (top), deseasonalized mixing ratios (middle), and growth rates (buttom). Zonally averaged mixing ratios are calculated for each 20° zone. Deseasonalized mixing ratios and growth rates are derived as described in Chapter 2.

8. Carbon Monoxide (CO)

Basic information on CO with regard to environmental issues

Carbon monoxide (CO) is not a significant greenhouse gas as it absorbs little infrared radiation from the Earth. However, it does have an influence on oxidisation in the atmosphere through interaction with hydroxyl radicals (OH), which also react with methane, halocarbons and tropospheric ozone. The eventual indirect influence of current CO emission on radiative forcing has been estimated to be greater than the direct influence of N_2O (Daniel and Solomon, 1998). In addition, CO is identified in IPCC (2001) as an important indirect greenhouse gas.

Sources of atmospheric CO include fossil fuel combustion and biomass burning along with the oxidisation of both natural and anthropogenic methane and non-methane hydrocarbons (NMHC). Major sinks are primarily reaction with OH and surface deposition. The lifetime of CO in the atmosphere is relatively short (a few months), so that anthropogenic CO emission does not lead to CO accumulation in the atmosphere, unlike CO_2. Furthermore, uneven distribution of the sources causes large spatial and temporal variation of CO. Using this feature, CO could be used as a tracer of anthropogenic pollution.

CO measurements in ice cores have indicated that the CO mixing ratio of about 50 ppb had not changed markedly during the last two millennia over central Antarctica and that it increased to 110 ppb in 1950 in Greenland (Haan and Raynaud, 1998). CO mixing ratio had increased at a rate of 1% per year since 1950, but started to decrease in the late of 1980s (WMO, 1998). At present, the CO mixing ratio is decreasing at about 0.5 ppb per year, except for temporal enhancement from outbreaks of large biomass burning (Novelli *et al*., 2004). In recent years, CO emission from large scale forest fires has been widely noticed, and CO emission from biomass burning including forest fires is considered to account for 30% of the total CO emission in the globe (Holloway *et al*., 2000).

The global CO distribution and the budget have been estimated using satellite observations and inverse methods, but estimated anthropogenic emissions are larger than the inventories from industrial statistics (Bergamaschi *et al*., 2000; Kasihbhatla *et al.*, 2002; Arellano Jr *et al*., 2004).

Annual variation of CO in the atmosphere

The map at the beginning of this chapter shows observation sites that have submitted CO data to the WDCGG.

The time series of monthly mean CO data from all the stations that submitted to WDCGG are shown in Plate 8.1. Mixing ratio levels are illustrated in different colours. Global, hemispheric and zonal mean mixing ratios were calculated based on selected stations (see the caption for Plate 8.2).

The three-dimensional representations of latitudinal distribution of atmospheric CO mixing ratios, deseasonalized mixing ratios and growth rate (yearly difference in mixing ratio) are shown in Plate 8.2.

Please note that the CO data are reported in various units, *i.e.*, ppb, $\mu g/m^3$-25°C, $\mu g/m^3$-20°C and mg/m^3-25°C. All units can be converted to ppb as follows:

$$X_p\,[ppb] = (R * T / M / P_0) * 10 * X_g\,[\mu g/m^3]$$
$$X_p\,[ppb] = (R * T / M / P_0) * 10^4 * X_g\,[mg/m^3]$$

where R is the molar gas constant (8.31451 [J/K/mol]),
T is the absolute temperature reported by an individual station,
M is the molecular weight of CO (28.0101),
P_0 is the standard pressure (1013.25 [hPa]).

Plates 8.2 and 8.3 show that the seasonal variation of CO is largest in the middle latitudes in the Northern Hemisphere and is small in the Southern Hemisphere. The deseasonalized mixing ratio is highest in the middle latitudes in the Northern Hemisphere and low in the Southern Hemisphere. These results are practically consistent with the global CO distribution derived from a combination of satellite observations and computational models. (Bergamaschi *et al.*, 2000; Holloway *et al*., 2000; Clerbaux *et al*., 2001). The latitudinal gradient of CO is large from the Northern middle latitudes to Southern low latitudes, and is small in Southern Hemisphere. This is due to that the numerous CO sources exist in the Northern middle latitudes and CO being destroyed in the tropics where OH radicals are abundant.

The global monthly mean mixing ratios, their deseasonalized long-term trends and growth rates are shown in Figure 8.1. Growth rates were high in 1993/1994, 1997/1998 and 2002, and low in 1992 and 1998/1999. The global annual mean mixing ratio was about 94 ppb in 2004.

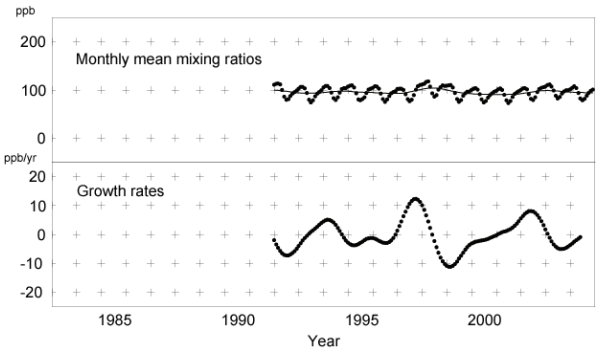

Fig. 8.1 Global monthly mean mixing ratios (thick line and dots) and deseasonalized long-term trends (thin line) (top) and the growth rate (bottom) from 1992 to 2004.

Figure 8.2 shows the monthly mean mixing ratios and their deseasonalized long-term trends for each 30° latitudinal zone. A seasonal variation is seen in both hemispheres. In the Northern Hemisphere, the mixing ratio is higher in the winter season. Amplitudes of the seasonal cycle are larger in the Northern Hemisphere than in the Southern Hemisphere.

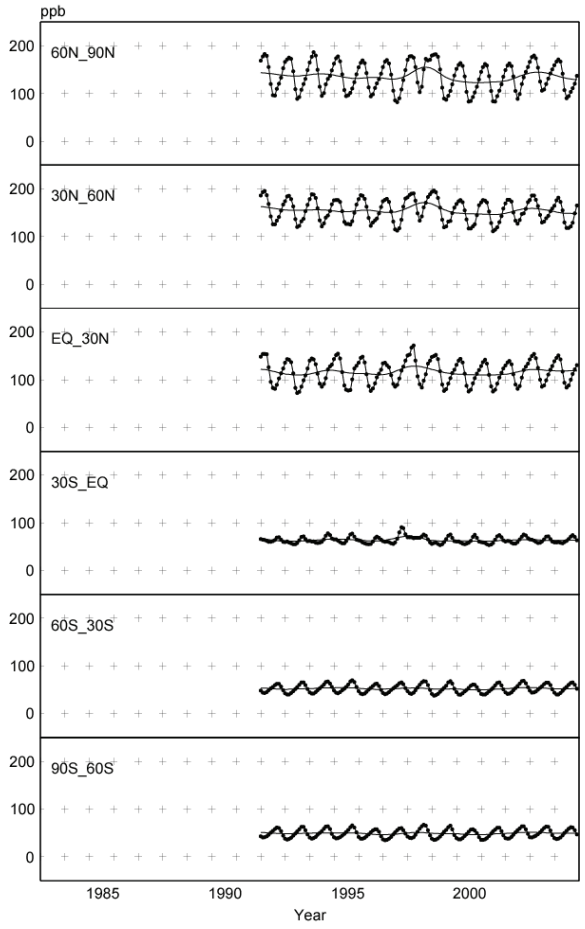

Fig. 8.2 Monthly mean CO mixing ratios (thick lines and dots) and deseasonalized long-term trends (thin lines) from 1992 to 2004 for each 30° latitudinal zone.

Figure 8.3 shows the deseasonalized long-term trends and growth rates for each 30° latitudinal zone. CO mixing ratios are generally higher in northern than in southern regions.

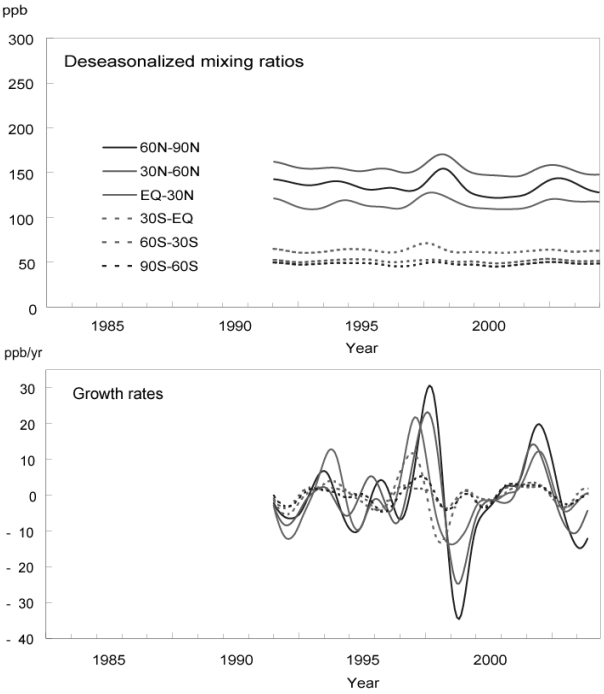

Fig. 8.3 Deseasonalized long-term trends (top) and growth rates (bottom) for each 30° latitudinal zone.

Annual variation of atmospheric flow can influence CO mixing ratio variation as shown by Allen *et al.* (1996). However, a negative growth rate was seen in 1992 in all latitudes. Novelli *et al.* (1998) showed a clear decline in CO mixing ratios from late 1991 through mid-1993, with a subsequent recovery from mid-1993 through mid-1994. The decline in CO mixing ratios almost coincides with the decrease in growth rate of the CH_4 mixing ratio, which can be ascribed to the variations in their common sink. Enhanced stratospheric ozone depletion due to the increase in volcanic aerosols from the eruption of Mt. Pinatubo in 1991 may have increased the mixing ratio of OH, which reacts with both CO and CH_4 (Dlugokencky *et al.*, 1996). Increases in CO mixing ratios were observed from 1997 to 1998 in northern latitudes and southern low latitudes. This increase was attributed to the large biomass burning around Indonesia in late 1997 and that around Siberia between summer and autumn 1998 (Novelli *et al.*, 1998). The regular observation using passenger aircraft of Japan Air Line showed enhanced CO mixing ratios over the tropical Pacific at 10 km altitudes and model simulation showed that the large biomass burning in Southeast Asia brought about this CO enhancement (Matsueda *et al.*, 1998; Matsueda *et al.*, 2002; Taguchi

et al., 2002). Duncan *et al.* (2003) also suggested that CO emission in 1997 and 1998 was 19-32% greater than that in 1999. The mixing ratios returned to normal levels after 1999, but the growth rates in the Northern Hemisphere increased again substantially in 2002. This increase in CO mixing ratios in 2002 might be also attributed to large biomass burning.

Seasonal cycle of CO in the atmosphere

Figure 8.4 shows the average seasonal cycles for each 30° latitudinal zone from which the long-term trends were subtracted. The seasonal cycle of CO is mainly driven by seasonal variations in OH mixing ratio, which acts as a CO sink. Furthermore, emission and oxidation as CO sources and the large-scale transportation of CO are additional factors, although the seasonality of emission and oxidation is relatively weak compared with that of the OH mixing ratio. This seasonality and the roughly a few months lifetime of CO produce a sharp decrease in early summer and a relatively gradual increase in autumn. Semi-annual features evident in the southern low latitudes may be attributed to the cross-equatorial transportation of CO from the Northern Hemisphere.

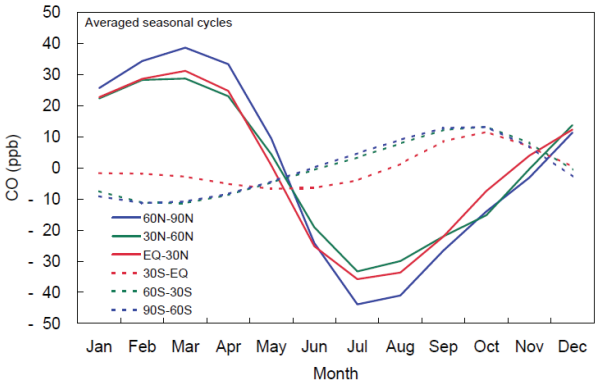

Fig. 8.4 Average seasonal cycles for each 30° latitudinal zone from which the long-term trends were subtracted.

Direct CO emission also brings about intense seasonal variation on some occasions. Novelli *et al.* (1998) showed with a model of a box representing the well-mixed northern layer and a box representing the southern boundary layer that seasonal cycles are strongly affected by changes in emission from biomass burning in both hemispheres. Using observation data for the upper troposphere, Matsueda *et al.* (1998) showed that high CO mixing ratios in southern low latitudes from October to November were enhanced by tropical biomass burning.

9.
NITROGEN MONOXIDE (NO)
and
NITROGEN DIOXIDE (NO_2)

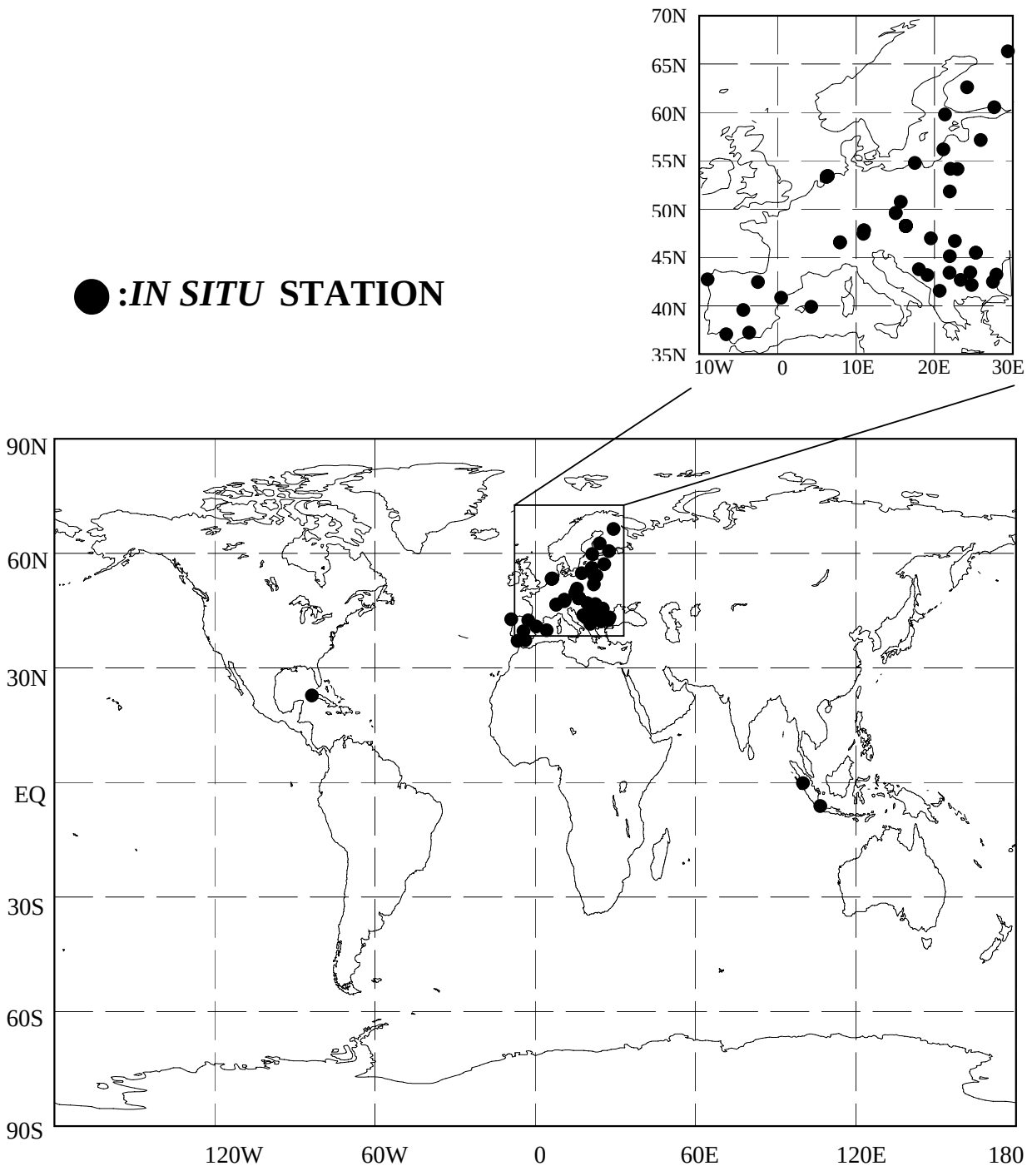

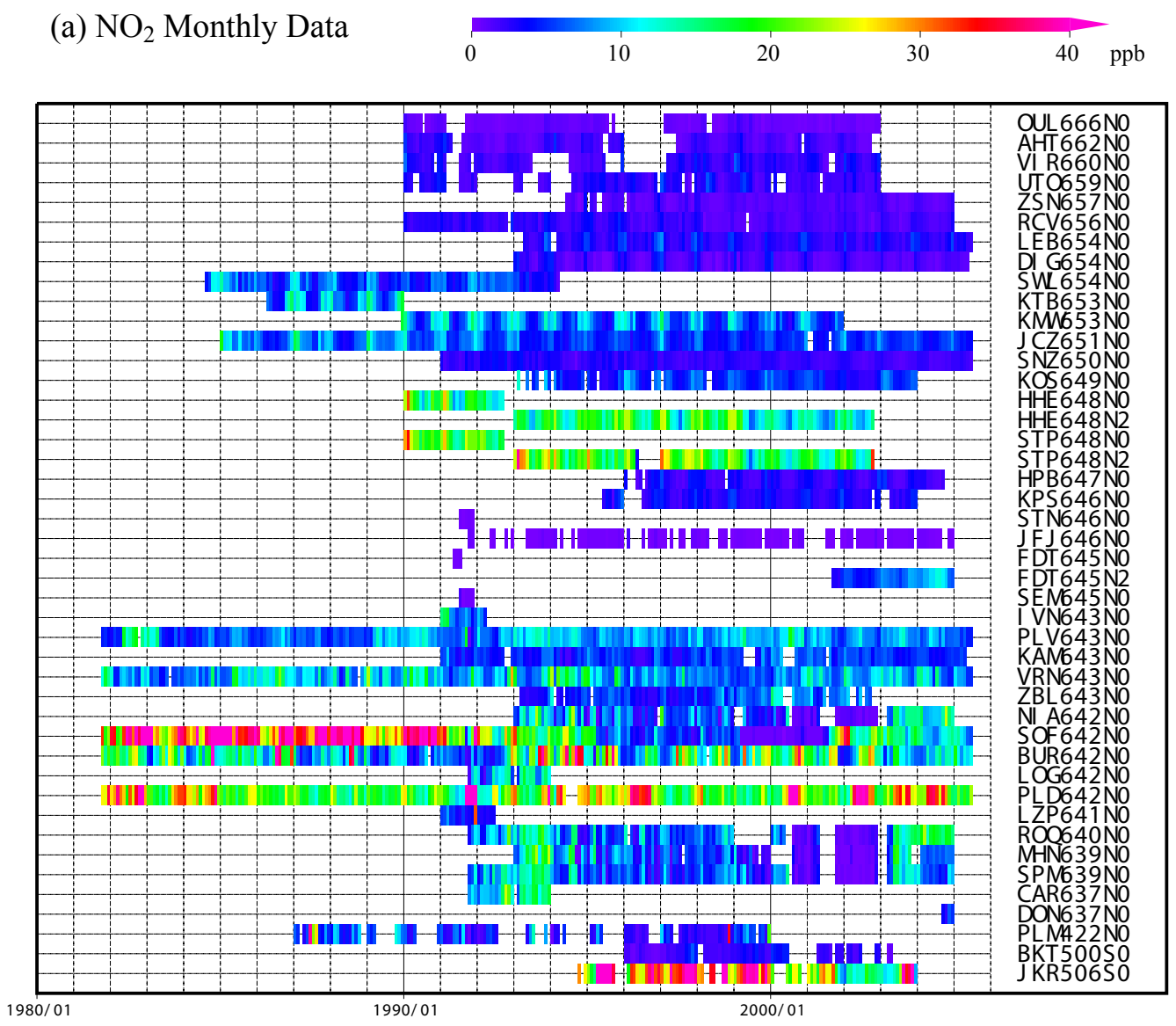

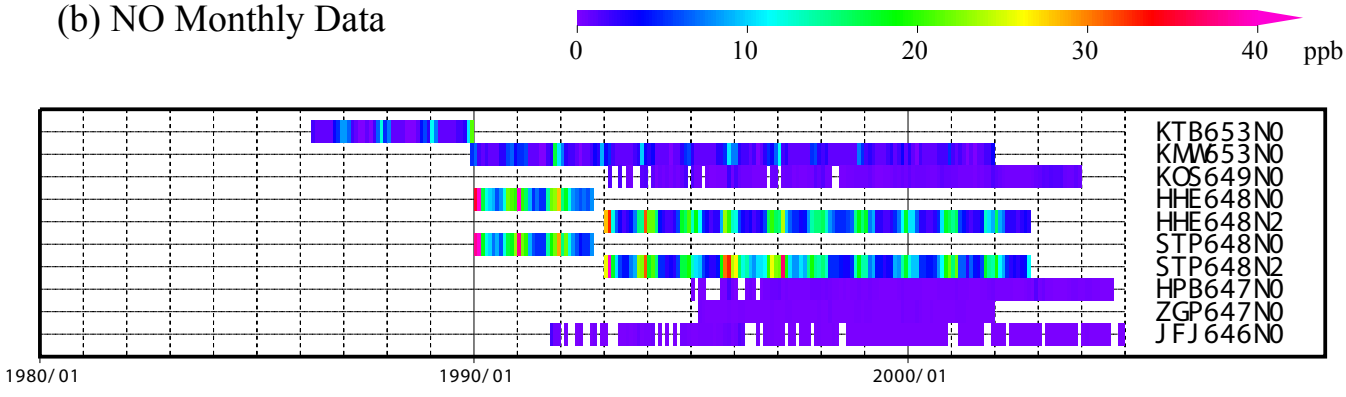

Plate 9.1 Monthly mean (a) NO_2 and (b) NO mixing ratios for all sites reported to the WDCGG illustrated in colors that change with the mixing ratio. The sites are set from north to south.

9. Nitrogen Monoxide (NO) and Nitrogen Dioxide (NO_2)

Basic information on NO and NO_2 with regard to environmental issues

Nitrogen oxides (NO_x, *i.e.*, NO and NO_2) are not greenhouse gases, but affect hydroxyl radicals (OH), which control many substances in the atmosphere such as methane (CH_4), carbon monoxide (CO) and hydrochlorofluorocarbons (HCFCs). In the presence of NO_x, CO and hydrocarbons are oxidised to produce ozone (O_3) in the troposphere, which is one of strong greenhouse gases. Thus, NO_x can influence the Earth's radiative balance and, by generating OH, alter the oxidisation capacity of the atmosphere.

Sources of NO_x include fossil fuel combustion, biomass burning, lightning and soil (IPCC, 2001). The dominant sink of NO_x in the atmosphere is its conversion into nitric acid (HNO_3) and peroxyacetylnitrate (PAN), which are eventually removed by dry or wet deposition. In some cases, NO_x are removed from the atmosphere directly by dry deposition. Anthropogenic emission of NO_x is currently one of the major causes of acid rain and deposition. NO_x mixing ratios show large variability in both space and time because of the species' short lifetimes and uneven source distribution.

Annual variation of NO and NO_2

Observation stations that submitted data for NO_2 and NO to the WDCGG are shown on the map at the beginning of this chapter. Most of the contributing stations are located in Europe.

The time series of monthly mean NO and NO_2 data from all stations submitted to the WDCGG are shown in Plate 9.1. In this plate, mixing ratio levels are illustrated in different colours. Please note that the data for NO_x are reported in various units, *i.e.*, ppb, $\mu g/m^3$-25°C, $\mu g/m^3$-20°C, $\mu gN/m^3$-25°C and mg/m^3-25°C.

All units can be converted to ppb as follows:

$$X_p\,[ppb] = (R * T / M / P_0) * 10 * X_g\,[\mu g/m^3]$$
$$X_p\,[ppb] = (R * T / M / P_0) * 10^4 * X_g\,[mg/m^3]$$
$$X_p\,[ppb] = (R * T / M_N / P_0) * 10 * X_g\,[\mu gN/m^3]$$

where R is the molar gas constant (8.31451 [J/K/mol]),
T is the absolute temperature reported by an individual station,
M is the molecular weight of NO (30.00614) or NO_2 (46.00554),
M_N is the atomic weight of N (14.00674), and
P_0 is the standard pressure (1013.25 [hPa]).

As their sources are localised and their lifetimes are short, the distributions of NO and NO_2 are also localised and vary over time. Due to the high temporal variability of NO_2 mixing ratios for each observation site, it was difficult to identify a long-term trend. A number of stations located in southern Europe showed higher mixing ratios, and some stations exhibited a winter enhancement of NO_2.

As the number of observation sites for NO is quite small, it is difficult to identify increasing or decreasing trends for NO mixing ratios.

10.
SULPHUR DIOXIDE
(SO_2)

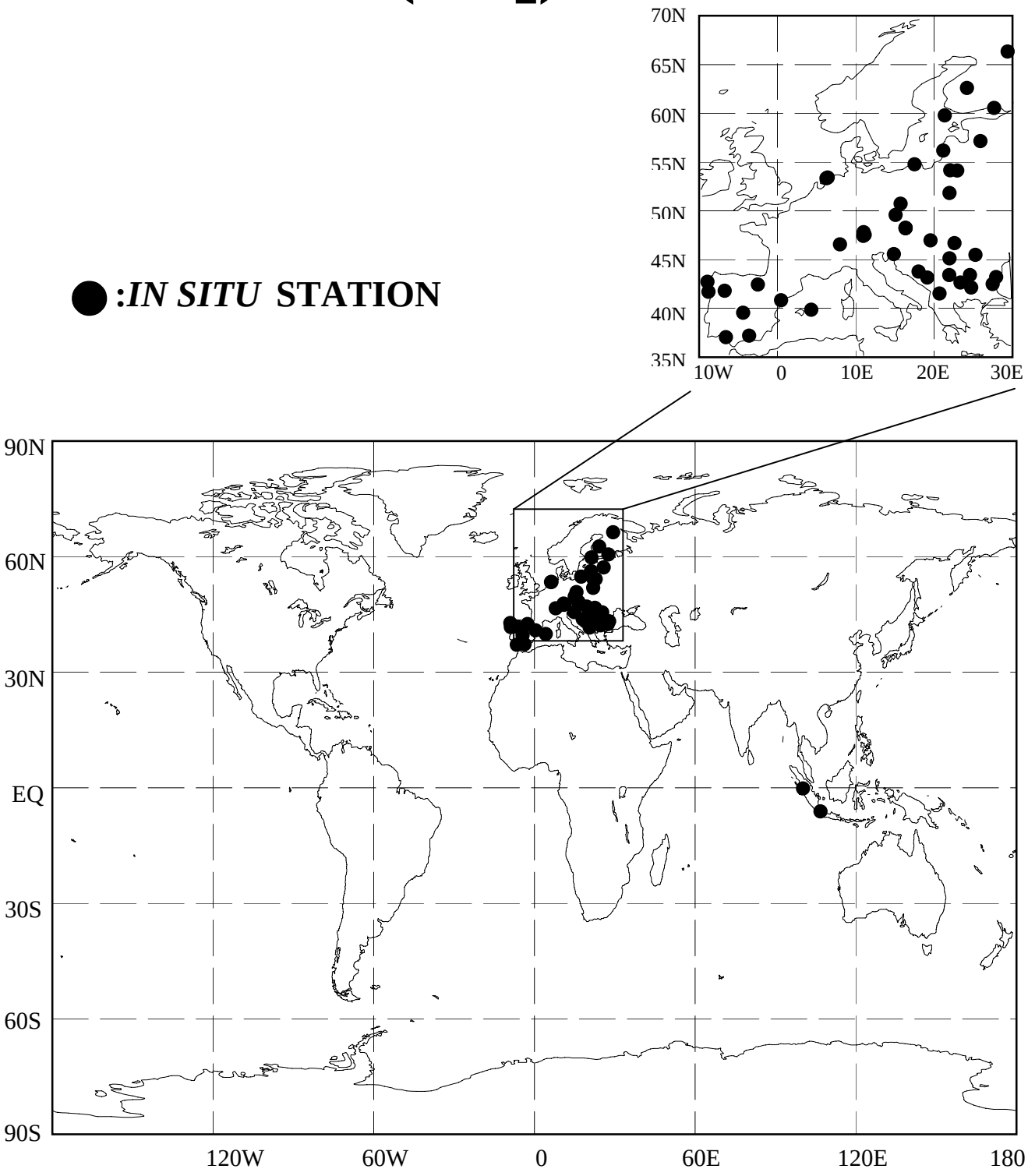

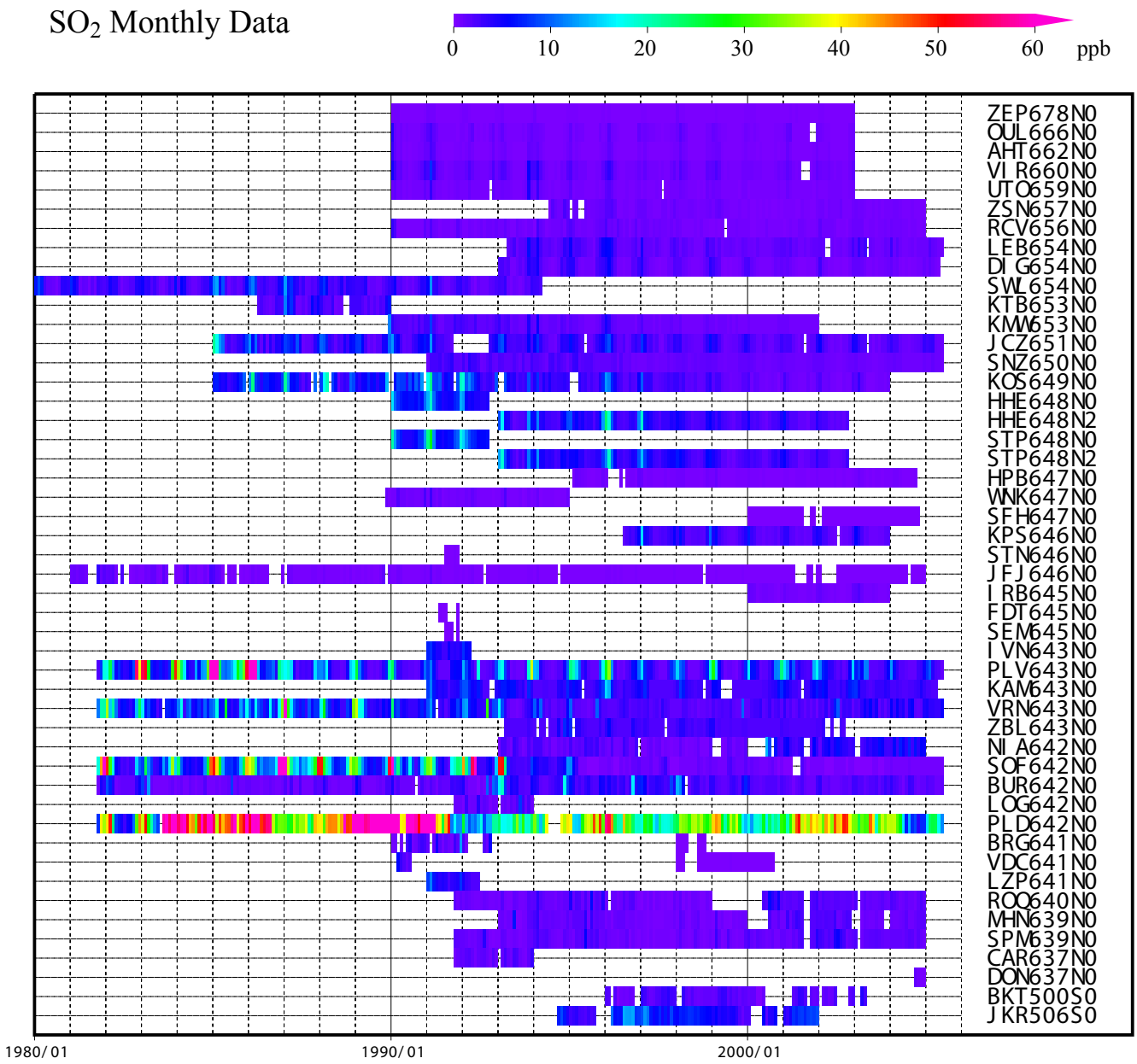

Plate 10.1 Monthly mean SO_2 mixing ratios for all sites reported to the WDCGG illustrated in colors that change with the mixing ratio. The sites are set from north to south.

10. Sulphur Dioxide (SO_2)

Basic information on SO_2 with regard to environmental issues

Sulphur dioxide (SO_2) is not a greenhouse gas, but a precursor of atmospheric sulphuric acid (H_2SO_4) or sulphate aerosol. SO_2 is oxidised by hydroxyl radicals (OH) to form sulphuric acid, which then produces aerosols through photochemical gas-to-particle conversion. While the SO_2 reaction with OH is much slower than with NO_2, SO_2 dissolves readily in suspended liquid droplets in the atmosphere.

Sources of SO_2 include fossil fuel combustion by industry, biomass burning, volcanoes and the oxidation of dimethylsulphide (DMS) from the oceans (IPCC, 2001). Major SO_2 sinks are oxidation by OH and deposition onto wet surfaces. Anthropogenic SO_2 has caused acid rain and deposition throughout the industrial era. SO_2 mixing ratios show large variations in both space and time because of the species' short lifetime and uneven anthropogenic source distribution.

Annual variation of SO_2

The map at the beginning of this chapter shows observation sites that have submitted SO_2 data to the WDCGG. Most of the contributing stations are located in Europe.

The monthly mean SO_2 data from all stations submitted to the WDCGG are shown in Plate 10.1. In this plate, mixing ratio levels are illustrated in different colours. Please note that the data for SO_2 are reported in various units, *i.e.*, ppb, $\mu g/m^3$, mg/m^3 and $\mu gS/m^3$.

All units can be converted to ppb as follows:

$$X_p\,[ppb] = (R * T / M / P_0) * 10 * X_g\,[\mu g/m^3]$$
$$X_p\,[ppb] = (R * T / M / P_0) * 10^4 * X_g\,[mg/m^3]$$
$$X_p\,[ppb] = (R * T / M_S / P_0) * 10 * X_g\,[\mu gS/m^3]$$

where R is the molar gas constant (8.31451 [J/K/mol]),
T is the absolute temperature reported by an individual station,
M is the molecular weight of SO_2 (64.0648),
M_S is the atomic weight of S (32.066), and
P_0 is the standard pressure (1013.25 [hPa]).

Certain stations in southern Europe showed higher mixing ratios. However, it was difficult to identify an increasing or decreasing trend for SO_2 mixing ratios.

References

Allen, D. J., P. Kasibhatla, A. M. Thompson, R. B. Rood, B. G. Doddridge, K. E. Pickering, R. D. Hudson, and S.-J. Lin, Transport-induced interannual variability of carbon monoxide determined using a chemistry and transport model, *J. Geophys. Res.,* **101**, 28655-28669, 1996.

Angert A., S. Biraud, C. Bonfils, W. Buermann, I. Fung, CO_2 seasonality indicates origins of post-Pinatubo sink, *Geophys. Res. Lett.*, **31**, L11103, doi:10.1029/2004GL019760, 2004.

Arellano Jr., A. F., P. S. Kasibhatla, L. Giglio, G. R. Werf, J. T. Randerson, Top-down esitmates of global CO sources using MOPITT measurements, *Geophys. Res. Lett*., **31**, L01104, doi:10.1029/2004GL018609, 2004.

Bartlett, B. B., G. W. Sache, T. Slate, C. Haward, and D. D. Blake, Large-scale distribution of CH_4 in the western Pacific: Sources and transport from the Asian continent, *J. Geophys. Res*., **108 (D20),** 8807, doi:10.1029/2002JD003076, 2003.

Bekki, S., K. S. Law, and J. A. Pyle, Effects of ozone depletion on atmospheric CH_4 and CO concentrations, *Nature*, **371**, 595-597, 1994.

Bekki, S., K. S. Law, Sensitivity of atmospheric CH_4 growth rate to global temperature change observed from 1980 to 1992, *Tellus*, **49B**, 409-416, 1997.

Bergamaschi, P., R. Hein, M. Heimann, and P. J. Crutzen, Inverse modeling of the global CO cycle, 1. Inversion of CO mixing ratios, *J. Geophys. Res.,* **105(D2)**, 1909-1928, 10.1029/1999JD900818, 2000.

Ciais, P., P. P. Tans, M. Trolier, J. W. C. White, and R. J. Francey, A large northern hemisphere terrestrial CO_2 sink indicated by the $^{13}C/^{12}C$ ratio of atmospheric CO_2, *Science*, **269**, 1098-1102, 1995.

Clerbaux, C, J. Hadji-Lazaro, D. Hauglustaine, G. Megie, B. Khattatov, and J-F. Lamarque, Assimilation of carbon monoxide meaured from satellite in a three-dimensional chemistry-transport model. *J. Geophys. Res.,* **106(D14)**, 15385-15394, 2001.

Cleveland, W. S., S. J. Devlin, Locally weighted regression: an approach to regression analysis by local fitting, *J. Amer. Statist. Assn.*, **83**, 596-610, 1988.

Conway, T. J., P. P. Tans, L. S. Waterman, K. W. Thoning, D. R. Kitzis, K. A. Masarie, and N. Zhang, Evidence for interannual variability of the carbon cycle from the National Oceanic and Atmospheric Administration/Climate Monitoring and Diagnostics Laboratory global air sampling network, *J. Geophys. Res.*, **99**, 22831-22855, 1994.

Daniel, J. S. and S. Solomon, On the climate forcing of carbon monoxide. *J. Geophys. Res.,* **103(D11)**, 13249-13260, 1998.

Dettinger, M. D. and M. Ghill, Seasonal and interannual variations of atmospheric CO_2 and climate, *Tellus*, **50B**, 1-24, 1998.

Dlugokencky, E. J., L. P. Steele, P. M. Lang, and K. A. Masarie, The grouth rate and distribution of atmospheric methane, *J. Geophys. Res*., **99**, 17021-17043, 1994.

Dlugokencky, E. J., E. G. Dutton, P. C. Novelli, P. P. Tans, K. A. Masarie, K. O. Lantz, and S. Mardronich, Changes in CH_4 and CO growth rates after the eruption of Mt. Pinatubo and their link with changes in tropical tropospheric UV flux, *Geophys. Res. Lett.*, **23**, 2761-2764, 1996.

Dlugokencky, E. J., K. A. Masarie, P. M. Lang, and P. P. Tans, Continuing decline in the growth rate of the atmospheric methane burden, *Nature*, **393**, 447-450, 1998.

Dlugokencky, E. J., B. P. Walter, K. A. Masarie, P. M. Lang and E. S. Kasischke, Measurements of an anomalous global methane increase during 1998, *Geophys. Res. Lett.*, **28**, 499-502, 2001.

Duchon, C. E., Lanczos filtering in one and two dimensions, *J. Appl. Meteor.*, **18**, 1016-1022, 1979.

Duncan, B. N., I. Bey, M. Chin, L. J. Mickley, T. D. Fairlie, R. V. Martin, and H. Matsueda, Indonesian wildfires of 1997: Impact on tropospheric chemistry, *J. Geophys. Res*., **108 (D15)**, 4458, doi:10.1029/2002JD003195, 2003.

Etherridge, D. M., L. P. Steele, R. J. Francey, and R. L. Langenfelds, Atmospheric methane between 1000 A.D. and present: Evidence of anthropogenic emissions and climatic variability, *J. Geophys. Res.*, **103**, 15979-15993, 1998.

Francey, R. J., P. P. Tans, C. E. Allison, I. G. Enting, J. W. C. White, and M. Trolier, Changes in oceanic and terrestrial carbon uptake since 1982, *Nature*, **373**, 326-330, 1995.

Gu, L., D. D. Baldocchi, S. C. Wofsy, J. W. Munger, J. J. Michalsky, S. P. Urbanski, and T. A. Bonden, Response of a deciduous forest to the Mount Pinatubo eruption enhanced photosysthesis, *Science*, **299**, 2035-2038, 2003.

Haan, D. and D. Raynaud, Ice core record of CO variations during the last two millennia: atmospheric implications and chemical

interactions within the Greenland ice, *Tellus*, **50B**, 253-262, 1998.

Hansen, J., A.Lacis, R. Ruedy, and M. Sato, Potential Clim. Impact of Mount-Pinatubo Eruption, *Geophys. Res. Lett.,* **19(2)**, 215-218, 1992.

Holloway, T., H. Levy II, and P. Kasibhatla, Global distribution of carbon monoxide. *J. Geophys. Res.,* **105(D10)**, 12123-12148, 2000.

IPCC, Climate Change 2001: The Science Basis, Contribution of Working Group I to the Third Assessment Report of the Intergovernmental Panel on Climate Change, Cambridge University Press, Cambridge, United Kingdom and New York, NY, USA, 881pp, 2001.

Kasibhatla, P., A. Arellano, J. A. Logan, P. I. Palmer, and P. Novelli, Top-down estimate of a large source of atmospheric carbon monoxide associated with fuel combustion in Asia. *Geophys. Res. Lett.,* 29(19), 1900, doi:10.1029/2002GL015581, 2002.

Keeling, C. D., R. B. Bacastow, A. F. Carter, S. C. Piper, T. P. Whorf, M. Heimann, W. G. Mook, and H. Roeloffzen, A three-dimensional model of atmospheric CO_2 transport based on observed winds: 1. Analysis of observational data, in aspects of climate variability in the Pacific and the Western Americas, edited by D. H. Peterson, *Geophysical Monograph* **55**, 165-236, American Geophysical Union, Washington, D.C, 1989.

Keeling, C. D., T. P. Whorf, M. Wahlen, and J. van der Plicht, Interannual extremes in the rate of rise of atmospheric carbon dioxide since 1980, *Nature*, **375**, 666-670, 1995.

Lambert, G., P. Monfray, B. Ardouin, G. Bonsang,, A.Gaudry, V. Kazan and G. Polian, Year-to-year changes in atmospheric CO_2, *Tells*, **47B**, 35-55,1995.

Lelieveld, J., P. J. Crutzen, and F. J. Dentener: Changing concentration, lifetime and climate forcing of atmospheric methane, *Tellus*, **50B**, 128-150, 1998.

Lowe, D. C., M. R. Manning, G. W. Brailsford, and A. M. Bromley, The 1991-1992 atmospheric methane anomaly: Southern hemisphere ^{13}C decrease and growth rate fluctuations, *Geophys. Res. Lett.*, **24**, 857-860, 1997.

Marenco, A, and F. Said: Meridional and vertical ozone distribution in the background troposphere from Scientific aircraft measurements during the STRATOZ III experiment. *Atmos. Env.,* **23**, 201-214, 1989.

Matsueda, H., H. Inoue, Y. Sawa, Y. Tsutsumi, and M. Ishii, Carbon monoxide in the upper troposphere over the western Pacific between 1993 and 1996, *J. Geophys. Res.*, **103**, 19093-19110, 1998.

Matsueda, H., S. Taguchi, H.Y. Inoue, and M. Ishii, A large impact of tropical biomass burning on CO and CO_2 in the upper troposphere. *Science in China (Series C)*, **45**, 116-125, 2002.

Morimoto, S., T. Nakazawa, K. Higuchi, and S. Aoki, Latitudinal distribution of atmospheric CO_2 sources nad sinks inferred by $\delta\ ^{13}C$ measurements from 1985 to 1991. *J. Geophys. Res*., **105(D19)**, 24,315-24,326, 2000.

Nakazawa, T., K. Miyashita, S. Aoki, and M. Tanaka, Temporal and spatial variations of upper tropospheric and lower stratospheric carbon dioxide, *Tellus*, **43B**, 106-117, 1991.

Nakazawa, T., S. Morimoto, S. Aoki and M. Tanaka, Time and space variations of the carbon isotopic ratio of tropospheric carbon dioxide over Japan, *Tellus*, **45B**, 258-274, 1993.

Nakazawa, T., S. Morimoto, S. Aoki and M. Tanaka, Temporal and spatial variations of the carbon isotopic ratio of atmospheric carbon dioxide in the western Pacific region, *J. Geophys. Res.*, **102**, 1271-1285, 1997a.

Nakazawa, T., S. Murayama, M. Toi, M. Ishizawa, K. Otonashi, S. Aoki and S. Yamamoto, Temporal variations of CO_2 concentration and its carbon and oxygen isotopic ratios in a temperate forest in the central part of the main island of Japan, *Tellus*, **49B**, 364-381, 1997b.

Nemry, B., L. Francois, P. Warnant, F. Robinet, and J.C. Gerard, The seasonality of the CO_2 exchange between the atmosphere and the land biosphere: A study with a global mechanistic vegetation model, *J. Geophys. Res.*, **101**, 7111-7125, 1996.

Novelli, P. C., K. A. Masarie, and P. M. Lang, Distributions and recent changes of carbon monoxide in the lower troposphere, *J. Geophys. Res.*, **103**, 19015-19033, 1998.

Novelli, P. C., K. A. Masarie, P. M. Lang, B. D. Hall, R. C. Myers, and J. W. Elkins, Reanalysis of tropospheric CO trends: Effects of the 1997-1998 wildfires. *J. Geophys. Res.,* **108(D15)**, 4464, doi:10.1029/2002JD003031, 2004.

Prinn, R. G., J. Huang, R. F. Weiss, D. M. Cunnold, P. J. Fraser, P. G. Simmonds, A. McCulloch, C. Harth, P. Salameh, S. O'Doherty, R. H. J. Wang, L. Porter and B. R. Miller, Evidence for substantial variations of atmospheric hydroxyl radicals in the past two decades, *Science*, **292**, 1882-1888, 2001.

Rayner, P. J., I. G. Enting, R. J. Francey and R. Langenfelds, Reconstructing the recent carbon cycle from atmospheric CO_2,$\delta^{13}C$ and O_2/N_2 observations, *Tellus*, **51B**, 213-232, 1999.

Ramonet, M. and P. Monfray, CO_2 baseline concept in

3-D atmospheric transport models, *Tellus*, **48B**, 502-520, 1996.

Stenchikov, G., A.Robock, V. Ramaswamy, M. D. Schwarzkopf, K. Hamilton, and S. Ramachandran, Arctic Oscillation response to the 1991 Mount Pinatubo eruption: Effects of volcanic aerosols and ozone depletion, J. Geophys. Res., **107(D24)**, 4803, doi:10.1029/2002JD002090., 2002.

Taguchi, S., H. Matsueda, H. Y. Inoue, and Y. Sawa, Long-range transport of carbon monoxide from tropical ground to upper troposphere: a case study for South East Asia in October 1997. Tellus, **54B**, 22-40, 2002.

Tanaka, M., T. Nakazawa, S. Aoki, Seasonal and meridional variations of atmospheric carbon dioxide in the lower troposphere of the northern and southern hemispheres, *Tellus*, **39B**, 29-41, 1987.

Tsutsumi, Y, Y. Makino, and J. B. Jensen: Vertical and latitudinal distributions of tropospheric ozone over the western Pacific: Case studies from the PACE aircraft missions. J. Geophys. Res., 108(D8), 4251, doi:10.1029/2001JD001374, 2004.

Thoning, K. W., P. P. Tans, and W. D. Komhyr, Atmospheric carbon dioxide at Mauna Loa observatory, 2. Analysis of the NOAA GMCC data, 1974-1985, *J. Geophys. Res.*, **94**, 8549-8565, 1989.

Wittenberg, U., M. Heimann, G. Esser, A.D. Mcguire, and W. Sauf, On the influence of biomass burning on the seasonal CO_2 signal as observed at monitoring stations, *Global Biogeochem. Cycles*, **12**, 531-544, 1998.

WMO, Scientific assessment of ozone depletion: 1998. WMO global ozone research and monitoring project - Report No. 44, World Meteorological Organization, Geneva, 1999a.

WMO, WMO statement on the status of the global climate in 1998, WMO- No.896, World Meteorological Organization, Geneva, 1999b.

WMO, World Data Centre for Greenhouse Gases (WDCGG) Data Summary, WDCGG No. 22, 84pp, 2000.

WMO, Strategy for the Implementation of the Global Atmosphere Watch Programme (2001-2007), WMO/GAW - Report No. 142, 62pp, 2001.

WMO, World Data Centre for Greenhouse Gases (WDCGG) Data Summary, WDCGG No. 28, 98pp, 2004.

APPENDICES

Appendix A Calibration and Standard Scales

1. Calibration System in the GAW programme

Under the Global Atmosphere Watch (GAW) programme, World Calibration Centres (WCCs) are responsible for maintaining calibration standards for certain species, establishing instrument calibrations and providing training to the stations. A Reference Standard is designated for each species to be used for all GAW measurements of that species at Central Calibration Laboratories. Table 1 lists the organizations that serve as WCCs and CCLs for GAW [*WMO*, 2001, 2004].

Table 1. Overview of the GAW Central Calibration Laboratories (GAW-CCL, Reference Standard) and World Calibration Centres for Greenhouse and Other Related Gases (as of December 2003). The World Calibration Centres Have Assumed Global Responsibilities, Except Where Indicated (Am, Americas; E/A, Europe and Africa; A/O, Asia and the South-West Pacific)

Species	Central Calibaration Laboratory (Reference Standard)	World Calibration Centre
Carbon Dioxide (CO_2)	ESRL/GMD	ESRL/GMD
Methane (CH_4)	ESRL/GMD	EMPA (Am, E/A) JMA (A/O)
Nitrous Oxide (N_2O)	ESRL/GMD	IFU
Chlorofluorocarbons (CFCs)		
Surface Ozone (O_3)	NIST	EMPA
Carbon Monoxide (CO)	ESRL/GMD	EMPA
Volatile Organic Compounds (VOCs)		IFU
Sulphur Dioxide (SO_2)		
Nitrogen Oxides (NO_x)		

2. Carbon Dioxide (CO_2)

In 1995, NOAA Earth System Research Laboratory/Global Monitoring Division (ESRL/GMD, former CMDL) took over the role of CCL from the Scripps Institution of Oceanography (SIO) in San Diego, California, USA. ESRL/GMD, Boulder, Colorado, USA has been designated by WMO as the Central Calibration Laboratory (CCL) responsible for maintenance of the GAW Reference Standard for CO_2. As the World Calibration Centre (WCC) for CO_2, ESRL/GMD maintains a high-precision manometric system for absolute calibration of CO_2 as the reference used for GAW measurements throughout the world [*Zhao et al.*, 1997]. It is recommended that the standards of the GAW measurement laboratories be calibrated every two years at the CCL (WMO, 2003).

Under the WMO calibration system, there have been several calibration scales for CO_2 data, *e.g.*, SIO-based X74, X85, X87 and X93 scales and the ESRL/GMD-based WMO Mole Fraction Scale partially based on the past SIO scales. The ESRL/GMD and SIO are working to resolve the possible small differences between their scales. The CCL will adopt the WMO X2002 scale, reflecting historical manometric calibrations of the WMO CCL set of 15 cylinders and the possible small differences between SIO and ESRL/GMD calibrations [*ESRL/GMD*, 2002].

To assess the differences in standard scales among CO_2 measuring laboratories, ESRL/GMD organizes intercomparisons or Round Robin experiments endorsed by WMO every few years. Many laboratories participated in the experiments organized in 1991-1992, 1996-1997 and 1999-2000. Table 2 shows the results of the experiments performed in 1996-1997 in which the mixing ratios measured by various laboratories are compared with the mixing ratios measured by NOAA/ESRL/GMD [*Peterson et al.*, 1999]. In addition, many laboratories compare their standards bilaterally or multilaterally among themselves.

Table 3 lists laboratories contributing CO_2 measurement data to WDCGG with standard scales of reported data and history of participation in the WMO intercomparison experiments.

Table 2. Round Robin Results for Carbon Dioxide Mixing ratio. Differences Between the Mixing ratios Measured by Various Laboratories and the Mixing ratio Measured by NOAA (Laboratory minus NOAA, ppm)

Laboratory	Analysis Date	Mixing ratio Difference (ppm)

		Low 340-350 ppm	Medium 350-360 ppm	High 370-380 ppm
NIWA	1996-02	0.02	0.10	0.20
CSIRO	1996-05	-0.07	-0.02	-0.02
AES	1997-06	-0.04	0.00	-0.02
CMA	1995-12	-0.07	-0.01	-0.02
Tohoku Univ.	1996-06	-0.01	0.04	0.02
NIES	1996-08	-0.02	0.09	0.12
MRI	1996-12	0.04	0.07	0.14
JMA	1997-01	0.07	0.31	0.30
SNU	1997-03	0.24	0.13	0.29
CFR	1996-01	0.10	0.08	0.16
IMS	1996-03	0.04	0.06	0.07
ENEA	1996-04	-0.29	-0.06	0.19
UBA	1996-07	0.00	-0.02	0.11
HMS	1996-12	-1.22	-1.04	-0.80

Table 3. Status of Standard Scales and Calibration/Intercomparison for Carbon Dioxide at Laboratories Contributing to the WDCGG as of December 2005.

Laboratory	WDCGG Site Index	Calibration Scale	Most Recent Calibration	WMO Intercomparison
Aichi	MKW234N0	WMO	JMA	
CAMS	WLG236N0	WMO	1994-01 at SIO	96/97, 99/00
CESI	PLR645N00	WMO	2001-12 at ESRL/GMD	99/00
ESRL/GMD	BRW471N0, MLO519N0, SPO789S0, SMO514S0, ESRL/GMD flask network*	WMO	2002-07 at ESRL/GMD	91/92, 96/97, 99/00
CNR	JBN762S0	WMO	ENEA	
CSIRO	CGR540S0, CSIRO flask network**	WMO	2001-11 at ESRL/GMD	91/92, 96/97, 99/00
ENEA	LMP635N0	WMO	2000-08 at ESRL/GMD	91/92, 96/97, 99/00
FMI	PAL667N0	WMO		
Heidelberg		WMO	1998-10 at CMDL	96/97, 99/00
HMS	KPS646N0	WMO	2000-05 at ESRL/GMD	91/92, 96/97, 99/00
IFU	WNK647N0, ZSP647N00	SIO 1974		99/00
IGP	HUA312S0	X81		
IMS	CMN644N0	WMO	1998-10 at ESRL/GMD	91/92, 96/97
INM	IZA128N0	WMO	2002-03 at ESRL/GMD	91/92, 96/97, 99/00
NIWA	BAR541S0	WMO	1995-11 at SIO	91/92, 96/97, 99/00
METRI/SNU	KSN233N0	WMO	2001-09	96/97
JMA	MNM224N0, RYO239N0, YON224N0, ALG99990, EOM99990, RYF99990	WMO	2002-03 at ESRL/GMD	91/92, 96/97, 99/00
KMA	AMY236N0			
KSNU	ISK242N0		MGO	
LSCE	AMS137S0, MHDH653N2	WMO	2002-02 at ESRL/GMD	91/92, 96/97, 99/00
MGO	BER255N0, KOT276N0,	X97	1991 at SIO	

	KYZ240N0, STC652N0, TER669N0			
MISU/NILU	ZEP678N0	WMO	1996-07 at ESRL/GMD	96/97, 99/00
MRI	TKB236N0, INS9999A, HKH99990, KIY99990, NTU99990, RFM99990, WLT99990	MRI 1997		91/92, 96/97, 99/00
MSC	ALT482N0, CSJ451N0, SBL443N0	WMO	2001-12 at ESRL/GMD	91/92, 96/97, 99/00
NIES	COI243N0, HAT224N0	NIES 95	2001-09 at ESRL/GMD	96/97, 99/00
NIMH	FDT645N20		SIAD SpA, Italy	
NIST		NIST		91/92, 96/97, 99/00
RIVM	KMW653N0	NIST		
Saitama	DDR236N0, URW235N0	WMO	JMA	
SAWS	CPO134S0	WMO	1997-06 at ESRL/GMD	99/00
Shizuoka	HMM234N0		Nippon Sanso	
SIO		SIO		91/92, 96/97, 99/00
Tohoku Univ.	SYO769S0	Tohoku		91/92, 96/97, 99/00
UBA	BRT648N0, DEU649N0, NGL653N0, SFH647NA0, SSL647N0, LGB652N0, WST654N0, ZGT654N0, ZGP647N0	WMO	1998-10 at ESRL/GMD	91/92, 96/97, 99/00
ZAMG	SNB647N00	WMO	UBA	

* ESRL/GMD flask network: ALT482N10, AMS137S10, ASC107S10, ASK123N10, BAL655N10, BRW471N10, BSC644N10, NMB123S10, CGO540S10, KUM519N10, CHR501N10, CBA455N10, CRZ146S10, GOZ636N10, EIC329S10, ITN435N10, GMI513N10, HBA775S10, SUM672N10, STM666N10, HUN646N10, ICE663N10, SIS660N30, OPW448N10, CMO445N10, PTA438N10, KZD244N10, KZM243N10, IZO128N10, KEY425N10, MHD653N10, KCO204N10, SEY104S10, MLO519N10, MBC476N10, WLG236N10, NWR440N10, ZEP678N10, STC654N10, STM666N10, POC9XXX10, PSA764S10, LEF445N10, RPB413N10, MID528N10, WIS631N10, SHM452N10, SCS9XXX10, SPO789S10, BMW432N10, AVI417N10, BME432N10, SYO769S10, TAP236N10, AZR638N10, TDF354S10, SMO514S10, UUM244N10, UTA439N10

** CSIRO flask network: AIA999930, ALT482N30, CFA519S30, CGR540S30, EPC449N30, MQA554S30, MLO519N30, MAA767N30, SIS660N30, SPO789S30

3. Methane (CH_4)

The GAW programmes have established two World Calibration Centres (WCCs) for methane: the Swiss Federal Laboratory for Materials Testing and Research (EMPA), Dübendorf, Switzerland and the Japan Meteorological Agency (JMA), Tokyo, Japan [*WMO*, 2001]. In addition, the Central Calibration Centre for methane has been established in NOAA Earth System Research Laboratory/Global Monitoring Division (NOAA/ESRL/GMD) [*WMO*, 2004; *Dlugokencky, et. al.*, 2005].

The new NOAA04 scale has been designated as the Reference Standards of GAW programme. This scale results in CH4 mole fractions that are a factor of 1.0124 greater than the NOAA previous scale. [*Dlugokencky et al.*, 2005]

Table 4 summarizes the methane standard scales used in the laboratories contributing to the WDCGG and lists tentative multiplying conversion factors applied for the analysis in the present issue of *Data Summary* to make the data on different scales more intercomparable. The standard is the NOAA04 scale and conversion factors are calculated from the results of intercomparisons of the mixing ratios with other laboratories bilaterally or multilaterally performed before the establishment of GAW Standards. The conversion factors will be abolished when a station employs the NOAA04 scale.

The former CMDL scale is lower than an absolute gravimetric scale [*Aoki et al.*, 1992] by ~1.5% [*Dlugokencky et al.*, 1994] and lower than the AES (MSC) scale by a factor of 1.0151 [*Worthy et al.*, 1998]. The CSIRO scale can be converted to the Tohoku University standard by multiplying by 1.0119 [*Cunnold et al.*, 2002]. So we adopt the conversion

factors 1.0124/1.0151=0.997 and 1.0119*1.0124/1.0151= 1.0092 to intercompare with the new WMO scale, NOAA04..

Table 4. Status of Methane Standard Scales at Laboratories Contributing to the WDCGG with Conversion Factors Used in the Present Issue of *Data Summary*.

Laboratory	WDCGG Site Index	Calibration Scale	Conversion Factor
AGAGE	CGR540SX, MAT514SX, CME445NX, MCH653NX, RGP413NX, TRH441N0	Tohoku	0.997
CESI	PLR645N00	CMDL	1.0124
CHMI	KOS649N0	NIST	0.9973
ESRL/GMD	BRW471N0, MLO519N0, ESRL/GMD flask network**	NOAA04	1
CSIRO	CSIRO flask network***	CSIRO 94	1.0119
ENEA	LMP635N0	ENEA	0.9973
INM	IZA128N0	CMDL	1.0124
JMA	MNM224N0, RYO239N0, YON224N0, RYF99990, RYF9999A	JMA	0.9973
METRI/SNU	KSN233N0	CMDL	1.0124
MRI	EOM99990, INS9999A, MRI9999A, TKB236N0	MRI	0.9973
NIES	COI243N0, HAT224N0	NIES	0.9973
RIVM	KMW653N0	NIST	0.9973
SAWS	CPO134S0	CMDL	1.0124
Tohoku Univ.	MZH770S0, GRL666N0	Tohoku	0.9973
UBA	DEU649N00, NGL653N00, SFH647NA0, SSL647N00, ZGP647N0	CMDL	1.0124

** ESRL/GMD flask network: ALT482N10, AMS137S10, ASC107S10, ASK123N10, BAL655N10, BRW471N10, SGI354S10, BSC644N10, CGO540S10, KUM519N10, CHR501N10, CBA455N10, CRZ146S10, GOZ636N10, EIC329S10, ITN435N10, GMI513N10, HBA775S10, HUN646N10, ICE663N10, KEY425N10, MHD653N10, SEY104S10, MLO519N10, MBC476N10, WLG236N10, NWR440N10, ZEP678N10, STM666N10, POC9XXX10, PSA764S10, LEF445N10, RPB413N10, MID528N10, WIS631N10, SHM452N10, SCS9XXX10, SPO789S10, BMW432N10, AVI417N10, BME432N10, SYO769S10, TAP236N10, AZR638N10, TDF354S10, SMO514S10, UUM244N10, UTA439N10, PTA438N10, CMO445N10, IZO128N10, KPA432N10, KZD244N10, KZM243N10, MCM777S10, NMB123S10, NZL543S10, OPW448N10, SIO432N10, SUM672N10

*** CSIRO flask network: AIA999930, ALT482N30, CFA519S30, CGR540S30, EPC449N30, MQA554S30, MLO519N30, MAA767N30, SIS660N30, SPO789S30

4. Nitrous Oxide (N_2O)

The Halocarbons and other Atmospheric Trace Species (HATS) Group of the Climate Monitoring and Diagnostics Laboratory (CMDL), NOAA, USA, maintains a set of standards for N_2O [*Hall et al.*, 2001, *Hall et al.*, 2002]. These standards have been designated as Reference Standards of the GAW programme. The HATS Group analyses the standards of laboratories, including the Meteorological Service of Canada (MSC) and the Australian Commonwealth Scientific and Industrial Research Organisation (CSIRO). The Fraunhofer Institut für Atmosphärische Umweltforschung (IFU) in Garmisch-Partenkirchen, Germany, serves as the GAW World Calibration Centre (WCC).

The NOAA CMDL N_2O calibration scale agrees to within 0.3% of that predicted using NIST Standard Reference Materials (at 300 and 330 ppb). According to a results of the Nitrous Oxide and Halocarbons Intercalibration Experiment (NOHALICE) implemented under the International Global Atmospheric Chemistry (IGAC) programme, the difference between the scales of AGAGE (SIO-98) and NOAA/CMDL is 1% or less [*Prinn et al.*, 2000].

Table 5. Status of N_2O Standard Scales at Laboratories Contributing to the WDCGG.

Laboratory	WDCGG Site Index	Calibration Scale
AGAGE	ADR652NA, CGR540SX, MAT514SX,	SIO 1998

	CME445NX, MCH653NX, RGP413NX, TRH441N0	
ESRL/GMD	ALT482NX, BRW471NX, MLO519NX, KUM519N, NWR440NX, SPO789SX, SMO514SX	CMDL 2000
ENEA	LMP635N0	CMDL 2000
JMA	RYO239N0	JMA
KMA	AMY236N0	
METRI	KSN233N0	SIO
MISU	ZEP678N0	
NIES	HAT224N0	NIES
SAWS	CPO134S0	CMDL 2000

5. Surface Ozone (O_3)

The National Institute of Standards and Technology (NIST) has developed and deployed Standard Reference Photometers (SRPs) in the USA and other countries. The GAW has designated the SRP #2 maintained at NIST as the Reference Standard for the GAW programme. The Swiss Federal Laboratory for Materials Testing and Research (EMPA) maintains NIST SRP #15 as the reference for the activities for the GAW World Calibration Centre for Surface Ozone [*Hofer et al.,* 1998]. The traceability and uncertainty of surface ozone within the GAW network were reported by Klausen *et al.,* (2003). Regional Calibration Centres have been established at the Czech Hydrometeorological Institute (CHMI) in Prague, Czech Republic, and Servicio Meteorológico Nacional (SMN) in Buenos Aires, Argentina [*WMO,* 2001]. The former maintains the SRP #17 directly purchased by NIST.

Table 6. Status of Surface Ozone Standard Scales at Laboratories Contributing to the WDCGG.

Laboratory	WDCGG Site Index	Calibration Scale	Audit EMPA-WCC
AWI/DWD	NMY770S0		
AQRB	ALG447N0, BRA450N, CHA446N0, CPS449N0, EGB444N0, EST451N0, ELA449N0, KEJ444N0, LON442N0, SAT448N0, SUT445N0		
BMG	BKT500S0	WMO (NIST & EMPA)	1999, 2001
CAMS	(Mt. Waliguan)	WMO (NIST & EMPA)	2000
CHMI	KOS649N0		
CSIRO	CGR540S0	WMO (NIST & EMPA)	2002
DEFRA	EDM655N0		
DWD	HPB647N0,	WMO (NIST & EMPA)	1997
EARS	IRB645N0, KVK646N0, KVV646N0, ZRN646N0	WMO (NIST & EMPA)	
EMPA	JFJ646N0	WMO (NIST & EMPA)	1999
ESRL/GMD	BRW471N4, ICE663N4, MLO519N4, NWR440N4, RPB413N4, SPO789S4, BME432N4, SUM672N4, SMO514S4, LAV545S4, MCM777S4, NTL440N4, TRH441N4	ESRL/GMD	
FMI	AHT662N0, OUL666N0, PAL667N0, UTO659N0, VIR660N0		
HKPU	HKG222N0		

HMS	KPS646N0		
IM	ANG638N0, BEJ638N0, CAS639N0, FUN132N0, LIS638N0, MVH638N0, PEN640N0		
INM	IZA128N0, MHN639N0, NIA642N0, ROQ640N0, SPM639N0	NPL(U. K.)	1996, 1998, 2000 (Izana)
INMET	(Arembepe)	WMO (NIST & EMPA)	2001
INMH	FDT645N2		
IOEP	DIG654N0		
IVL	VDL664N0		
JMA	RYO239N0, MNM224N0, YON224N0, SYO769S20	JMA	2005 (Ryori)
JMA/AO	TKB236N3		
KMD	(Mt. Kenya)	WMO (NIST & EMPA)	2000, 2002
KSNU	ISK242N0		
LHMA	RCV656N0	WMO (NIST & EMPA)	
MMD	TAR504N0		
NILU	ZEP678N0	WMO (NIST & EMPA)	1997, 2001
NIWA	BAR541S0	WMO (NIST & EMPA)	
NUI	MHD653N0	WMO (NIST & EMPA)	1996, 1998, 2002
ONM	ASK123N0		
Roshydromet	DAK654N0, SHP659N0		
RIVM	KMW653N0		
SAWS	CPO134S0	WMO (NIST & EMPA)	1997, 1998, 2002
SMN	USI354S0	WMO (NIST & EMPA)	1998
UBA	BRT648N0, DEU649N0, NGL653N0, SSL647N0, SNB647N0, LGB652N0, WST654N0, ZGT654N0, ZGP647N0, SFH647NA	WMO (NIST & EMPA)	1996, 1997, 2001 (Zugspitze)
UBA Austria	SNB647N0	WMO (NIST & EMPA)	1998
UM	GLH636N0		

6. Carbon Monoxide (CO)

The Swiss Federal Laboratory for Materials Testing and Research (EMPA) serves as the World Calibration Centre (WCC) under GAW based on its secondary standards calibrated against the standard at NOAA/ESRL/GMD designated as the Reference Standard for GAW.

Table 7. Status of Carbon Monoxide Standard Scales at Laboratories Contributing to the WDCGG.

Laboratory	WDCGG Site Index	Calibration Scale	Audit EMPA-WCC
AGAGE	CGR540SX, MCH653NX	SIO 98	
CAMS	(Mt. Waliguan)	WMO (CMDL & EMPA)	2000
CHMI	KOS649N0	Observer	
CMDL	CMDL flask network*	WMO (CMDL & EMPA)	
CSIRO	CSIRO flask network**	WMO (ESRL/GMD & EMPA)	
DWD	HPB647N0	WMO (ESRL/GMD & EMPA)	
EMPA	JFJ646N0	WMO (ESRL/GMD & EMPA)	1999
ESRL/GMD	ESRL/GMD flask network*	WMO (ESRL/GMD & EMPA)	

HKPU	HKG222N0	Observer	
INM	(Izaña)	WMO (CMDL & EMPA)	2000
JMA	RYO239N0, MNM224N0, YON224N0	JMA	
NILU	(Ny Ålesund/Mt. Zeppelin)	WMO (CMDL & EMPA)	2001
NIWA	ARH778SX, BAR541SX		
NUI	(Mace Head)	WMO (ESRL/GMD & EMPA)	1998, 2002
RIVM	KTB653N0, KMW653N0	National	
SAWS	CPO134S0	WMO (ESRL/GMD & EMPA)	1998, 2002
SMN	USI354S0	WMO (ESRL/GMD & EMPA)	1998
UBA	ZGP647N0	WMO (ESRL/GMD & EMPA)	2001
UBA Austria	SNB647N0, SFH647NA	WMO (ESRL/GMD & EMPA)	1998 (Sonnblick)
UM	GLH636N0	Observer	

* ESRL/GMD flask network: ALT482N10, ASC107S10, ASK123N10, BAL655N10, BRW471N10, BSC644N10, CGO540S10, KUM519N10, CHR501N10, CBA455N10, CRZ146S10, GOZ636N10, EIC329S10, ITN435N10, GMI513N10, HUN646N10, ICE663N10, KEY425N10, MHD653N10, SEY104S10, MLO519N10, MBC476N10, WLG236N10, NWR440N10, ZEP678N10, POC9XXX10, PSA764S10, LEF445N10, RPB413N10, MID528N10, SHM452N10, SCS9XXX10, SPO789S10, BMW432N10, BME432N10, SYO769S10, TAP236N10, AZR638N10, SMO514S10, UUM244N10, UTA439N10, CMO445N10, IZO128N10, KZD244N10, KZM243N10, HBA775S10, STM666N10, PAL667N10, PTA438N10, WIS631N10, TDF354S10

** CSIRO flask network: AIA999930, ALT482N30, CFA519S30, CGR540S30, EPC449N30, MQA554S30, MLO519N30, MAA767S30, SIS660N30, SPO789S30

Acronyms and Abbreviations:

AES: Atmospheric Environment Service (presently MSC)
Aichi: Aichi Prefecture, Japan
AGAGE: Advanced Global Atmospheric Gases Experiment
AWI: Alfred Wegener Institute, Germany
BMG: Bureau of Meteorology and Geophysics, Indonesia
CAMS: Chinese Academy of Meteorological Sciences, China
CESI: Italian Electrical Experimental Center, Italy
CFR: Laboratoire des Sciences du Climat et de l'Environnement, CEA-CNRS, France
CHMI: Czech Hydrometeorological Institute, Prague, Czech Republic
CMA: Chinese Academy of Meteorological Sciences, China Meteorological Administration
CMDL: Climate Monitoring and Diagnostics Laboratory, NOAA, USA (presently ESRL/GMD)
CNR: Istituto di Fisica dell'Atmosfera, Consiglio Nazionale delle Ricerche, Italy
CSIRO: Commonwealth Scientific and Industrial Research Organisation, Australia
DEFRA: Department for Environment, Food and Rural Affairs, London, United Kingdom
DWD: Deutscher Wetterdienst, Germany
EARS: Environmental Agency of the Republic of Slovenia
EMPA: Swiss Federal Laboratories for Materials Research and Testing, Dübendorf, Switzerland
ENEA: Italian National Agency for New Technology, Energy and the Environment, Italy
ESRL/GMD: Earth System Research Laboratory, Global Monitoring Division, NOAA, USA (formerly CMDL)
FMI: Finnish Meteorological Institute
HKPU: Hong Kong Polytechnik University, Hong Kong, China
HMS: Hungarian Meteorological Service, Hungary
IFU Fraunhofer Institut für Atmosphärische Umweltforschung, Garmich-Partenkirchen, Germany
IGP: Instituto Geofísico del Perú
IM: Instituto de Meteorologia, Portugal
IMS: Centro Aeronautico di Montagna, Italian Air Force Meteorological Service, Italy
INM: Instituto Nacional de Meteorología, Spain

INMET:	Instituto Nacional de Meteorologia, Brazil
INMH:	National Meteorological Administration, Romania
IOEP:	Institute of Environmental Protection, Warsaw
IVL:	Swedish Environmental Research Institute, Göteborg, Sweden
JMA:	Japan Meteorological Agency, Tokyo, Japan
JMA/AO:	Aerological Observatory, Japan Meteorological Agency, Tsukuba, Japan
KMA:	Korea Meteorological Administration, Republic of Korea
KMD:	Kenya Meteorological Department, Kenya
KSNU:	Kyrgyz State National University, Kyrgyzstan
LHMA:	Latvian Hydrometeorological Agency, Latvia
LSCE:	Laboratoire des Sciences du Climat et de l'Environnement, CEA-CNRS, France
METRI:	Meteorological Research Institute, KMA, Republic of Korea
MISU:	Department of Meteorology, Stockholm University, Sweden
MGO:	Main Geophysical Observatory, Russian Federation
MMD:	Malaysian Meteorological Department
MRI:	Meteorological Research Institute, Japan Meteorological Agency, Japan
MSC:	Meteorological Service of Canada (formerly AES)
NIES:	National Institute for Environmental Studies, Japan
NILU:	Norwegian Institute for Air Research, Norway
NIMH:	Institutul National de Meteorologie, Hidrologie si Gospodarirea Apelor, Romania
NIST:	National Institute of Standards and Technology, Gaithersburg MD, USA
NIWA:	National Institute of Water and Atmospheric Research, New Zealand
NUI:	National University of Ireland, Galway, Ireland
ONM:	Office National de la Météorologie, Algeria
RIVM:	National Institute of Public Health and the Environment, Bilthoven, Netherlands
Roshydromet	Russian Hydrometeorological Service
Saitama:	Saitama Prefecture, Japan
SAWS:	South African Weather Service, South Africa
Shizuoka:	Shizuoka University, Japan
SIO:	Scripps Institution of Oceanography, USA
SMN:	Servicio Meteorológico Nacional, Argentina
SNU:	Seoul National University, Republic of Korea
Tohoku Univ.:	Tohoku University, Japan
UBA:	Umweltbundesamt (Federal Environmental Agency), Germany
UBA Austria:	Umweltbundesamt (Federal Environmental Agency), Austria
UHEI-IUP:	Institut für Umweltphysik, Universität Heidelberg, Germany
UM:	University of Malta
ZAMG:	Central Institute of Meteorology and Geodynamics, Austria

References

Aoki, S., T. Nakazawa, S. Murayama and S. Kawaguchi, Measurements of atmospheric methane at the Japanese Antarctic station, Syowa, *Tellus, Ser. B,* **44**, 273-281, 1992.

CMDL, Climate Monitoring and Diagnostics Laboratory Summary Report No.26 2000-2001, 2002.

Cunnold, D. M., L. P. Steele, P. J. Fraser, P. G. Simmonds, R. G. Prinn, R. F. Weiss, L. W. Porter, S. O'Doherty, R. L. Langenfelds, P. B. Krummel, H. J. Wang, L. Emmons, X. X. Tie, and E. J. Dlugokencky, In situ measurements of atmospheric methane at GAGE/AGAGE sites during 1985-2000 and resulting source inferences, *J. Geophys, Res,* **107**（**D14**）, 10.1029/2001JD001226, 2002.

Dlugokencky, E. J., L. P. Steele, P. M. Lang, and K. A. Masarie, The growth rate and distribution of atmospheric methane, *J. Geophys. Res.,* **99**, 17021-17043, 1994.

Dlugokencky, E. J., R. C. Myers, P. M. Lang, K. A. Masarie, A. M. Crotwell, K. W. Thoning, B. D. Hall, J. W. Elkins, and L. P. Steele, Conversion of NOAA atmospheirc dry air CH4 mole fractions to a gravimetrically prepared standard scale, *J. Geophys. Res.,***110**, D18306, doi: 10.1029/2005JD006035, 2005.

Hall, B. D. (ed.), J. W. Elkins, J. H. Butler, S. A. Montzka, T. M. Thompson, L. Del Negro, G. S. Dutton, D. F. Hurst, D. B. King, E. S. Kline, L. Lock, D. Mactaggart, D. Mondeel, F. L. Moore,

J. D. Nance, E. A. Ray, and P. A. Romashkin, Halocarbons and Other Atmospheric Gases, Section 5 in Climate Monitoring and Diagnostics Laboratory, Summary Report N. 25, 1998-1999, R. S. Schnell, D. B. King, R. M. Rosson (eds.), NOAA-CMDL, Boulder, CO., USA, 2001.

Hall, B. D. (ed.), J. H. Butler, A. D. Clarke, G. S. Dutton, J. W. Elkins, D. F. Hurst, D. B. King, E. S. Kline, J. Lind, L. Lock, D. Mondeel, F. L. Moore, S. A. Montzka, J. D. Nance, E. A. Ray, P. A. Romashkin, and T. M. Thompson, Halocarbons and Other Atmospheric Gases, Section 5 in Climate Monitoring and Diagnostics Laboratory, Summary Report N. 26, 2000-2001, D. B. King, R. C. Schnell, C. Sweet, R. M. Rosson (eds.), NOAA-CMDL, Boulder, CO., USA, 2002.

Hofer, P., B. Buchmann and A. Herzog, Traceability, Uncertainty and Assessment Criteria of Surface Ozone Measurements, *EMPA-WCC Report 98/5*, 20 pp, 1998.

Klausen, J., C. Zellweger, B. Buchmann, and P. Hofer, Uncertainty and bias of surface ozone measurements at selected Global Atmosphere Watch sites, *J. Geophys. Res.,* **108(D19)**, 4622, doi:10.1029/2003JD003710, 2003.

Peterson, J., P. Tans, and D. Kitzis, "CO_2 Round-Robin Reference Gas Intercomparison" in Report of the Ninth WMO Meeting of Experts on Carbon Dioxide Concentration and Related Tracer Measurement Techniques, Aspendale, Vic. Australia, 1 - 4 September 1997, edited by R. Francey, WMO/GAW Report No. 132, 1999.

WMO, Strategy for the Implementation of the Global Atmosphere Watch Programme (2001-2007), WMO/GAW Report No. 142, 62pp, 2001.

WMO, Report of the Eleventh WMO/IAEA Meeting of Experts on Carbon Dioxide Concentration and Related Tracer Measurement Techniques, Global Atmosphere Watch Report Series No.148, 2003.

WMO, Addendum for the Period 2005-2007 To the Strategy for the Implementation of the Global Atmosphere Watch Programme (2001-2007), WMO/GAW Report No. 142, WMO/GAW Report No. 156, 2004.

Worthy, D. E. J., I. Levin, N. B. A. Trivett, A. J. Kuhlmann, J. F. Hopper and M. K. Ernst, Seven years of continuous methane observations at a remote boreal site in Ontario, Canada, *J. Geophys. Res.,* **103***,* 15995-16007, 1998.

Zhao, C. L., P. P. Tans, and K. W. Thoning, A high precision manometric system for absolute calibrations of CO_2 in dry air, *J. Geophys. Res.,* **102**, 5885-5894, 1997.

LIST OF OBSERVING STATIONS

Station	Country/Territory	Index Number	Location Latitude (° ')	Location Longitude (° ')	Altitude (m)	Parameter
REGION I (Africa)						
Amsterdam Island	France	AMS137S00	37 48 S	77 32 E	65	CO_2
Amsterdam Island	France	AMS137S10	37 57 S	77 31 E	150	CO_2, CH_4
Ascension Island	United Kingdom	ASC107S10	7 55 S	14 25 W	54	CO_2, CH_4, CO, H_2, $^{13}CO_2$, $C^{18}O_2$
Assekrem	Algeria	ASK123N00	23 16 N	5 38 E	2710	O_3
Assekrem	Algeria	ASK123N10	23 10 N	5 25 E	2728	CO_2, CH_4, CO, H_2, $^{13}CO_2$, $C^{18}O_2$
Cape Point	South Africa	CPO134S00	34 21 S	18 29 E	230	CO_2, CH_4, O_3, CO, N_2O
Crozet	France	CRZ146S10	46 27 S	51 51 E	120	CO_2, CH_4, CO, H_2, $^{13}CO_2$, $C^{18}O_2$
Funchal	Portugal	FUN132N00	32 39 N	16 53 W	58	O_3
Gobabeb	Namibia	NMB123S10	23 34 S	15 01 E	461	CO_2, CH_4, $^{13}CO_2$
Izaña	Spain	IZA128N00	28 18 N	16 30 W	2367	CO_2, CH_4, O_3
Mahe Island	Seychelles	SEY104S10	4 40 S	55 10 E	7	CO_2, CH_4, CO, H_2, $^{13}CO_2$, $C^{18}O_2$
Tenerife	Spain	IZO128N10	28 18 N	16 28 W	2360	CO_2, CH_4, CO, H_2, $^{13}CO_2$, $C^{18}O_2$
REGION II (Asia)						
Anmyeon-do	Rep. of Korea	AMY236N00	36 32 N	126 19 E	47	CO_2, CH_4, N_2O, CFCs
Bering Island	Russian Federation	BER255N00	55 12 N	165 59 E	13	CO_2
Cape Ochi-ishi	Japan	COI243N00	43 09 N	145 30 E	45	CO_2, CH_4
Gosan	Rep. of Korea	KSN233N00	33 17 N	126 10 E	72	CO_2, CH_4, N_2O, CFCs
Hamamatsu	Japan	HMM234N00	34 43 N	137 43 E	35	CO_2
Hateruma	Japan	HAT224N00	24 03 N	123 48 E	10	CO_2, CH_4, N_2O
Hok Tsui	Hong Kong, China	HKG222N00	22 13 N	114 15 E	60	CO, O_3
Issyk-Kul	Kyrgyzstan	ISK242N00	42 37 N	76 59 E	1640	CO_2, O_3, CH_4
Kaashidhoo	Maldives	KCO204N10	4 58 N	73 28 E	1	CO_2, CH_4, $^{13}CO_2$
Kisai	Japan	KIS236N00	36 05 N	139 33 E	13	CO_2
Kotelny Island	Russian Federation	KOT276N00	76 00 N	137 52 E	5	CO_2
Kyzylcha	Uzbekistan	KYZ240N00	40 52 N	66 09 E	340	CO_2
Memanbetsu	Japan	MMB243N00	43 55 N	144 12 E	32.9	N_2O
Mikawa-Ichinomiya	Japan	MKW234N00	34 51 N	137 26 E	50	CO_2
Minamitorishima	Japan	MNM224N00	24 17 N	153 59 E	8	CO_2, CH_4, CO, O_3
Mt. Dodaira	Japan	DDR236N00	36 00 N	139 11 E	840	CO_2
Mt. Waliguan	China	WLG236N00	36 17 N	100 54 E	3810	CO_2
Mt. Waliguan	China	WLG236N10	36 17 N	100 54 E	3810	CO_2, CH_4, CO, H_2, $^{13}CO_2$, $C^{18}O_2$
Nagoya	Japan	NGY235N00	35 09 N	136 58 E	35	N_2O
Plateau Assy	Kazakhstan	KZM243N10	43 15 N	77 52 E	2519	CO_2, CH_4, CO, H_2, $^{13}CO_2$
Ryori	Japan	RYO239N00	39 02 N	141 49 E	260	CO_2, CH_4, N_2O, CFCs, CCl_4, CH_3CCl_3, CO, O_3
Sary Taukum	Kazakhstan	KZD244N10	44 27 N	75 34 E	412	CO_2, CH_4, CO, H_2, $^{13}CO_2$
Tae-ahn Peninsula	Rep. of Korea	TAP236N10	36 43 N	126 07 E	20	CO_2, CH_4, CO, H_2, $^{13}CO_2$, $C^{18}O_2$
Takayama	Japan	TKY236N00	36 08 N	137 25 E	1420	CO_2
Tsukuba	Japan	TKB236N00	36 03 N	140 08 E	26	CH_4
Tsukuba	Japan	TKB236N20	36 03 N	140 08 E	26	CO_2
Tsukuba	Japan	TKB236N30	36 03 N	140 08 E	25	O_3
Ulaan Uul	Mongolia	UUM244N10	44 27 N	111 05 E	914	CO_2, CH_4, CO, H_2, $^{13}CO_2$, $C^{18}O_2$
Urawa	Japan	URW235N00	35 52 N	139 36 E	10	CO_2
Yonagunijima	Japan	YON224N00	24 28 N	123 01 E	30	CO_2, CH_4, CO, O_3
REGION III (South America)						
Arembepe	Brazil	ABP312S00	12 46 S	38 10 W	0	O_3
Bird Island	United Kingdom	SGI354S10	54 00 S	38 03 W	30	CO_2, CH_4
Easter Island	Chile	EIC329S10	27 08 S	109 27 W	50	CO_2, CH_4, CO, H_2, $^{13}CO_2$, $C^{18}O_2$

LIST OF OBSERVING STATIONS (continued)

Station	Country/Territory	Index Number	Location Latitude (° ')	Location Longitude (° ')	Altitude (m)	Parameter
Huancayo	Peru	HUA312S00	12 04 S	75 32 W	3313	CO_2
Tierra del Fuego	Argentina	TDF354S10	54 52 S	68 28 W	20	CO_2, CH_4, CO, H_2, $^{13}CO_2$, $C^{18}O_2$
Tierra del Fuego	Argentina	TDF354S20	54 52 S	68 29 W	20	CFCs, HCFCs, CH_3CCl_3
Tierra del Fuego	Argentina	TDF354SX0	54 52 S	68 29 W	20	HFCs
Ushuaia	Argentina	USI354S00	54 51 S	68 19 W	18	O_3, CO
REGION IV (North and Central America)						
Alert	Canada	ALT482N00	82 27 N	62 31 W	210	CO_2
Alert	Canada	ALT482N10	82 27 N	62 31 W	210	CO_2, CH_4, CO, H_2, $^{13}CO_2$, $C^{18}O_2$
Alert	Canada	ALT482N20	82 27 N	62 31 W	210	CFCs, HCFCs, CH_3CCl_3, C_2Cl_4, CH_2Cl_2, SF_6, N_2O
Alert	Canada	ALT482N30	82 27 N	62 31 W	210	CO_2, CH_4, CO, H_2
Alert	Canada	ALT482NX0	82 27 N	62 31 W	210	HFCs
Algoma	Canada	ALG447N00	47 02 N	84 23 W	411	O_3
Barrow	U. S. A.	BRW471N00	71 19 N	156 36 W	8	CO_2, CH_4
Barrow	U. S. A.	BRW471N10	71 19 N	156 35 W	11	CO_2, CH_4, CO, H_2, $^{13}CO_2$, $^{13}CH_4$, $C^{18}O_2$
Barrow	U. S. A.	BRW471N20	71 19 N	156 36 W	8	CFCs, HCFCs, CH_3CCl_3, C_2Cl_4, CH_2Cl_2, SF_6, N_2O
Barrow	U. S. A.	BRW471N40	71 19 N	156 36 W	8	O_3
Barrow	U. S. A.	BRW471NX0	71 19 N	156 36 W	8	N_2O, CFCs, HFCs, CCl_4, CH_3CCl_3, SF_6, HCFCs
Bratt's Lake	Canada	BRA450N00	50 12 N	104 12 W	588	O_3
Cape Meares	U. S. A.	CME445NX0	45 29 N	123 58 W	30	CH_4, N_2O, CFCs, CCl_4, CH_3CCl_3
Cape Meares	U. S. A.	CMO445N10	45 28 N	123 58 W	30	CO_2, CH_4, CO, H_2, $^{13}CO_2$, $C^{18}O_2$
Cape St. James	Canada	CSJ451N00	51 56 N	131 01 W	89	CO_2
Chalk River	Canada	CHA446N00	46 04 N	77 24 W	184	O_3
Chapais	Canada	CPS449N00	49 49 N	74 59 W	381	O_3
Cold Bay	U. S. A.	CBA455N10	55 12 N	162 43 W	25	CO_2, CH_4, CO, H_2, $^{13}CO_2$, $C^{18}O_2$
Egbert	Canada	EGB444N00	44 14 N	79 47 W	253	O_3
Estevan Point	Canada	EPC449N30	49 23 N	126 32 W	39	CO_2, CH_4, CO, H_2
Esther	Canada	EST451N00	51 40 N	110 12 W	707	O_3
Experimental Lakes Area	Canada	ELA449N00	49 40 N	93 43 W	369	O_3
Grifton	U. S. A.	ITN435N10	35 21 N	77 22 W	505	CO_2, CH_4, CO, H_2, $^{13}CO_2$, $C^{18}O_2$
Grifton	U. S. A.	ITN435N20	35 21 N	77 23 W	9	CFCs, SF_6, N_2O
Harvard Forest	U. S. A.	HFM442N20	42 54 N	72 18 W	340	CFCs, HCFCs, CH_3CCl_3, SF_6, N_2O
Harvard Forest	U. S. A.	HFM442NX0	42 54 N	72 18 W	340	HFCs
Kejimkujik	Canada	KEJ444N00	44 26 N	65 12 W	127	O_3
Key Biscayne	U. S. A.	KEY425N10	25 40 N	80 12 W	3	CO_2, CH_4, CO, H_2, $^{13}CO_2$, $C^{18}O_2$
Kitt Peak	U. S. A.	KPA432N10	32 N	112 W	2083	CH_4
La Jolla	U. S. A.	SIO432N10	32 50 N	117 16 W	14	CH_4
La Palma	Cuba	PLM422N00	22 45 N	83 32 W	47	NO_2
Longwoods	Canada	LON442N00	42 53 N	81 29 W	239	O_3
Moody	U. S. A.	WKT431N10	31 19 N	97 19 W	708	CH_4
Mould Bay	Canada	MBC476N10	76 15 N	119 20 W	58	CO_2, CH_4, CO, H_2, $^{13}CO_2$, $C^{18}O_2$
Niwot Ridge	U. S. A.	NWR440N10	40 02 N	105 34 W	3526	CO_2, CH_4, CO, H_2, $^{13}CO_2$, $^{13}CH_4$, $C^{18}O_2$
Niwot Ridge	U. S. A.	NWR440N20	40 03 N	105 35 W	3475	CFCs, HCFCs, HFCs, CH_3CCl_3, C_2Cl_4, CH_2Cl_2, SF_6, N_2O
Niwot Ridge	U. S. A.	NWR440N40	40 02 N	105 32 W	3022	O_3

LIST OF OBSERVING STATIONS (continued)

Station	Country/Territory	Index Number	Location Latitude (° ')	Location Longitude (° ')	Altitude (m)	Parameter
Niwot Ridge	U. S. A.	NWR440NX0	40 03 N	105 35 W	3475	N_2O, CFCs, HFCs, CCl_4, CH_3CCl_3, SF_6, HCFCs
Niwot Ridge (Saddle)	U. S. A.	NTL440N40	40 03 N	105 35 W	3538	O_3
Niwot Ridge C-1	U. S. A.	NWC440N20	40 00 N	105 36 W	3475	HFCs
Olympic Peninsula	U. S. A.	OPW448N10	48 15 N	124 25 W	488	CO_2, CH_4, H_2
Park Falls	U. S. A.	LEF445N10	45 55 N	90 16 W	868	CO_2, CH_4, CO, H_2, $^{13}CO_2$, $C^{18}O_2$
Park Falls	U. S. A.	LEF445N20	45 56 N	90 16 W	868	CFCs, CH_3CCl_3, HCFCs, SF_6, N_2O
Park Falls	U. S. A.	LEF445NX0	45 56 N	90 16 W	868	HFCs
Point Arena	U. S. A.	PTA438N10	38 57 N	123 43 W	17	CO_2, CH_4, CO, $^{13}CO_2$
Ragged Point	Barbados	RGP413NX0	13 10 N	59 26 W	45	CH_4, N_2O, CFCs, CCl_4, $CHCl_3$, CH_3CCl_3
Ragged Point	Barbados	RPB413N10	13 10 N	59 25 W	45	CO_2, CH_4, CO, H_2, $^{13}CO_2$, $C^{18}O_2$
Ragged Point	Barbados	RPB413N40	13 10 N	59 26 W	45	O_3
Sable Island	Canada	SBL443N00	43 56 N	60 01 W	5	CO_2
Saturna	Canada	SAT448N00	48 47 N	123 08 W	178	O_3
Shemya Island	U. S. A.	SHM452N10	52 43 N	174 05 E	40	CO_2, CH_4, CO, H_2, $^{13}CO_2$, $C^{18}O_2$
Southern Great Plains	U. S. A.	SGP436N10	36 47 N	97 30 W	314	CO_2, CH_4,
St. Croix	U. S. A.	AVI417N10	17 45 N	64 45 W	3	CO_2, CH_4
St. David's Head	United Kingdom	BME432N10	32 22 N	64 39 W	30	CO_2, CH_4, CO, H_2, $^{13}CO_2$, $C^{18}O_2$
Sutton	Canada	SUT445N00	45 05 N	72 41 W	243	O_3
Trinidad Head	U. S. A.	TRH441N00	41 03 N	124 09 W	120	CH_4, N_2O, CFCs, CCl_4, $CHCl_3$, CH_3CCl_3
Trinidad Head	U. S. A.	TRH441N10	41 02 N	124 09 W	107	CO_2, CH_4
Trinidad Head	U. S. A.	TRH441N20	41 03 N	124 09 W	120	CFCs, HCFCs, SF_6, N_2O, CH_3CCl_3
Trinidad Head	U. S. A.	TRH441N40	41 03 N	124 09 W	120	O_3
Trinidad Head	U. S. A.	TRH441NX0	41 03 N	124 09 W	120	HFCs
Tudor Hill	United Kingdom	BMW432N10	32 16 N	64 52 W	30	CO_2, CH_4, CO, H_2, $^{13}CO_2$, $C^{18}O_2$
Tudor Hill	Bermuda, United Kingdom	BMW432N40	32 22 N	64 39 W	30	O_3
Wendover	U. S. A.	UTA439N10	39 53 N	113 43 W	1320	CO_2, CH_4, CO, H_2, $^{13}CO_2$, $C^{18}O_2$
REGION V (South-West Pacific)						
Baring Head	New Zealand	BAR541S00	41 25 S	174 52 E	85	CH_4, CO, CO_2, N_2O, O_3
Baring Head	New Zealand	BAR541SA0	41 25 S	174 52 E	85	CO
Bukit Koto Tabang	Indonesia	BKT500S00	0 12 S	100 19 E	864.5	NO_2, SO_2, O_3
Bukit Koto Tabang	Indonesia	BKT500S10	0 12 N	100 19 E	864.5	CH_4
Cape Ferguson	Australia	CFA519S30	19 17 S	147 03 E	2	CO_2, CH_4, CO, H_2
Cape Grim	Australia	CGO540S10	40 40 S	144 40 E	94	CO_2, CH_4, CO, H_2, $^{13}CO_2$, $^{13}CH_4$, $C^{18}O_2$
Cape Grim	Australia	CGO540S20	40 41 S	144 41 E	94	CFCs, HCFCs, CH_3CCl_3, C_2Cl_4, CH_2Cl_2, SF_6, N_2O
Cape Grim	Australia	CGO540SX0	40 41 S	144 41 E	94	HFCs
Cape Grim	Australia	CGR540S00	40 41 S	144 41 E	94	CO_2, O_3
Cape Grim	Australia	CGR540S30	40 41 S	144 41 E	94	CO_2, CH_4, CO, H_2
Cape Grim	Australia	CGR540SX0	40 41 S	144 41 E	94	CH_4, N_2O, CFCs, HFCs, HCFCs, CCl_4, $CHCl_3$, CH_3CCl_3, CO, H_2, CH_3Cl, CH_3Br
Cape Kumukahi	U. S. A.	KUM519N10	19 31 N	154 49 W	3	CO_2, CH_4, CO, H_2, $^{13}CO_2$, $C^{18}O_2$
Cape Kumukahi	U. S. A.	KUM519N20	19 31 N	154 49 W	3	CFCs, HCFCs, CH_3CCl_3, C_2Cl_4, CH_2Cl_2, SF_6, N_2O
Cape Kumukahi	U. S. A.	KUM519ND0	19 31 N	154 49 W	3	HFCs

LIST OF OBSERVING STATIONS (continued)

Station	Country/Territory	Index Number	Location Latitude (° ')	Location Longitude (° ')	Altitude (m)	Parameter
Cape Matatula	U. S. A.	MAT514SX0	14 15 S	170 34 W	42	CH_4, N_2O, CFCs, CCl_4, $CHCl_3$, CH_3CCl_3
Cape Matatula	American Samoa, U. S. A.	SMO514S40	14 15 S	170 34 W	42	O_3
Christmas Island	Kiribati	CHR501N10	1 42 N	157 10 W	3	CO_2, CH_4, CO, H_2, $^{13}CO_2$, $C^{18}O_2$
Danum Valley GAW Baseline Station	Malaysia	DMV504N00	4 58 N	117 50 E	426	CO_2
Guam	U. S. A.	GMI513N10	13 26 N	144 47 E	2	CO_2, CH_4, CO, H_2, $^{13}CO_2$, $C^{18}O_2$
Jakarta	Indonesia	JKR506S00	6 11 S	106 50 E	7	NO_2, SO_2
Kaitorete Spit	New Zealand	NZL543S10	43 50 S	172 38 E	3	CH_4
Lauder	New Zealand	LAU545S40	45 02 S	169 40 E	370	O_3
Macquarie Island	Australia	MQA554S30	54 29 S	158 58 E	12	CO_2, CH_4, CO, H_2
Mauna Loa	U. S. A.	MLO519N00	19 32 N	155 34 W	3397	CO_2, CH_4
Mauna Loa	U. S. A.	MLO519N10	19 32 N	155 34 W	3397	CO_2, CH_4, CO, H_2, $^{13}CO_2$, $^{13}CH_4$, $C^{18}O_2$
Mauna Loa	U. S. A.	MLO519N20	19 32 N	155 35 W	3397	CFCs, HCFCs, HFCs, CH_3CCl_3, C_2Cl_4, CH_2Cl_2, SF_6, N_2O
Mauna Loa	U. S. A.	MLO519N30	19 32 N	155 35 W	3397	CO_2, CH_4, CO, H_2
Mauna Loa	U. S. A.	MLO519N40	19 32 N	155 35 W	3397	O_3
Mauna Loa	U. S. A.	MLO519NX0	19 32 N	155 35 W	3397	N_2O, CFCs, HFCs, CCl_4, CH_3CCl_3, SF_6, HCFCs
Sand Island	U. S. A.	MID528N10	28 12 N	177 22 W	7.7	CO_2, CH_4, CO, H_2, $^{13}CO_2$, $C^{18}O_2$
Tanah Rata	Malaysia	TAR504N00	4 28 N	101 23 E	1545	O_3
Tutuila	U. S. A.	SMO514S00	14 14 S	170 34 W	42	CO_2
Tutuila	U. S. A.	SMO514S10	14 14 S	170 34 W	42	CO_2, CH_4, CO, H_2, $^{13}CO_2$, $^{13}CH_4$, $C^{18}O_2$
Tutuila	U. S. A.	SMO514S20	14 15 S	170 34 W	42	CFCs, HCFCs, CH_3CCl_3, C_2Cl_4, CH_2Cl_2, SF_6, N_2O
Tutuila	U. S. A.	SMO514SX0	14 15 S	170 34 W	42	N_2O, CFCs, HFCs, CCl_4, CH_3CCl_3, SF_6, HCFCs
REGION VI (Europe)						
Adrigole	Ireland	ADR652NA0	52 N	10 W	50	N_2O, CFCs, CCl_4, CH_3CCl_3
Ähtäri	Finland	AHT662N00	62 35 N	24 12 E	180	NO_2, SO_2, O_3
Angra do Heroismo	Portugal	ANG638N00	38 40 N	27 13 W	74	O_3
Baltic Sea	Poland	BAL655N10	55 21 N	17 13 E	28	CO_2, CH_4, CO, H_2, $^{13}CO_2$, $C^{18}O_2$
Beja	Portugal	BEJ638N00	38 01 N	7 52 W	246	O_3
Black Sea	Romania	BSC644N10	44 10 N	28 40 E	3	CO_2, CH_4, CO, H_2, $^{13}CO_2$, $C^{18}O_2$
Braganca	Portugal	BRG641N00	41 48 N	6 44 W	690	SO_2
Brotjacklriegel	Germany	BRT648N00	48 49 N	13 13 E	1016	CO_2, O_3
Brotjacklriegel	Germany	BRT648N60	48 49 N	13 13 E	1016	VOCs
Burgas	Bulgaria	BUR642N00	42 29 N	27 29 E	16	NO_2, SO_2
Campisabalos	Spain	CAM641N60	41 17 N	3 09 W	1360	VOCs
Castelo Branco	Portugal	CAS639N00	39 50 N	7 28 W	386	O_3
Danki	Russian Federation	DAK654N00	54 54 N	37 48 E	140	O_3
Deuselbach	Germany	DEU649N00	49 46 N	7 03 E	480	CO_2, O_3, CH_4
Doñana	Spain	DON637N00	37 03 N	6 33 W	5	NO_2, SO_2, O_3
Donon	France	DNN649N60	48 30 N	7 08 E	775	VOCs
Dwejra Point	Malta	GOZ636N10	36 03 N	14 11 E	30	CO_2, CH_4, CO, H_2, $^{13}CO_2$, $C^{18}O_2$
Eskdalemuir	United Kingdom	EDM655N00	55 19 N	3 12 W	242	O_3
Fundata	Romania	FDT645N00	45 28 N	25 18 E	1371	NO_2, SO_2
Fundata	Romania	FDT645N20	45 28 N	25 18 E	1383.5	CO_2, NO_2, O_3
Giordan Lighthouse	Malta	GLH636N00	36 04 N	14 13 E	167	O_3, CO

LIST OF OBSERVING STATIONS (continued)

Station	Country/Territory	Index Number	Location Latitude (° ')	Location Longitude (° ')	Altitude (m)	Parameter
Hegyhatsal	Hungary	HUN646N00	46 57 N	16 39 E	248	CO_2
Hegyhatsal	Hungary	HUN646N10	46 57 N	16 38 E	344	CO_2, CH_4, CO, H_2, $^{13}CO_2$, $C^{18}O_2$
Heimaey	Iceland	ICE663N10	63 20 N	20 17 W	100	CO_2, CH_4, CO, H_2, $^{13}CO_2$, $C^{18}O_2$
Heimaey	Iceland	ICE663N40	63 24 N	20 17 W	100	O_3
Hohe Warte	Austria	HHE648N00	48 15 N	16 22 E	202	NO, NO_2, SO_2
Hohe Warte	Austria	HHE648N20	48 15 N	16 22 E	202	NO, NO_2, SO_2
Hohenpeissenberg	Germany	HPB647N00	47 48 N	11 01 E	985	CO, NO, NO_2, NOx, NOy, SO_2, ROOH, H_2O_2, O_3, PAN
Hohenpeissenberg	Germany	HPB647N20	47 48 N	11 01 E	985	VOCs
Hohenpeissenberg	Germany	HPB647N50	47 48 N	11 01 E	985	^{222}Rn
Iskrba	Slovenia	IRB645N00	45 34 N	14 52 E	520	SO_2, O_3
Ivan Sedlo	Bosnia and Herzegovina	IVN643N00	43 46 N	18 02 E	970	NO_2, SO_2
Jarczew	Poland	JCZ651N00	51 49 N	21 59 E	180	NO_2, SO_2
Jungfraujoch	Switzerland	JFJ646N00	46 33 N	7 59 E	3578	CO, O_3, NO, NO_2, NOx, SO_2,
K-puszta	Hungary	KPS646N00	46 58 N	19 33 E	125	CO_2, NO_2, SO_2, O_3
Kamenicki Vis	Serbia and Montenegro	KAM643N00	43 24 N	21 57 E	813	NO_2, SO_2
Kloosterburen	Netherlands	KTB653N00	53 24 N	6 25 E	0	CO, NO, NOx, NO_2, SO_2
Kollumerwaard	Netherlands	KMW653N00	53 20 N	6 17 E	0	CO_2, CH_4, CO, NO, NOx, NO_2, SO_2, O_3
Kosetice	Czech Republic	KOS649N00	49 35 N	15 05 E	534	CH_4, CO, NO, NO_2, SO_2, O_3
Kosetice	Czech Republic	KOS649N60	49 35 N	15 05 E	534	VOCs
Kovk	Slovenia	KVK646N00	46 07 N	15 06 E	600	O_3
Krvavec	Slovenia	KVV646N00	46 18 N	14 32 E	1720	O_3
La Cartuja	Spain	CAR637N00	37 12 N	3 36 W	720	NO_2, SO_2
La Tardiere	France	LAT647N60	46 39 N	0 45 W	133	VOCs
Lampedusa	Italy	LMP635N00	35 31 N	12 38 E	45	CO_2, CH_4, N_2O, CFCs
Lazaropole	The former Yugoslav Republic of Macedonia	LZP641N00	41 32 N	20 42 E	1320	NO_2, SO_2
Leba	Poland	LEB654N00	54 45 N	17 32 E	2	NO_2, SO_2
Lisboa / Gago Coutinho	Portugal	LIS638N00	38 46 N	9 08 W	105	O_3
Logroño	Spain	LOG642N00	42 27 N	2 30 W	370	NO_2, SO_2
Mace Head	Ireland	MCH653N20	53 20 N	9 54 W	25	CFCs, HCFCs, CH_3CCl_3, SF_6, N_2O
Mace Head	Ireland	MCH653NX0	53 20 N	9 54 W	25	CH_4, N_2O, CFCs, HFCs, HCFCs, CCl_4, $CHCl_3$, CH_3CCl_3, CO, H_2, CH_3Cl, CH_3Br
Mace Head	Ireland	MHD653N00	53 20 N	9 54 W	25	O_3
Mace Head	Ireland	MHD653N10	53 19 N	9 54 W	25	CO_2, CH_4, CO, H_2, $^{13}CO_2$, $C^{18}O_2$
Mace Head	Ireland	MHD653N20	53 20 N	9 54 W	25	CO_2
Mace Head	Ireland	MHD653NX0	53 20 N	9 54 W	25	HFCs
Mahón	Spain	MHN639N00	39 52 N	4 19 E	78	NO_2, SO_2, O_3
Monte Cimone	Italy	CMN644N00	44 11 N	10 42 E	2165	CO_2, O_3
Monte Velho	Portugal	MVH638N00	38 05 N	8 48 W	43	O_3
Neuglobsow	Germany	NGL653N00	53 10 N	13 02 E	65	CO_2, O_3, CH_4
Noia	Spain	NIA642N00	42 44 N	8 55 W	685	NO_2, SO_2, O_3
Ny-Alesund	Norway	ZEP678N10	78 54 N	11 52 E	475	CO_2, CH_4, CO, H_2, $^{13}CO_2$, $C^{18}O_2$
Ocean Station "C"	U. S. A.	STC654N10	54 00 N	35 00 W	6	CO_2
Ocean Station "M"	Norway	STM666N10	66 00 N	2 00 E	5	CO_2, CH_4, CO, H_2, $^{13}CO_2$, $C^{18}O_2$
Ocean Station Charlie	Russian Federation	STC652N00	52 45 N	35 30 W	5	CO_2
Oulanka	Finland	OUL666N00	66 19 N	29 24 E	310	NO_2, SO_2, O_3
Pallas-Sammaltunturi	Finland	PAL667N00	67 58 N	24 07 E	565	CO_2, O_3
Pallas-Sammaltunturi	Finland	PAL667N10	67 58 N	24 07 E	560	CO_2, CH_4, CO
Pallas-Sammaltunturi	Finland	PAL667N60	68 00 N	24 09 E	340	VOCs
Penhas Douradas	Portugal	PEN640N00	40 25 N	7 33 W	1380	O_3

LIST OF OBSERVING STATIONS (continued)

Station	Country/Territory	Index Number	Location Latitude (° ')	Location Longitude (° ')	Altitude (m)	Parameter
Pezrusse Vieille	France	PVI644N60	43 37 N	0 11 E	200	VOCs
Plateau Rosö	Italy	PLR645N00	45 56 N	7 42 E	3480	CO_2, CH_4
Pleven	Bulgaria	PLV643N00	43 25 N	24 36 E	64	NO_2, SO_2
Plovdiv	Bulgaria	PLD642N00	42 08 N	24 45 E	179	NO_2, SO_2
Puszcza Borecka/Diabla Gora	Poland	DIG654N00	54 09 N	22 04 E	157	CO_2, NO_2, O_3, SO_2
Roquetes	Spain	ROQ640N00	40 49 N	0 29 E	50	NO_2, SO_2, O_3
Rucava	Latvia	RCV656N00	56 10 N	21 11 E	18	NO_2, SO_2, O_3
San Pablo de los Montes	Spain	SPM639N00	39 33 N	4 21 W	917	NO_2, SO_2, O_3
Schauinsland	Germany	SSL647N00	47 55 N	7 55 E	1205	CO_2, O_3, CH_4, N_2O, SF_6
Schmuecke	Germany	SCH651N60	50 39 N	10 46 E	937	VOCs
Sede Boker	Israel	WIS631N10	31 07 N	34 52 E	400	CO_2, CH_4, CO, H_2, $^{13}CO_2$, $C^{18}O_2$
Semenic	Romania	SEM645N00	45 07 N	21 58 E	1432	NO_2, SO_2
Shepelevo	Russian Federation	SHP659N00	59 58 N	29 07 E	4	O_3
Shetland	United Kingdom	SIS660N30	60 05 N	1 15 W	30	CO_2, CH_4, CO, H_2
Site J	Denmark	GRL666N00	66 30 N	46 12 W	2030	CH_4
Sniezka	Poland	SNZ650N00	50 44 N	15 44 E	1603	NO_2, SO_2
Sofia	Bulgaria	SOF642N00	42 39 N	23 23 E	586	NO_2, SO_2
Sonnblick	Austria	SNB647N00	47 03 N	12 57 E	3106	CO_2, O_3, CO
Starina	Slovakia	STA649N60	49 03 N	22 16 E	345	VOCs
Stephansplatz	Austria	STP648N00	48 13 N	16 23 E	171	NO, NO_2, SO_2
Stephansplatz	Austria	STP648N20	48 13 N	16 23 E	171	NO, NO_2, SO_2
Stîna de Vale	Romania	STN646N00	46 41 N	22 37 E	1116	NO_2, SO_2
Summit	Denmark	SUM672N10	72 34 N	38 28 W	3238	CH_4, CO_2
Summit	Denmark	SUM672N20	72 35 N	38 29 W	3238	CFCs, HCFCs, CH_3CCl_3
Summit	Greenland, Denmark	SUM672N40	72 35 N	38 29 W	3238	O_3
Summit	Denmark	SUM672NX0	72 35 N	38 29 W	3238	HFCs
Suwalki	Poland	SWL654N00	54 08 N	22 57 E	184	NO_2, SO_2
Terceira Island	Portugal	AZR638N10	38 46 N	27 22 W	40	CO_2, CH_4, CO, H_2, $^{13}CO_2$, $C^{18}O_2$
Teriberka	Russian Federation	TER669N00	69 12 N	35 06 E	40	CO_2, CH_4
Utö	Finland	UTO659N00	59 47 N	21 22 E	7	NO_2, SO_2, O_3
Utö	Finland	UTO659N60	59 47 N	21 23 E	7	VOCs
Varna	Bulgaria	VRN643N00	43 12 N	27 55 E	41	NO_2, SO_2
Viana do Castelo	Portugal	VDC641N00	41 42 N	8 48 W	16	SO_2
Vindeln	Sweden	VDL664N00	64 15 N	19 46 E	271	O_3
Virolahti	Finland	VIR660N00	60 32 N	27 40 E	4	NO_2, SO_2, O_3
Waldhof	Germany	LGB652N00	52 48 N	10 46 E	74	CO_2, O_3
Waldhof	Germany	LGB652N60	52 48 N	10 46 E	74	VOCs
Wank Peak	Germany	WNK647N00	47 31 N	11 09 E	1780	CO_2, NOx, SO_2
Westerland	Germany	WST654N00	54 56 N	8 19 E	12	CO_2, O_3
Zabljak	Serbia and Montenegro	ZBL643N00	43 09 N	19 08 E	1450	NO_2, SO_2
Zavodnje	Slovenia	ZRN646N00	46 26 N	15 00 E	770	O_3
Zeppelinfjellet	Norway	ZEP678N00	78 54 N	11 53 E	475	CO_2, N_2O, CFCs, CCl_4, CH_3CCl_3, O_3, SO_2
Zingst	Germany	ZGT654N00	54 26 N	12 44 E	1	CO_2, O_3, CH_4
Zingst	Germany	ZGT654N60	54 26 N	12 44 E	1	VOCs
Zoseni	Latvia	ZSN657N00	57 08 N	25 55 E	183	NO_2, SO_2
Zugspitze	Germany	ZGP647N00	47 25 N	10 59 E	2960	CO_2, CH_4, CO, NO, NOx, NOy, O_3
Zugspitze	Germany	ZSP647N00	47 25 N	10 59 E	2960	CO_2
Zugspitze/Schneefernerhaus	Germany	SFH647NA0	47 25 N	10 59 E	2656	CH_4, CO, CO_2, N_2O, NO, NO_2, NOy, O_3, SF_6
Zugspitze/Schneefernerhaus	Germany	SFH647N00	47 25 N	10 59 E	2656	SO_2

LIST OF OBSERVING STATIONS (continued)

Station	Country/Territory	Index Number	Location Latitude (° ')	Location Longitude (° ')	Altitude (m)	Parameter
ANTARCTICA						
Arrival Heights	Antarctica / New Zealand	ARH778S00	77 48 S	166 40 E	184	CH_4, CO, N_2O
Arrival Heights	Antarctica / New Zealand	ARH778SA0	77 48 S	166 40 E	184	CO
Halley Bay	United Kingdom	HBA775S10	75 34 S	26 30 W	33	CO_2, CH_4, CO, H_2, $^{13}CO_2$, $C^{18}O_2$
Jubany	Argentina	JBN762S00	62 14 S	58 40 W	15	CO_2
Mawson	Australia	MAA767S30	67 37 S	62 52 E	32	CO_2, CH_4, CO, H_2
McMurdo / Arrival Height	U. S. A. / New Zealand / Antarctica	MCM777S40	77 48 S	166 46 E	50	O_3
McMurdo Station	U. S. A.	MCM777S10	77 49 S	166 35 E	11	CH_4
Mizuho	Japan	MZH770S00	70 42 S	44 18 E	2230	CH_4
Neumayer	Germany	NMY770S00	70 39 S	8 15 W	42	O_3
Palmer Station	U. S. A.	PSA764S10	64 55 S	64 00 W	10	CO_2, CH_4, CO, H_2, $^{13}CO_2$, $C^{18}O_2$
Palmer Station	U. S. A.	PSA764S20	64 55 S	64 00 W	10	CFCs, HCFCs, CH_3CCl_3, SF_6, N_2O
Palmer Station	U. S. A.	PSA764SX0	64 55 S	64 00 W	10	HFCs
South Pole	U. S. A.	SPO789S00	89 58 S	24 48 W	2810	CO_2
South Pole	U. S. A.	SPO789S10	89 59 S	24 48 W	2810	CO_2, CH_4, CO, H_2, $^{13}CO_2$, $^{13}CH_4$, $C^{18}O_2$
South Pole	U. S. A.	SPO789S20	89 59 S	24 48 W	2810	CFCs, HCFCs, CH_3CCl_3, C_2Cl_4, CH_2Cl_2, SF_6, N_2O
South Pole	U. S. A.	SPO789S30	89 59 S	24 48 W	2810	CO_2, CH_4, CO, H_2
South Pole	U. S. A.	SPO789S40	89 59 S	24 48 W	2810	O_3
South Pole	U. S. A.	SPO789SX0	89 59 S	24 48 W	2810	N_2O, CFCs, HFCs, CCl_4, CH_3CCl_3, SF_6, HCFCs
Syowa Station	Japan	SYO769S00	69 00 S	39 35 E	29	CO_2
Syowa Station	Japan	SYO769S10	69 00 S	39 34 E	14	CO_2, CH_4, CO, H_2, $^{13}CO_2$, $C^{18}O_2$
Syowa Station	Japan	SYO769S20	69 00 S	39 35 E	29	O_3
MOBILE STATION						
Aircraft (over Bass Strait and Cape Grim)	Australia	AIA999930				CO_2, CH_4, CO, H_2
Akademik Korolev, R/V	U. S. A.	AKD999910				CH_4
Alligator liberty, M/V	Japan	ALG999900				CO_2
Discoverer 1983 & 1984, R/V	U. S. A.	DIS999910				CH_4
Discoverer 1985, R/V	U. S. A.	DSC999910				CH_4
Environmental observation and monitoring project	Japan	EOM999900				CO_2, CH_4
HATS Ocean Projects	U. S. A.	HOP9999X0				HFCs
INSTAC-I (International Strato/Tropospheric Air Chemistry Project)	Japan	INS9999A0				CO_2, CH_4, $^{13}CO_2$
John Biscoe, R/V	U. S. A.	JBS999910				CH_4
Keifu Maru, R/V	Japan	KEF999900				CO_2
Kofu Maru, R/V	Japan	KOF999900				CO_2
Korolev, R/V	U. S. A.	KOR999910				CH_4
Long Lines Expedition, R/V	U. S. A.	LLE999910				CH_4
Mexico Naval H-02, R/V	U. S. A.	MXN999910				CH_4

LIST OF OBSERVING STATIONS (continued)

Station	Country/Territory	Index Number	Location Latitude (° ')	Location Longitude (° ')	Altitude (m)	Parameter
MRI Research, 1978-1986, R/V	Japan	MRI9999A0				CH_4
MRI Research, Hakuho Maru, R/V	Japan	HKH999900				CO_2
MRI Research, Kaiyo Maru, R/V	Japan	KIY999900				CO_2
MRI Research, Mirai, R/V	Japan	MMR999900				CO_2
MRI Research, Natushima, R/V	Japan	NTU999900				CO_2
MRI Research, Ryofu Maru, R/V	Japan	RFM999900				CO_2
MRI Research, Wellington Maru, R/V	Japan	WLT999900				CO_2
Oceanographer, R/V	U. S. A.	OCE999910				CH_4
Pacific Ocean	U. S. A.	POC9XXX10			10	CO_2, CH_4, CO, H_2, $^{13}CO_2$, $C^{18}O_2$
Polar Star, R/V	U. S. A.	PLS999910				CH_4
Ryofu Maru, R/V	Japan	RYF999900				CO_2, CH_4, N_2O, CFCs
Ryofu Maru, R/V	Japan	RYF9999A0				CO_2, CH_4
South China Sea	U. S. A.	SCS9XXX10			15	CO_2, CH_4, CO, H_2, $^{13}CO_2$, $C^{18}O_2$
Surveyor, R/V	U. S. A.	SUR999910				CH_4
The Observation of Atmospheric Methane Over Japan	Japan	OAM999900				CH_4
The Observation of Atmospheric Sulfur Hexafluoride Over Japan	Japan	OAS999900				SF_6

LIST OF CONTRIBUTORS

Station Country/Territory	Name	Address
REGION I (Africa)		
Assekrem (Algeria)	Mimouni Mohamed	Office National de la Meteorologie POBox 31 Tamanrasset 11000, Algeria
Amsterdam Island (France)	M. Ramonet M. Schmidt P. Ciais V. Kazan S.G. Jennings	LSCE (Laboratoire des Sciences du Climat et de l'Environnement) UMR CEA-CNRS LSCE - CEA Saclay - Orme des Merisiers - Bat.709 91191 Gif-sur-Yvette, France
Funchal (Portugal)	Antonio Dias Baptista	Instituto de Meteorologia Rua C, Aeroporto 1749-077 Lisboa, Portugal
Cape Point (South Africa)	Casper Labuschagne Ernst-Günther Brunke and Gerrie Coetzee	South African Weather Service (Climate Division) SAWS, c/o CSIR (Environmentek), P.O. Box 320, Stellenbosch 7599, South Africa.
Izaña (Spain)	A.J. Gomez-Pelaez Ramon Ramos J. Perez-delaPuerta	Observatorio Atmosferico de Izana, Instituto Nacional de Meteorologia (Spain) C/ La Marina, 20, Planta 6 Apartado 880 38071 Santa Cruz de Tenerife, Spain
Izaña (Spain)	Carlos Marrero Ramon Ramos Julian Perez	Observatorio Atmosferico de Izana, Instituto Nacional de Meteorologia, Spain C/ La Marina, 20, Planta 6 Apartado 880 38071 Santa Cruz de Tenerife, Spain
REGION II (Asia)		
Mt. Waliguan (China)	Wen Yupu Zhang Xianchun	Chinese Academy of Meteorological Sciences 46 Zhongguancun Nandajie, Haidian, Beijing 100081, P.R. of China
Hok Tsui (Hong Kong, China)	Ka Se Lam	Department of Civil and Structural Engineering, Hong Kong Polytechnic University Hung Hom, Kowloon, Hong Kong
Takayama (Japan)	Shohei Murayama Susumu Yamamoto Nobuko Saigusa and Hiroaki Kondo	Research Institute for Environmental Management Technology National Institute of Advanced Industrial Science and Technology (AIST) AIST Tsukuba West, 16-1 Onogawa, Tsukuba, Ibaraki 305-8569, Japan
Cape Ochi-ishi Hateruma (Japan)	Yasunori Tohjima Hitoshi Mukai Toshinobu Machida Yasumi Fujinuma Masayuki Katsumoto	Center for Global Environmental Research, National Institute for Environmental Studies 16-2, Onogawa, Tsukuba-shi, Ibaraki, 305-8506, Japan

LIST OF CONTRIBUTORS (continued)

Station Country/Territory	Name	Address
Hateruma (Japan)	Yasunori Tohjima Hitoshi Mukai Toshinobu Machida Yasumi Fujinuma Masayuki Katsumoto	Center for Global Environmental Research, National Institute for Environmental Studies 16-2, Onogawa, Tsukuba-shi, Ibaraki, 305-8506, Japan
Tsukuba (Japan)	M. Hirota Y. Makino	Meteorological Research Institute 1-1, Nagamine, Tsukuba, Ibaraki 305-0052, Japan
Minamitorishima Ryori Yonagunijima (Japan)	Hideyuki SASAKI	Atmospheric Environment Division, Global Environment and Marine Department, Japan Meteorological Agency (JMA) 1-3-4 Otemachi, Chiyoda-ku, Tokyo 100-8122, Japan
Tsukuba (Japan)	H. Y. Inoue H. Matsueda M. Ishii	Geochemical Research Department, Meteorological Research Institute 1-1, Nagamine, Tsukuba, Ibaraki 305-0052, Japan
Kisai Mt. Dodaira Urawa (Japan)	Yosuke MUTO	Center for Environmental Science in Saitama 914 Kamitanadare, Kisai-machi, Kita-Saitama-gun, Saitama 347-0115, Japan
Mikawa-Ichinomiya (Japan)	Seiko Iwata	Aichi Environmental Research Center 7-6 Aza-Nagare, Tuji-machi, Kita-ku, Nagoya, Aichi 462-0032, Japan
Cape Ochi-ishi Hateruma (Japan)	Hitoshi Mukai Toshinobu Machida Yasumi Fujinuma Masayuki Katsumoto	Center for Global Environmental Research, National Institute for Environmental Studies 16-2, Onogawa, Tsukuba-shi, Ibaraki, 305-8506, Japan
Nagoya (Japan)	K. Kitagawa A. Matsunami	Research Center for Advanced Energy Conversion, Nagoya University Furo-cho, Chikusaku, Nagoya 464-8603, Japan
Hamamatsu (Japan)	Mitsuo TODA	Shizuoka University 3-5-1 Jyohoku, Hamamatsu 432-8561, Japan
Memanbetsu (Japan)	M. Hirota H. Muramatsu	Meteorological Research Institute Nagamine, Tsukuba, Ibaraki 305-0082, Japan
	F. Muromatsu M. Hashimoto T. Koike	Memanbetsu Magnetic Observatory Memanbetsu, Hokkaido 099-2356, Japan
Tsukuba (Japan)	Tosiro Kimura Hirotosi Baba Takeo Ueno Eiji Ogura Yuuzou Ikeda	Lower Aerological Observations Division, Aerological Observatory, Japan Meteorological Agency (JMA) Lower Aerological Observations Division, Aerological Observatory 1-2 Nagamine, Tsukuba, Ibaraki, 305-0052, Japan

LIST OF CONTRIBUTORS (continued)

Station Country/Territory	Name	Address
Issyk-Kul (Kyrgyzstan)	V. Semenov V. Sinyakov L. Sorokina N. Ignatova	Laboratory of Geophysics, Institute of Fundamental sciences at the Kyrgyz National University, Kyrgyzstan Manas Street 101, Bishkek, 720033, Kyrgyz Republic
	V. Aref'ev N. Kamenogradsky F. Kashin	Institute of Experimental Meteorology SPA 'Typhoon', Russia Lenin St. 82, Obninsk, Kaluga reg. 249020, Russian Federation
Gosan (Rep. of Korea)	Jae-Cheol Nam So-young Bang Kyung-Ryul Kim Mi-Kyung Park	Applied Meteorology Research Laboratory, Meteorological Research Institute (METRI), Korea Meteorological Administration (KMA) 460-18, Shindaebang-dong, Tongjak-gu, Seoul 156-720, Rep. of Korea
Anmyeon-do (Rep. of Korea)	Jeong-Sik Kim Ki-Jun Park	Climate Policy Division, Climate Bureau, Korea Meteorology Administration 460-18, Shindaebang-dong, Dongjak-gu Seoul 156-720, Republic of Korea
Bering Island Kotelny Island (Russian Federation)	A. Shashkov N. Paramonova V. Privalov A. Reshetnikov	Main Geophysical Observatory (MGO) Karbyshev Street 7, St. Petersburg, 194021, Russian Federation
Kyzylcha (Uzbekistan)	A. Shashkov N. Paramonova V. Privalov A. Reshetnikov	Main Geophysical Observatory (MGO) Karbyshev Street 7, St. Petersburg, 194021, Russian Federation
REGION III (South America)		
Ushuaia (Argentina)	Miguel Pereyra Sergio Luppo	Servicio Meteorológico Nacional - Gobierno de Tierra del Fuego Subsecretaria de Planeamiento Fagnano 486, Planta Alta 9410 Ushuaia, Tierra del Fuego, Argentina
Arembepe (Brazil)		
Huancayo (Peru)	M. Ishituka	Observatorio de Huancayo, Instituto Geofisico del Peru Apartado 46, Huancayo, Peru
REGION IV (North and Central America)		
Alert Cape St. James Sable Island (Canada)	V. Hudec C.S. Wong	Meteorological Service of Canada (MSC) 4905 Dufferin Street, Downsview, Ontario, Canada, M3H 5T4

LIST OF CONTRIBUTORS (continued)

Station Country/Territory	Name	Address
Algoma Bratt's Lake Chalk River Chapais Egbert Esther Experimental Lakes Area Kejimkujik Longwoods Saturna Sutton (Canada)		Environment Canada Meteorological Service of Canada Air Quality Research Branch 4905 Dufferin St. Toronto, Ontario CANADA M3H 5T4
La Palma (Cuba)	Osvaldo Cuesta Santos	Institute of Meteorology, Atmospheric Environment Research Center Apdo. 17032, Postal Code 11700, Havana 17, Cuba
Barrow (U. S. A.)	Edward J. Dlugokencky Patricia M. Lang Tom Mefford	NOAA/ESRL Global Monitoring Division 325 Broadway R/GMD1 Boulder, CO 80305-3328
Barrow (U. S. A.)	Pieter P. Tans Kirk Thoning Lee Waterman Thomas Mefford	NOAA/ESRL Global Monitoring Division 325 Broadway R/GMD1 Boulder, CO 80305-3328, U.S.A
REGION V (South-West Pacific)		
Cape Grim (Australia)	Paul Fraser	Commonwealth Scientific and Industrial Research Organization (CSIRO) CSIRO, Division of Atmospheric Research 107-121 Station Street, Aspendale, Victoria 3195, Australia Postal adress: PMB 1 Aspendale Vic 3195
Cape Grim (Australia)	Ian Galbally	Commonwealth Scientific and Industrial Research Organization (CSIRO) CSIRO, Division of Atmospheric Research 107-121 Station Street, Aspendale, Victoria 3195, Australia Postal address: PMB 1 Aspendale Vic 3195
Bukit Koto Tabang (Indonesia)	WMO EMPA-Switzerland	Global GAW Bukit Kototabang Jl. Angkasa I No. 2, Kemayoran, Jakarta JAKARTA 10720
Bukit Koto Tabang Jakarta (Indonesia)	Tuti Mulyani	Bureau of Meteorology and Geophysics Jalan Angkasa 1 No.2 Jakarta 10720, Indonesia
Danum Valley GAW Baseline Station Tanah Rata (Malaysia)		Malaysian Meteorological Department

LIST OF CONTRIBUTORS (continued)

Station Country/Territory	Name	Address
Baring Head (New Zealand)	M.R. Manning A.J. Gomez G.W. Brailsford S.E. Nichol	National Institute of Water & Atmospheric Research Ltd. 301 Evans Bay Parade, Greta Point Private Bag 14-901, Kilbirnie, Wellington, New Zealand
Mauna Loa (U. S. A.)	Edward J. Dlugokencky Patricia M. Lang Tom Mefford	NOAA/ESRL Global Monitoring Division 325 Broadway R/GMD1 Boulder, CO 80305-3328
Mauna Loa Tutuila (U. S. A.)	Pieter P. Tans Kirk Thoning Lee Waterman Thomas Mefford	NOAA/ESRL Global Monitoring Division 325 Broadway R/GMD1 Boulder, CO 80305-3328, U.S.A
REGION VI (Europe)		
Hohe Warte Stephansplatz (Austria)	Wolfgang Spangl	Federal Environmental Agency Spittelauer L?de 5 A-1090 Wien, Austria wolfgang.spangl@umweltbundesamt.at
Sonnblick (Austria)	Wolfgang Spangl	Federal Environment Agency Austria Spittelauer Lande 5, A-1090 Wien, Austria
Hohe Warte Stephansplatz (Austria)	Guenther Schermann	Municipal Department 22 - Environmental Protection Air quality subdepartment, City of Vienna Ebendorferstrasse 4, A-1082 Vienna, Austria
Ivan Sedlo (Bosnia and Herzegovina)	Enes Sarac	Meteoroloski zavod Bosne i Hercegovine Bardakcije 12, 71000 Sarajevo, Bosnia and Herzegovina
Burgas Pleven Plovdiv Sofia Varna (Bulgaria)	N. Valkov E. Batchvarova	National Institute of Meteorology and Hydrology 66 Tzarigradsko chaussee, 1784 Sofia, Bulgaria
Kosetice (Czech Republic)	Milan Vana	Air Quality Protection Department, Czech Hydrometeorological Institute Czech Hydrometeorological Institute, Kosetice Observatory, 394 22 Kosetice, Czech Republic
Kosetice (Czech Republic)	Sverre Solberg	Norwegian Institute for Air Research P.O.Box 100 NO-2027 Kjeller

LIST OF CONTRIBUTORS (continued)

Station Country/Territory	Name	Address
Site J (Denmark)	S. Morimoto G. Hashida	National Institute of Polar Research Kaga 1-9-10, Itabashi-ku, Tokyo 173-8515, Japan
	S. Aoki T. Nakazawa	Center for Atmospheric and Oceanic Studies, Graduate School of Science, Tohoku University Sendai 980-8578, Japan
Pallas-Sammaltunturi (Finland)	Dr. Tuula Aalto	Finnish Meteorological Institute P.O.Box 503, FI-00101 Helsinki, Finland
Pallas-Sammaltunturi Utö (Finland)	Sverre Solberg	Norwegian Institute for Air Research P.O.Box 100 NO-2027 Kjeller
Ähtäri Oulanka Pallas-Sammaltunturi Utö Virolahti (Finland)	Virpi Tarvainen Yrjo Viisanen	Finnish Meteorological Institute Erik Palmenin aukio 1, P.O.Box 503, FIN-00101 Helsinki, Finland
Donon La Tardiere Pezrusse Vieille (France)	Sverre Solberg	Norwegian Institute for Air Research P.O.Box 100 NO-2027 Kjeller
Hohenpeissenberg (Germany)	U.Kaminski	Deutscher Wetterdienst (DWD) Meteorologisches Observatorium Hohenpeissenberg Albin-Schwaiger-Weg 10 D-82383 Hohenpeissenberg, Germany
Brotjacklriegel Schmuecke Waldhof Zingst (Germany)	Sverre Solberg	Norwegian Institute for Air Research P.O.Box 100 NO-2027 Kjeller
Hohenpeissenberg Zugspitze/Schneefernerhaus (Germany)	Stefan Gilge	German Meteorological Service (DWD) Meteorological Observatory Hohenpeissenberg Albin-Schwaiger-Weg 10 D-82383 Hohenpeissenberg, Germany
Brotjacklriegel Deuselbach Neuglobsow Schauinsland Waldhof Westerland Zingst Zugspitze Zugspitze/Schneefernerhaus (Germany)	K. Uhse L. Ries U. Treffert F. Meinhardt O. Bath R. Graul	Federal Environmental Agency (Umweltbundesamt) Federal Environmental Agency (Umweltbundesamt) Monitoring site Zingst Landstrasse 3 D-18874 Zingst
Wank Peak Zugspitze (Germany)	H.E. Scheel R. Sladkovic	Fraunhofer-Institute for Atmospheric Environmental Research, since 1.1.2002: Forschungszentrum Karlsruhe, IMK-IFU D-82467 Garmisch-Partenkirchen, Germany

LIST OF CONTRIBUTORS (continued)

Station Country/Territory	Name	Address
Hohenpeissenberg (Germany)	Christian Plass-Duelmer Harald Berresheim	Deutscher Wetterdienst (DWD), Meteorologisches Observatorium Hohenpeissenberg Albin-Schwaiger-Weg 10 D-82383 Hohenpeissenberg, Germany
Hegyhatsal K-puszta (Hungary)	L. Horvath	Hungarian Meteorological Service P.O. Box 39 H-1675 Budapest, Hungary
Mace Head (Ireland)	Gerard Spain	National University of Ireland, Galway (NUI) Mace Head Research Station Carna, Co. Galway, Ireland
Mace Head (Ireland)	M. Ramonet M. Schmidt P. Ciais V. Kazan S.G. Jennings	LSCE (Laboratoire des Sciences du Climat et de l'Environnement) UMR CEA-CNRS LSCE - CEA Saclay - Orme des Merisiers - Bat.709 91191 Gif-sur-Yvette, France
Monte Cimone (Italy)	Riccardo Santaguida Francesco De Nile Luigi Lauria	Italian Air Force Meteorological Service C.A.M.M. Mt. CIMONE, Via delle Ville 40, 41029-Sestola (MO), Italy
Lampedusa (Italy)	F. Artuso S. Piacentino A. di Sarra,S. Chiavarini P. Grigioni F. Monteleone L. De Silvestri.	Italian National Agency for New Technology, Energy and the Environment (ENEA) ENEA CLIM-OSS Via Anguillarese 301, 00060 S. >00060 Maria di Galeria, Rome, Italy.
Plateau Rosö (Italy)	Claudio Vannini	Italian Electrical Experimental Center - Research (CESI RICERCA) Via Rubattino, 54, 20134 Milano, Italy
Monte Cimone (Italy)	Paolo Bonasoni Paolo Cristofanelli	National Research Council, Institute of Atmospheric Sciences and Climate, Mt. Cimone Station Via Gobetti 101 40129 Bologna, Italy
Rucava Zoseni (Latvia)	Iraida Lyulko	Observation Network Department, Latvian Environment, Geology and Meteorology Agency, Ministry of Environmental 165 Maskavas str. LV-1019, Riga, Latvia
Giordan Lighthouse (Malta)	Raymond Ellul Martin Saliba	Atmospheric Research Unit / Physics Department /University of Malta Msida MSD 06, Malta
Kloosterburen Kollumerwaard (Netherlands)	J.P. Beck	Air Research Laboratory, National Institute of Public Health and the Environment P.O. Box 1, 3720 BA Bilthoven, Netherlands
Zeppelinfjellet (Norway)	Johan Strom	Department of Applied Environmental Science (ITM), Stockholm University SE-106 91 Stokholm, Sweden

LIST OF CONTRIBUTORS (continued)

Station Country/Territory	Name	Address
Zeppelinfjellet (Norway)	Ove Hermansen	Norwegian Institute for Air Research (NILU) P. O. Box 100 Instituttveien 18, N-2027 Kjeller, Norway
Puszcza Borecka/Diabla Gora (Poland)	Institute of Environmental Protection Warsaw	Institute of Environmental Protection Kolektorska 4 01-692 Warsaw, Poland
Jarczew Leba Sniezka Suwalki (Poland)	prof. dr eng. Henryk Slota	Laboratory of Atmospheric Chemistry, Institute of Meteorology and Water Management (IMWM) Podlesna Street 61, 01-673 Warszawa, POLAND
Angra do Heroismo Beja Braganca Castelo Branco Lisboa / Gago Coutinho Monte Velho Penhas Douradas Viana do Castelo (Portugal)	Antonio Dias Baptista	Instituto de Meteorologia Rua C, Aeroporto 1749-077 Lisboa, Portugal
Fundata Semenic Stîna de Vale (Romania)	Daniela ZISU	National Research and Development Institute for Environmental Protection Splaiul Independentei nr. 294, sector 6, 77703 Bucuresti Romania
Fundata (Romania)	Adriana Nicodim Florin Nicodim	National Meteorological Administration Sos. Bucuresti-Ploiesti nr. 97, 71552 Bucharest, Romania
Ocean Station Charlie Teriberka (Russian Federation)	A. Shashkov N. Paramonova V. Privalov A. Reshetnikov	Main Geophysical Observatory (MGO) Karbyshev Street 7, St. Petersburg, 194021, Russian Federation
Danki Shepelevo (Russian Federation)		
Kamenicki Vis Zabljak (Serbia and Montenegro)	Dragan Djordjevic	Republic Hydrometeorological Service of Serbia P.O. Box 37, Kneza Viseslava 66 11030 Belgrade, Serbia and Montenegro
Starina (Slovakia)	Sverre Solberg	Norwegian Institute for Air Research P.O.Box 100 NO-2027 Kjeller
Iskrba Kovk Krvavec Zavodnje (Slovenia)	Brigita Jesenovec	Ministry of Environment and Spatial Planning Environmental Agency of the Republic of Slovenia (EARS) Vojkova 1/b, Sl-1000 Ljubljana, Slovenia

LIST OF CONTRIBUTORS (continued)

Station Country/Territory	Name	Address
Campisabalos (Spain)	Sverre Solberg	Norwegian Institute for Air Research P.O.Box 100 NO-2027 Kjeller
Doñana La Cartuja Logroño Mahón Noia Roquetes San Pablo de los Montes (Spain)	J.M. Saenz R.G. Marin	Instituto Nacional de Meteorologia, Ministerio de Medio Ambiente Leonardo Prieto Castro, 8, 28071 Madrid, Spain
Vindeln (Sweden)	Karin Sjoberg	Swedish Environmental Research Institute (IVL) P.O.Box 5302 S-400 14 Goteborg, Sweden
Jungfraujoch (Switzerland)	Brigitte Buchmann	EMPA, Swiss Federal Laboratories for Materials Testing and Research Air Pollution / Environmental Technology Uberlandstrasse 129 CH-8600 Dubendorf, Switzerland
Lazaropole (The former Yugoslav Republic of Macedonia)	Suzana Alcinova Monevska	Hydrometeorological Service Skupi bb, 1000 Skopie, The former Yugoslav Republic of Macedonia
Eskdalemuir (United Kingdom)	Peter Kuria	Air and Environment Quality Division, DEFRA 4/F15, Ashdown House 123 Victoria Street London, SW1E 3DE, United Kingdom
ANTARCTICA		
Arrival Heights (Antarctica / New Zealand)	M.R. Manning A.J. Gomez G.W. Brailsford S.E. Nichol	National Institute of Water & Atmospheric Research Ltd. 301 Evans Bay Parade, Greta Point Private Bag 14-901, Kilbirnie, Wellington, New Zealand
Jubany (Argentina)	L. Ciattaglia	Consiglio Nazionale delle Ricerche Istituto di Scienze dell'Atmosfera e del Clima (CNR-ISAC) Area della Ricerca di Roma Tor Vergata via Fosso del Cavaliere, 100, 00133 Rome, Italy
	J. Araujo H.Rodriguez	Direccion Nacional del Antartico Instituto Antmgtico Argentino (DNA-IAA) Cerrito 1248, 1010 Buenos Aires, Argentina
Neumayer (Germany)	Rolf Weller	Alfred Wegener Institute Am Handelshafen 12, 27570 Bremerhaven, Germany
	Uwe Kaminski	Deutscher Wetterdienst, Meteorologisches Observatorium, GAW Global station Albin-Schwaiger-Weg 10, 82383 Hohenpeissenberg, Germany

LIST OF CONTRIBUTORS (continued)

Station Country/Territory	Name	Address
Syowa Station (Japan)	S. Morimoto G. Hashida	National Institute of Polar Research Kaga 1-9-10, Itabashi-ku, Tokyo 173-8515, Japan
	S. Aoki T. Nakazawa	Center for Atmospheric and Oceanic Studies, Graduate School of Science, Tohoku University Sendai 980-8578, Japan
Mizuho (Japan)	Takakiyo Nakazawa	Center for Atmospheric and Oceanic Studies, Graduate School of Science, Tohoku University Aoba, Sendai 980-8578, Japan
Syowa Station (Japan)	Yasuo Shudou	Office of Antarctic Observations, Japan Meteorological Agency (JMA) 1-3-4 Otemachi, Chiyoda-ku, Tokyo 100-8122, Japan
South Pole (U. S. A.)	Pieter P. Tans Kirk Thoning Lee Waterman Thomas Mefford	NOAA/ESRL Global Monitoring Division 325 Broadway R/GMD1 Boulder, CO 80305-3328, U.S.A
MOBILE STATION		
The Observation of Atmospheric Methane Over Japan (Japan)	M. Hirota Y. Makino	Meteorological Research Institute 1-1, Nagamine, Tsukuba, Ibaraki 305-0052, Japan
Keifu Maru, R/V Kofu Maru, R/V Ryofu Maru, R/V (Japan)	T. Miyao	Climate and Marine Department, Japan Meteorological Agency 1-3-4 Otemachi, Chiyoda-ku, Tokyo 100-8122, Japan
	H. Matsueda	Meteorological Research Institute 1-1 Nagamine, Tsukuba, Ibaraki 305-0052, Japan
	K. Saitou	Kobe Marine Observatory 1-4-3 Wakinohama-Kaigandori, Chuo-ku, Kobe 651-0073, Japan
MRI Research 1978-1986, R/V Hakuho Maru, R/V Kaiyo Maru, R/V Natushima, R/V Ryofu Maru, R/V Wellington Maru, R/V (Japan)	H. Matsueda H. Yoshikawa	Geochemistry Research Department, Meteorological Research Institute Nagamine 1-1, Tsukuba, Ibaraki 305-0052, Japan
Alligator liberty, M/V (Japan)	S. Kato	Foundation for Promoting Perspnal Mobility and Ecological Transportation (Eco-Mo Foundation) 808, Syuwakioicho-TBR-Building, 5-7, Koujimachi, Chiyodaku, Tokyo 102-0083, Japan
	J. Oyama	Pollutants Chemical Analysis Center, Marine Division, Climate and Marine Department, Japan Meteorological Agency (JMA) 1-3-4 Otemachi, Chiyoda-ku, Tokyo 100-8122, Japan

LIST OF CONTRIBUTORS (continued)

Station Country/Territory	Name	Address
Environmental observation and monitoring project INSTAC-I (International Strato/Tropospheric Air Chemistry Project) (Japan)	H. Matsueda H. Yoshikawa M. Ishii	Geochemical Research Department, Meteorological Research Institute Nagamine 1-1, Tsukuba, Ibaraki 305-0052, Japan
The Observation of Atmospheric Sulfur Hexafluoride Over Japan (Japan)	M. Hirota H. Muramatsu	Meteorological Research Institute/JMA 1-1 Nagamine, Tsukuba, Ibaraki 305-0052, Japan
MRI Research Mirai, R/V (Japan)	Masao Ishii	Geochemistry Research Department, Meteorological Research Institute Nagamine 1-1, Tsukuba, Ibaraki 305-0052, Japan

NOAA/CMDL Flask Network

Halley Bay (United Kingdom / Antarctica)	P. P. Tans* T. J. Conway* (CO_2)	(*) NOAA/ESRL Global Monitoring Division 325 Broadway R/GMD1 Boulder, CO 80305-3328, U.S.A. (**) Institute of Arctic and Alpine Research (INSTAAR) Campus box 450, University of Colorado, Boulder, CO 80309-0450, U.S.A.
Tierra del Fuego (Argentina) Cape Grim (Australia)	Edward J. Dlugokencky* Patricia M. Lang* Kenneth A. Masarie* (CH_4)	
Ragged Point (Barbados)	Paul C. Novelli* Kenneth A. Masarie* (CO)	
Alert Mould Bay (Canada)	Paul C. Novelli* (H_2)	
Easter Island (Chile)	James White** Bruce Vaughn** ($^{13}CO_2$ and $C^{18}O_2$)	
Mt. Waliguan (China) Summit (Denmark)	John Miller* James White** ($^{13}CH_4$)	
Pallas-Sammaltunturi (Finland)		
Amsterdam Island Crozet (France)		
Hegyhatsal (Hungary)		
Heimaey (Iceland)		

LIST OF CONTRIBUTORS (continued)

Station Country/Territory	Name	Address
Bukit Koto Tabang (Indonesia)		
Mace Head (Ireland)		
Sede Boker (Israel)		
Syowa Station (Japan / Antarctica)		
Plateau Assy Sary Taukum (Kazakhstan)		
Christmas Island (Kiribati)		
Kaashidhoo (Maldives)		
Dwejra Point (Malta)		
Ulaan Uul (Mongolia)		
Gobabeb (Namibia)		
Kaitorete Spit (New Zealand)		
Ny-Alesund Ocean Station "M" (Norway)		
Baltic Sea (Poland)		
Terceira Island (Portugal)		
Tae-ahn Peninsula (Rep. of Korea)		
Black Sea (Romania)		
Mahe Island (Seychelles)		
Tenerife (Spain)		
Akademik Korolev, R/V		

LIST OF CONTRIBUTORS (continued)

Station Country/Territory	Name	Address
Barrow		
Cape Kumukahi		
Cape Meares		
Cold Bay		
Discoverer 1983 & 1984, R/V		
Discoverer 1985, R/V		
Grifton		
Guam		
John Biscoe, R/V		
Key Biscayne		
Kitt Peak		
Korolev, R/V		
La Jolla		
Long Lines Expedition, R/V		
Mauna Loa		
Mexico Naval H-02, R/V		
Moody		
Niwot Ridge		
Ocean Station "C"		
Oceanographer, R/V		
Olympic Peninsula		
Pacific Ocean		
Park Falls		
Point Arena		
Polar Star, R/V		
Sand Island		
Shemya Island		
South China Sea		
Southern Great Plains		
St. Croix		
Surveyor, R/V		
Trinidad Head		
Tutuila		
Wendover		
(U. S. A.)		
McMurdo Station		
Palmer Station		
South Pole		
(U. S. A. / Antarctica)		
Ascension Island		
Bird Island		
St. David's Head		
Tudor Hill		
(United Kingdom)		
Assekrem		
(Algeria)		

LIST OF CONTRIBUTORS (continued)

Station Country/Territory	Name	Address
NOAA/CMDL/HATS Network		
Summit (Denmark) Cape Grim (Australia) Alert (Canada) Tierra del Fuego (Argentina) Mace Head (Ireland) Barrow Cape Kumukahi Grifton Harvard Forest HATS Ocean Projects Mauna Loa Niwot Ridge Niwot Ridge C-1 Park Falls Trinidad Head Tutuila (U. S. A.) Palmer Station South Pole (U. S. A. / Antarctica)	James W. Elkins James H. Butler Thayne M. Thompson Geoffrey S. Dutton Stephen A. Montzka Bradley D. Hall	Halocarbons and Other Atmosphere Trace Species Group (HATS) /NOAA/ESRL Global Monitoring Division 325 Broadway R/GMD1 Boulder, CO 80305-3328, U.S.A
NOAA/CMDL Surface Ozone Network		
McMurdo / Arrival Height (U. S. A. / New Zealand / Antarctica) Ragged Point (Barbados) Tudor Hill (Bermuda, United Kingdom) Summit (Greenland, Denmark) Heimaey (Iceland) Lauder (New Zealand) Barrow Mauna Loa	Sam Oltmans	NOAA/ESRL Global Monitoring Division 325 Broadway R/GMD1 Boulder, CO 80305-3328, U.S.A

LIST OF CONTRIBUTORS (continued)

Station Country/Territory	Name	Address
Niwot Ridge Niwot Ridge (Saddle) Trinidad Head (U. S. A.)		
South Pole (U. S. A. / Antarctica)		
Cape Matatula (American Samoa, U. S. A.)		

CSIRO Flask Network

Aircraft (over Bass Strait and Cape Grim) Cape Ferguson Cape Grim Macquarie Island (Australia)	Paul Steele Paul Krummel Ray Langenfelds Roger Francey	Commonwealth Scientific and Industrial Research Organisation (CSIRO) CSIRO Marine and Atmospheric Research 107-121 Station Street, Aspendale, Victoria 3195, Australia Postal address: PMB 1, Aspendale, Victoria 3195, Australia
Mawson (Australia / Antarctica)		
Alert Estevan Point (Canada)		
Mauna Loa (U. S. A.)		
South Pole (U. S. A. / Antarctica)		
Shetland (United Kingdom)		

ALE/GAGE/AGAGE Network

Cape Grim (Australia)	R. Prinn	TEPCO Professor of Atmospheric Chemistry, Director, Center for Global Change Science Head, Dept. of Earth, Atmospheric & Planetary Sciences MIT, Bldg. 54-1312, Cambridge, MA 02139-4307, U.S.A.
Ragged Point (Barbados)		
	D. Cunnold	School of Earth and Atmospheric Sciences, Georgia Institute of Technology 30332-0340 Atlanta, GA, U.S.A.
Adrigole Mace Head (Ireland)	R. H. J. Wang	
	P. Fraser	CSIRO Atmospheric Research, PMB #1 Aspendale Victoria 3195, Australia
Cape Matatula Cape Meares Trinidad Head (U. S. A.)	L. P. Steele	
	R. Weiss	Scripps Institution of Oceanography, University of California, San Diego, La Jolla, California 92093-0244, U.S.A.
	P. Salameh	
	P. Simmonds	39 Avon Castle Drive, Ringwood, Hants, BH24 2BB, United Kingdom
	S. O'Poherty	

GLOSSARY

AGENCIES AND PROGRAMMES:

AGAGE	Advanced Global Atmospheric Gases Experiment
ALE	Atmospheric Lifetime Experiment
AES	Atmospheric Environment Service (Canada, presently MSC)
CAMS	Chinese Academy of Meteorological Sciences (China)
CESI	Italian Electrical Experimental Center (Italy)
CFR	Centre des Faibles Radioactivites (France)
CHMI	Czech Hydrometeorological Institute (Czech Republic)
CMA	China Meteorological Administration (China)
CMDL	Climate Monitoring and Diagnostics Laboratory (USA/NOAA, presently ESRL/GMD)
CNR	Consiglio Nazionale delle Ricerche (Italy)
CNRS	Centre National de la Recherche Scientifique (France)
CSIRO	Commonwealth Scientific and Industrial Research Organisation (Australia)
DNA-IAA	Direccion Nacional del Antartico-Instituto Antartico Argentino (Argentina)
DWD	Deutscher Wetterdienst (German Meteorological Service, Germany)
EMPA	Swiss Federal Laboratories for Material Testing and Research (Switzerland)
ENEA	Italian National Agency for New Technology, Energy and the Environment (Italy)
ESRL/GMD	Earth System Research Laboratory/Global Monitoring Division (USA/NOAA, formerly CMDL)
GAGE	Global Atmospheric Gases Experiment
GAW	Global Atmosphere Watch (WMO)
HATS	Halocarbons and other Atmospheric Trace Species
HMS	Hungarian Meteorological Service (Hungary)
IFU	Institute of the Research of the Atmospheric Environment (Germany)
IGP	Instituto Geofísico del Perú (Peru)
IMS	Centro Aeronautico di Montagna, Italian Air Force Meteorological Service (Italy)
INM	Instituto Nacional de Meteorología (Spain)
JMA	Japan Meteorological Agency (Japan)
KMA	Korea Meteorological Administration (Republic of Korea)
LSCE	Laboratoire des Sciences du Climat et de l'Environnement (France)
METRI	Meteorological Research Institute (Republic of Korea /KMA)
MGO	Main Geophysical Observatory (Russian Federation)
MISU	Department of Meteorology, Stockholm University (Sweden)
MRI	Meteorological Research Institute (Japan/JMA)
MSC	Meteorological Service of Canada (Canada, formerly AES)
NCEP	National Centers for Environmental Prediction (USA/NOAA)
NIES	National Institute for Environmental Studies (Japan)
NILU	Norwegian Institute for Air Research (Norway)
NIMH	Institutul National de Meteorologie, Hidrologie si Gospodarirea Apelor (Romania)
NIST	National Institute of Standards and Technology (USA)
NIWA	National Institute of Water & Atmospheric Research (New Zealand)
NOAA	National Oceanic and Atmospheric Administration (USA)
NCEP	National Centers for Environmental Prediction (USA/NOAA)
RIVM	National Institute for Health and Environment (Netherlands)

SAWS	South African Weather Service (South Africa)
SIO	Scripps Institution of Oceanography, University of California at San Diego (USA)
UBA	Umweltbundesamt (Germany)
WDCGG	World Data Centre for Greenhouse Gases, operated by JMA, Japan (WMO)
WMO	World Meteorological Organization
ZAMG	Central Institute of Meteorology and Geodynamics (Austria)

ATMOSPHERIC SPECIES:

CCl_4	tetrachloromethane (carbon tetrachloride)
CFC-11	chlorofluorocarbon-11 (trichlorofluoromethane, CCl_3F)
CFC-12	chlorofluorocarbon-12 (dichlorodifluoromethane, CCl_2F_2)
CFC-113	chlorofluorocarbon-113 (1,1,2-trichlorotrifluoroethane, CCl_2FCClF_2)
CFCs	chlorofluorocarbons
HCFC-141b	hydrochlorofluorocarbon-141b (1,1-dichloro-1-fluoroethane, CH_3CCl_2F)
HCFC-142b	hydrochlorofluorocarbon-142b (1,1-difluoro-1-chloroethane, CH_3CClF_2)
HCFCs	hydrochlorofluorocarbons
CH_4	methane
CH_3CCl_3	trichloroethane (methyl chloroform)
CO	carbon monoxide
CO_2	carbon dioxide
N_2O	nitrous oxide
NO	nitrogen monoxide
NO_2	nitrogen dioxide
NO_X	nitrogen oxides
O_3	ozone
SO_2	sulphur dioxide

UNITS:

ppb	parts per billion
ppm	parts per million
ppt	parts per trillion

Others:

ENSO	El Niño-Southern Oscillation
M/V	merchant vessel
R/V	research vessel
SOI	Southern Oscillation Index
SST	Sea Surface Temperature

LIST OF WMO WDCGG PUBLICATIONS

DATA REPORTING MANUAL:

WDCGG No. 1	January	1991

WMO WDCGG DATA REPORT:

			(period of data accepted)				
WDCGG No. 2 Part A	October	1992	October	1990	~	August	1992
WDCGG No. 2 Part B	October	1992	October	1990	~	August	1992
WDCGG No. 3	October	1993	September	1992	~	March	1993
WDCGG No. 5	March	1994	April	1993	~	September	1993
WDCGG No. 6	September	1994	September	1993	~	March	1994
WDCGG No. 7	March	1995	April	1994	~	December	1994
WDCGG No. 9	September	1995	January	1995	~	June	1995
WDCGG No.10	March	1996	July	1995	~	December	1995
WDCGG No.11	September	1996	January	1996	~	June	1996
WDCGG No.12	March	1997	July	1996	~	November	1996
WDCGG No.14	September	1997	December	1996	~	June	1997
WDCGG No.16	March	1998	July	1997	~	December	1997
WDCGG No.17	September	1998	January	1998	~	June	1998
WDCGG No.18	March	1999	July	1998	~	December	1998
WDCGG No.20	September	1999	January	1999	~	June	1999
WDCGG No.21	March	2000	July	1999	~	December	1999
WDCGG No.23	September	2000	January	2000	~	June	2000
WDCGG No.25	March	2001	July	2000	~	December	2000

WMO WDCGG DATA CATALOGUE:

WDCGG No. 4	December	1993
WDCGG No.13	March	1997
WDCGG No.19	March	1999
WDCGG No.24	March	2001

WMO WDCGG DATA SUMMARY:

WDCGG No. 8	October	1995
WDCGG No.15	March	1998
WDCGG No.22	March	2000
WDCGG No.26	March	2002
WDCGG No.27	March	2003
WDCGG No.28	March	2004
WDCGG No.29	March	2005
WDCGG No.30	March	2006

WMO WDCGG CD-ROM:

			(period of data accepted)				
CD-ROM No. 1	March	1995	October	1990	~	December	1994
CD-ROM No. 2	March	1996	October	1990	~	June	1995
CD-ROM No. 3	March	1997	October	1990	~	June	1996
CD-ROM No. 4	March	1998	October	1990	~	December	1997
CD-ROM No. 5	March	1999	October	1990	~	December	1998
CD-ROM No. 6	March	2000	October	1990	~	December	1999
CD-ROM No. 7	March	2001	October	1990	~	December	2000
CD-ROM No. 8	March	2002	October	1990	~	January	2002
CD-ROM No. 9	March	2003	October	1990	~	December	2002
CD-ROM No.10	March	2004	October	1990	~	December	2003
CD-ROM No.11	March	2005	October	1990	~	December	2004
CD-ROM No.12	March	2006	October	1990	~	December	2005